

Distribution Agreement

In presenting this thesis or dissertation as a partial fulfillment of the requirements for an advanced degree from Emory University, I hereby grant to Emory University and its agents the non-exclusive license to archive, make accessible, and display my thesis or dissertation in whole or in part in all forms of media, now or hereafter known, including display on the world wide web. I understand that I may select some access restrictions as part of the online submission of this thesis or dissertation. I retain all ownership rights to the copyright of the thesis or dissertation. I also retain the right to use in future works (such as articles or books) all or part of this thesis or dissertation.

Signature:

Michael F. Thees

Date

Uncovering the Unexpected Role Chain Connectivity has on Altering Dynamics of
Thin Glassy Polymer Films Near Interfaces

By

Michael F. Thees
Doctor of Philosophy

Physics

Connie B. Roth, Ph.D.
Advisor

Sven H. Behrens, Ph.D.
Committee Member

Stefan Boettcher, Ph.D.
Committee Member

Juston C. Burton, Ph.D.
Committee Member

Eric R. Weeks, Ph.D.
Committee Member

Accepted:

Lisa A. Tedesco, Ph.D.
Dean of the James T. Laney School of Graduate Studies

Date

Uncovering the Unexpected Role Chain Connectivity has on Altering Dynamics of
Thin Glassy Polymer Films Near Interfaces

By

Michael F. Thees
B.A., Boston University, MA, 2012

Advisor: Connie B. Roth, Ph.D.

An abstract of
A dissertation submitted to the Faculty of the
James T. Laney School of Graduate Studies of Emory University
in partial fulfillment of the requirements for the degree of
Doctor of Philosophy
in Physics
2020

Abstract

Uncovering the Unexpected Role Chain Connectivity has on Altering Dynamics of
Thin Glassy Polymer Films Near Interfaces
By Michael F. Thees

Polymer glasses are a widely studied system in thin films, with perturbations to dynamics due to the presence of interfaces being a topic of ever growing interest. Such interface confinement effects have generally been understood as being enthalpic in nature, with these property changes at interfaces forming a gradient in dynamics propagating into the film. However, recent studies have begun reporting differences in confinement effects associated with chain length, stiffness, and architecture indicating that entropic effects may play a modifying role to dynamics near interfaces. Here, we explore the effects that chain connectivity and entropy have on the local and film average glass transition dynamics near interfaces.

We measured the average glass transition temperature (T_g) and aging rate (β) in bulk (>200 nm thick) and thin 31 nm thick films for molecular weights (MWs) up to 10,100 kg/mol, where β is observed to decrease in all thin films. For thin films of ultra-high molecular weight PS (MWs $>6,500$ kg/mol) an increased β is observed compared to thin films of merely high molecular weight PS (MWs $<3,500$ kg/mol). This increase in β for thin films is attributed to a diminished gradient in dynamics at ultra-high molecular weights, associated with chain connectivity.

Motivated by studies recently proposing that chain adsorption may be altering dynamics in thin films, we evaluate the procedure for forming adsorbed layers by washing off unadsorbed chains from melt annealed films, called the “Guiselin experiment”. We demonstrate that the adsorbed amount measured is highly dependent on the substrate cleaning and solvent washing protocol used. Measuring the effect that these adsorbed layers have on average dynamics, we observe no significant change to either the average T_g or average β . Adsorption and desorption of layers formed directly in solutions was also investigated at different concentrations for comparison with those formed by washing off melt annealed films. Local T_g adjacent to adsorbed layers formed by washing off melt films for different times or grown directly in solution were examined to determine how different adsorbed layers affect local T_g . We found that the local T_g adjacent to adsorbed layers only increased for adsorbed layers formed by washing for short times well-annealed melt films, provided good chain interpenetration was obtained for the system. Adsorbed layers well equilibrated in solution showed no corresponding changes in T_g .

Uncovering the Unexpected Role Chain Connectivity has on Altering Dynamics of
Thin Glassy Polymer Films Near Interfaces

By

Michael F. Thees
B.A., Boston University, MA, 2012

Advisor: Connie B. Roth, Ph.D.

A dissertation submitted to the Faculty of the
James T. Laney School of Graduate Studies of Emory University
in partial fulfillment of the requirements for the degree of
Doctor of Philosophy
in Physics
2020

Acknowledgments

I want to first thank my advisor Dr. Connie Roth, without whom none of this would have been possible. Ever since I came to Emory to work with Connie she has been an exceptionally welcoming and supportive advisor. In many ways she has challenged me to grow and be a better person both in academia and in life.

The members of the Roth Lab have been amazing to work with and have always kept me smiling. I want to thank a few people who have really been monumental in helping me to get here, namely Laura Gray, Roman Baglay, Yixuan (Louis) Han, and Benjamin Kasavan, you all were always good for a laugh, and I would not be the person I am without having known you. I hope that each of you has learned as much from me as I have from you.

To my committee, thank you for all the discussions we've had over the years both formal and informal. Certainly your ideas and thoughts about my work has been informative and influential.

The technical, administrative, and support staff at Emory are absolutely some of the best I have ever had the pleasure of working with. The effort that they go through to save the graduate students time and headaches deserves thanks and praise. I especially want to thank Horace Dale, and Jason Boss,

To my friends I've made along the way, you will not lose your special place in my heart. The Sunday golf outings with Robert, Yixuan (Louis), Ryan, and Dana have been a special part of my life. I've deeply enjoyed my discussions about physics and life with Joe, Roman, and Ben, and their never ending willingness to have a beer and talk things out.

Contents

1	Introduction and Scope	1
1.1	Introduction to Polymer Glasses	1
1.2	Confinement Effects in Thin Polymer Films	7
1.3	Outline	11
2	Unexpected Molecular Weight Dependence to the Physical Aging of Thin Polystyrene Films Present at Ultra High Molecular Weights	13
2.1	Introduction	13
2.2	Experimental Methods	17
2.3	Results and Discussion	19
2.3.1	Qualitative observations of differences in physical aging for thin films of ultra-high molecular weight polystyrene	19
2.3.2	Quantitative description of differences in physical aging for thin films of ultra-high molecular weight polystyrene	24
2.3.3	Attempting to understanding differences in physical aging for thin films of ultra-high molecular weight polystyrene	33
2.4	Conclusions	43
3	Review and Reproducibility of Forming Adsorbed Layers From Sol- vent Washing of Melt Annealed Films	46
3.1	Introduction	46

3.1.1	Summary of Recent Investigations on Adsorbed Layers Formed from Melt Films	48
3.1.2	Summary of the Understanding Developed of Chain Adsorption in Solution	55
3.2	Experimental Methods	63
3.3	Results and Discussion	66
3.3.1	Reliability of Measuring Adsorbed Layer Thickness h_{ads} with Ellipsometry	67
3.3.2	Reproducibility of Measuring Adsorbed Layer Thickness h_{ads} .	70
3.3.3	Impact of Multiple of Washings and Substrate Cleaning Method on Adsorbed Layer Thickness h_{ads}	80
3.3.4	Impact of Adsorbed Layers on Film Average $T_g(h)$ and Physical Aging	88
3.4	Conclusions: Summary, Implications and Open Questions	94
3.4.1	Summary of Findings	95
3.4.2	Open Questions	99
4	Role of Solvent Washing Conditions on the Creation of Adsorbed Layers from Melt Films and Its Impact on Local T_g Dynamics	104
4.1	Background	104
4.2	Experimental Methods	107
4.3	Results and Discussion	109
4.3.1	Formation and characterization of adsorbed layers by different methods	109
4.3.2	Local $T_g(z = 0)$ next to an adsorbed layer	119
4.4	Conclusions	129
5	Outlook and open questions	132

List of Figures

1.1	Cartoon depiction of how material properties undergo a continuous change as they pass through the glass transition.	3
1.2	Depiction of the evolution of volume or departure from equilibrium (left) as a function of log time during physical aging. Physical aging rate β versus the aging temperature (right).	4
2.1	Plot of the normalized film thickness h/h_0 versus log aging time at 40 °C comparing the physical aging response of 31 ± 1 nm thick PS films with those of bulk (>500 nm thick) films.	21
2.2	Comparison of 31 ± 1 nm thick PS films where the dashed yellow line delineates the slower aging response of MWs $\leq 3,500$ kg/mol (circles) from the faster aging observed for MWs $\geq 6,500$ kg/mol (triangles).	25
2.3	Comparison of bulk physical aging response measured at an aging temperature of 40 °C (a) and 65 °C (b) for representative molecular weights, where the black dashed curves are fits to Eq 2.1.	28
2.4	Plot of normalized film thickness h/h_0 versus log time for a series of samples with decreasing film thickness for (a) $M_w = 400$ kg/mol and (b) $M_w = 6,790$ kg/mol.	29
2.5	Thickness dependence of the physical aging rate measured at an aging temperature of 40 °C for two representative MWs.	30

2.6	Average physical aging rate β for 31 ± 1 nm thick PS films measure at 40 °C as a function of weight average molecular weight M_w	31
2.7	Fractional loss of aging F_β missing in 31 nm thin films relative to an equivalent material with bulk aging response, defined as $F_\beta = \frac{\beta_{\text{bulk}} - \beta(h,T)}{\beta_{\text{bulk}}}$ from the data shown in Fig. 2.6, as a function of weight average molecular weight M_w	33
2.8	(a) Temperature dependence of the film thickness $h(T)$ collected on cooling at 1 °C/min, where the data of the liquid-line has been superimposed at $T = 120$ °C. (b) Compilation of the average $T_g(h)$ values measured by ellipsometry from the literature and this work, referenced to their given studies' T_g^{bulk} value.	35
2.9	Temperature dependence of the thermal expansion coefficient $\alpha(T)$ of 31-nm thick films collected on cooling at three different cooling rates and cooling rate dependence of the glass transition temperature $T_g(h)$ for these 31 nm thick films.	37
2.10	Percent change in the effective average film density as a function of molecular weight for 31 nm thick PS films.	39
2.11	Plot of normalized film thickness h/h_0 vs. logarithmic aging time comparing the physical aging response of three different samples of $M_w = 400$ kg/mol with total thickness $h_{\text{total}} \approx 30\text{nm} = h_{\text{ads}} + h_{\text{float}}$	42
3.1	(a) Comparison of literature data for the residual adsorbed layer thickness $h_{\text{ads}}(t)$ remaining after solvent washing with toluene as a function of annealing time at 150 °C for PS films on piranha cleaned silicon wafers (b) Final residual thickness plateau h_∞ obtained at long annealing times on both piranha cleaned silicon (closed symbols) and HF treated silicon (open symbols) plotted as a function of radius of gyration, assuming $R_g \sim N^{1/2}$	52

3.2	Illustration of the basic experimental steps to be evaluated for forming adsorbed layers $h_{\text{ads}}(t)$ by solvent washing films that were annealed at an elevated temperature for some length of time t	55
3.3	(a) Cartoon of an adsorbed chain depicting trains, loops, and tails. (b) Schematic of a classic adsorption isotherm in solution, (c) Diagram illustrating the different interaction energies in the system	58
3.4	Reproducibility of the measured adsorbed layer thickness h_{ads} as a function of time the film was annealed at 150 °C under vacuum prior to solvent washing for 30 min in toluene.	71
3.5	Wider range of adsorbed layer thickness h_{ads} data (black open circles) plotted as a function of time the film was annealed at 150 °C under vacuum prior to solvent washing for 30 min in toluene, where no particular effort was done to make the samples in batches or minimized the time between steps in the experimental protocol outlined in Fig. 3.2	74
3.6	Decrease in film thickness h , normalized to the initial thickness h_0 , observed for bulk PS films ($M_w = 400$ kg/mol) as a function of aging time demonstrating the densification of the film that occurs following a solvent quench (purple diamonds.	77
3.7	Plots of the adsorbed layer thickness $h_{\text{ads}}(t)$ as a function of annealing time at 150 °C under vacuum for PS films (>200 nm thick, $M_w = 400$ kg/mol) on HCl acid cleaned silicon wafers (made as a single batch) where the films were subsequently solvent washed in 100 mL toluene for 30 min once (open circles), twice (half-filled circles), or three times (filled circles)	81

3.8	Comparison of the adsorbed layer thickness h_{ads} after one, two, or three 30 min washes in 100 mL of toluene, following 13 hours of annealing under vacuum at either 150 °C, 120 °C, or simply sitting at room temperature.	86
3.9	Comparison of PS films made with explicit adsorbed layers of thickness h_{ads} preformed on the surface followed by floating a layer of thickness h_{float} atop and annealing to create films of total thickness $h_{\text{total}} = h_{\text{ads}} + h_{\text{float}} \approx 31$ nm.	91
4.1	Plot of the adsorbed layer thickness versus the time samples spend in solution of various concentrations	109
4.2	Schematic of the adsorption and desorption process by increasing then decreasing the solution concentration.	112
4.3	Plot of the adsorbed layer thickness versus the time spent in pure solvent (toluene) after annealing films at 150 °C for 3, 6, and 23 hours.	115
4.4	Depiction of the regimes for creating adsorbed layers, where we show representative curves to guide the eye of adsorbed layer thickness versus time in solution for various cases of annealed films washed in solvent and adsorbed layers grown directly in solution.	118
4.5	Schematic of the film geometry used to measure the local fluorescence adjacent to the adsorbed layer.	119
4.6	Plot of the normalize fluorescence intensity at $\lambda = 379$ nm vs temperature for a local probe layer adjacent to adsorbed layers formed in either a 1 mg/mL solution (light green and dark green triangles) or by washing for 30 minutes of films annealed in the melt for 23 h at 150 °C (cyan and blue circles with a dot).	122

4.7	Plot of local local T_g for a dye-labeled layer adjacent to the adsorbed layer as a function of the time the dye-labeled layer was allowed to interpenetrate the adsorbed layer at 170 °C.	123
4.8	Plot of the normalize fluorescence intensity at $\lambda = 379$ nm vs temperature for a local probe layer adjacent to adsorbed layers made directly from a 1 mg/mL solution (green triangles) or from films annealed at 150°C for 23 h and washed for 30 minutes (blue circles with a dot), where both samples were interpenetrated for 24 h at 170 °C.	124
4.9	Plot of the normalize fluorescence intensity at $\lambda = 379$ nm vs temperature for a local probe layer adjacent to adsorbed layers formed by washing off melt annealed films for 30 min (circles with a dot) or 100+ h to the minimum adsorbed layer thickness h_{ads}^{min} $c \rightarrow 0$ mg/mL (dotted circles).	127

List of Tables

2.1	Polystyrenes used in the present study listing their weight average molecular weight M_w , polydispersity M_w/M_n , and supplier.	18
-----	---	----

Chapter 1

Introduction and Scope

1.1 Introduction to Polymer Glasses

Glasses are non-equilibrium materials that are highly prevalent in everyday life. The glass transition is characterized by large changes in dynamics (~ 10 - 14 orders of magnitude increase in viscosity) of a liquid during cooling over a small range in temperatures (~ 50 K) with minimal corresponding changes in structure.¹⁻³ Glasses do not form long range order but instead remain amorphous in their solid state, compared to crystals which exhibit long range order upon transitioning from a liquid to a solid. Glasses vary from small molecule glass formers such as SiO_2 (window glass) to polymeric glass formers (plastics) which are mass produced for industrial purposes every year. While the material properties of glasses have been well characterized, the fundamental understanding of how such large changes in dynamics on cooling can occur with minimal change in structure for glass forming materials remains largely an open question.

The glass transition is characterized by a departure of material properties (e.g. density) from their temperature dependent equilibrium values when cooling from high temperatures relatively quickly to avoid crystallization. Figure 1.1 shows the behav-

ior of a material's volume during cooling, which is shown to decrease on cooling in the equilibrium liquid. As the material passes through the glass transition temperature T_g the slope of the line, which corresponds to the thermal expansion of the material, changes indicating that the system has departed from the equilibrium liquid properties of the material. This transition is often reported as a single temperature corresponding to the midpoint of the transition on cooling. However several studies also make an effort to identify the onset of the transition on cooling called T_g^+ , as well as the temperature where the system is entirely glassy T_g^- .⁴ The state of the glass is frequently characterized by a quantity called the departure from equilibrium δ , where δ is typically defined volumetrically (or similarly calorimetrically) as the difference in the time dependent volume $V(t)$ from the equilibrium volume, normalized to the equilibrium volume: $\delta = (V(t) - V_\infty)/V_\infty$.⁵ The transition also is known to depend on the specific conditions under which the glass is formed, where cooling rate,⁶ and many other factors can increase or decrease T_g . This change in T_g means that at a given temperature, the departure from equilibrium for the glass will also depend on the conditions under which the glass was formed.

The molecular relaxation of glasses has been studied by various techniques down to only a few degrees, <10 K. Historically the relaxation mechanisms discovered have been labeled α , β , γ , and δ with decreasing temperature.⁷ Greiner and Schwarzl discussed changes in the slope of specific volume on cooling at a constant cooling rate in the context of these various relaxation mechanisms which they and others measured.^{7,8} They noted the coincidence of the α relaxation with the largest change in slope of specific volume, corresponding to T_g for the system. The slowing down of the primary α relaxation process on cooling has also been associated with the increased necessity of cooperative motion for the molecular structure to rearrange.⁹ This need for cooperation is believed to result from a packing frustration at the monomeric or segmental level in polymers.¹ Further cooling will result in additional

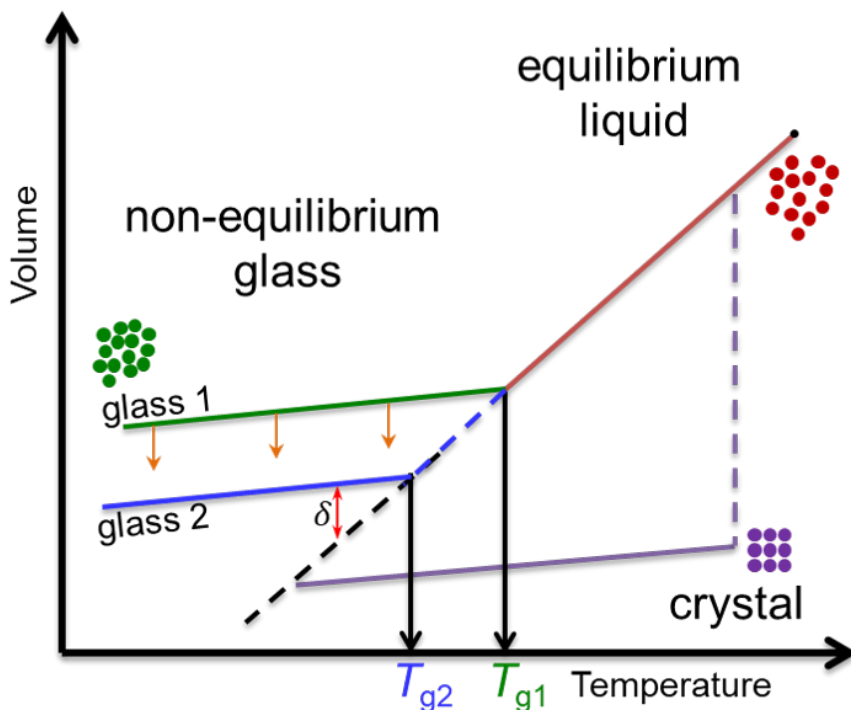


Figure 1.1: Cartoon depiction of how material properties undergo a continuous change as they pass through the glass transition. Plotting volume as a function of temperature the glass transition can be seen as the change in slope of the data. The black dashed line is a continuation of the equilibrium liquid line from high temperatures. The purple dashed line represents the phase transition to the crystal state. The cartoon insets are intended to illustrate how structure differs in various states. The departure from equilibrium is shown by the red double arrow and the physical aging behavior is given by the orange arrows indicating how one glass may evolve towards equilibrium.

molecular motions being locked out, with the δ relaxations often being attributed to the vibrational orientation of side groups at the monomeric level and γ relaxations having no clear molecular interpretation.

The locking out of the α relaxations near T_g for polymeric glasses associated with packing frustration on the segmental level also implies that there is an arrest of motions for a polymer chain at longer length scales than the segmental length scale at T_g . In general the glass transition is independent of chain connectivity effects with T_g for high molecular weight polymers being independent of chain length. Low molec-

ular weight polymers (oligomers) show a chain length dependence only up to some value.¹⁰ This dependence on the molecular weight has been interpreted as being due to polymer chains being too short for the chain conformations to exhibit Gaussian statistics.^{1,10,11} Above this molecular weight there is no dependence of molecular weight to T_g as one would expect due to the local nature of the glass transition.¹² Studies have examined T_g in bulk ranging from a few kg/mol up to several thousand kg/mol finding that above the molecular weight (MW) needed for the conformation of the polymer chain to exhibit Gaussian chain statistics ($M_n \gtrsim 20$ kg/mol for polystyrene) there is no dependence of the glass transition on MW.^{1,12} We can also then infer, that so long as we are above this MW there is no dependence of T_g on the total chain size and that glassy behavior and properties of polymeric glasses also should not depend on the molecular weight of the polymer being used.

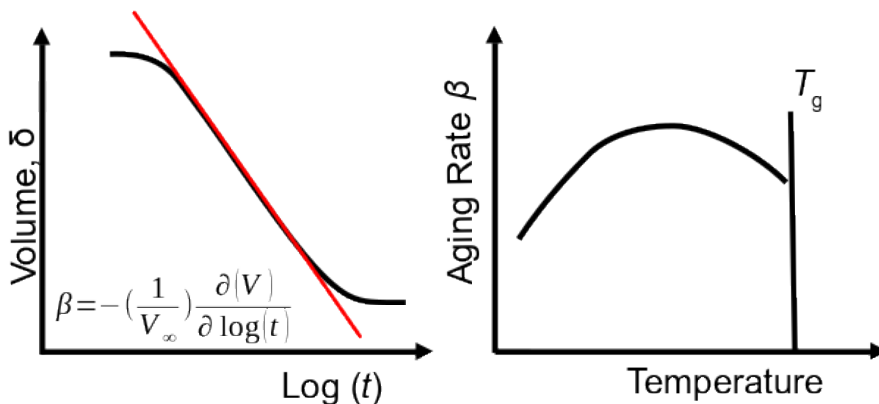


Figure 1.2: Depiction of the evolution of volume or departure from equilibrium (left) as a function of log time during physical aging. The linear regime is defined as the physical aging rate β for the system. Physical aging rate β versus the aging temperature (right), where the peak in physical aging rate is seen to occur at the temperature where the available thermal energy for relaxation begins to overcome the increasing enthalpic drive upon cooling to evolve to equilibrium.

The process of material properties such as density, modulus, enthalpy, or volume evolving towards their equilibrium values below T_g on logarithmic time scales is called physical aging. In Figure 1.1, the departure from equilibrium δ is shown by the red double arrow, where the associated physical aging behavior is shown by the orange

arrows depicting the evolution of the system at constant temperature back towards equilibrium. Figure 1.2 (left) shows a schematic depicting the physical aging behavior of materials, where the volume (or other material properties) evolve over time to the equilibrium value. The physical aging rate β is defined as the slope of this evolution in the linear portion on a log scale away from any curvature at short times or long times, $\beta = \frac{-d\delta(t)}{d\log(t)}$.⁵ This definition can be written in terms of any material property that is sufficiently carefully measured but has been commonly expressed in terms of the evolution of the volume as $\beta = (-1/V_\infty)(\frac{dV}{d\log(t)})$ as measured by dilatometry.⁵ The curvature at short and long times is understood to be due to the distribution of relaxation times necessary for aging to occur, where at short times aging will not occur until the shortest relaxation time for physical aging is reached and at long times aging will slow and stop once equilibrium for the system is reached.¹³ However, it is almost impossible to reach equilibrium through physical aging at temperatures more than a few K below T_g .

Physical aging is facilitated by an enthalpic drive in the material due to the departure from equilibrium on cooling, because the system wants to be in equilibrium in order to minimize its free energy. As you cool further below T_g the departure from equilibrium δ increases as measured by the difference in the volume at a given temperature compared to the extrapolated equilibrium volume from a continuation of the equilibrium liquid line, causing the associated enthalpic drive for physical aging to also increase. However, as you cool further below T_g the thermal energy available to facilitate physical aging also decreases, relaxations become harder to achieve and the lack of thermal energy eventually overcomes the increase in the enthalpic drive to return to equilibrium. Figure 1.2 (right) shows the physical aging rate β as a function of the aging temperature, where initially when cooling below T_g the aging rate increases due to the increase in the departure from equilibrium and resulting enthalpic drive. The competition between increasing enthalpic drive and the decreasing availability

of thermal energy to facilitate relaxation creates a curve in aging rate where upon cooling the physical aging rate then reaches a peak physical aging rate and begins to decrease. It is worth noting that the exact molecular mechanism for physical aging is unknown, but the peak in aging rate is often close to the β transition.⁷

Measuring the aging rate for polymer films in our lab is done by measuring linear changes in the film thickness as a function of log time with spectroscopic ellipsometry, where Baker et al.¹⁴ previously showed that this measure of physical aging was equivalent to measuring volume directly. This analogous measurement of physical aging is derived from Struik's original definition for volume, but with the added constraint that because the film is attached to a silicon substrate the area will not contract and the densification will occur only from the decrease in the perpendicular direction to the substrate (film thickness) as: $\beta = -\frac{1}{h_0} \frac{dh}{d\log(t)}$, where h_0 is the film thickness at an initial time of 10 min. Although the original work by Struik used the equilibrium volume at infinite aging times V_∞ to normalize physical aging data, Baker et al. showed that the measured aging rate using this h_0 to be equivalent to that normalizing the film thickness at the extrapolated equilibrium h_∞ .¹⁴ Spectroscopic ellipsometry is used to measure the relative change in the state of polarization Ψ and Δ after elliptically polarized light reflects from the sample. These changes in polarization are then modeled using a Cauchy layer model ($n(\lambda) = A + B/\lambda^2 + C/\lambda^4$) on top of a SiOx-Si substrate, where film thickness and index of refraction of the Cauchy layer are fit. This ellipsometry method used to measure aging is based on the Struik definition of physical aging, where for measurements on the ellipsometer the evolution of the film thickness is understood as being the only element of a volumetric evolution of the system as a supported polystyrene (PS) film is effectively constrained by the substrate from contracting. I developed a method that further streamlined the process by using the temperature stage to control the quench rate for the film during aging. This allows us to measure aging times significantly shorter than previously

measured in our lab. Samples are heated above T_g for long enough to erase thermal history, then quenched using liquid nitrogen at a rate of 55 K/min to the desired aging temperature.

Simon et al. examined the aging behavior near T_g in PS and saw that as they aged isothermally further below T_g it took longer to reach equilibrium, with equilibrium being hard to reach on experimental timescales as little as 10 °C below T_g .^{15,16} Other measures of physical aging have been done by measuring the excess enthalpy on heating in either a differential scanning calorimeter, or using an ellipsometer to measure the excess thermal expansivity. When done on heating with these techniques the fictive temperature T_f is defined as the temperature at which the volume crosses the equilibrium line on heating, where if the sample has not aged at all this will be the same value as T_g . Furthermore if the sample has aged significantly below T_g the behavior on heating will show a large overshoot in the enthalpy or thermal expansivity above T_f , which can be used as a measure of how much the sample has aged. Fully characterizing aging curves more than a few degrees below T_g is impossible because most glasses will never age to equilibrium. Recent work by McKenna and coworkers observed that for amber that had been aged for 20 million years there was a T_f 40 °C below T_g , but the amber was still not in equilibrium. For this reason when measuring physical aging using ellipsometry well below T_g we will only observe the initial portion of the aging curve presented in Figure 1.2 out to long enough times that we have reached the linear portion of the aging behavior to characterize our physical aging rate.

1.2 Confinement Effects in Thin Polymer Films

Previously work by Keddie et al.¹⁷ showed that for ultra-thin supported films of PS, there is a thickness dependent decrease in the average glass transition temperature

$T_g(h)$ as measured by ellipsometry. Ellison et al. also looked at the local T_g near the interfaces using a fluorescence technique, noting large T_g reductions at the free surface with bulk T_g being recovered only about $\sim 30 - 40$ nm into the film.¹⁸ This work showed that interfaces, such as the polymer-air ‘free-surface’, can affect dynamics tens of nanometers into a polymer glass and also that for PS on SiOx there is no local change to T_g at the polymer substrate interface. These observations strongly support the interpretation prevalent in the field that the free surface imparts some enhanced mobility to the film greatly reducing T_g in thin films. Furthermore, these long length scales for perturbations to bulk T_g are somewhat surprising when compared to other length scales that one typically associates with glassy dynamics, such as the length scale of an alpha relaxation which is the fundamental length scale for the glass transition. Work by Ellison et al. in 2005 showed that this $T_g(h)$ decrease in thin films was independent of the polymer molecular weight (up to 3×10^6 g/mol) confirming that glassy dynamics, even near interfaces, do not depend on the size of the polymer chain.¹⁹ Other efforts have been made to measure properties like the modulus of the polymer film on confinement with mixed results showing there may be an increase,²⁰ decrease,²¹⁻²³ or no change²⁴ to the polymer modulus in thin films.

Despite decades of study, the glass transition in bulk materials is still not well understood with many open questions remaining. We suspect for instance that a growing length scale for cooperative motion as you approach T_g exists and is an underlying principle of several theoretical treatments. Early confinement studies were motivated by the idea of perturbing this cooperative length scale for glass formation by making films or confining glass formers into areas that are comparable to the size scale for cooperative motion. However, interface effects become important in thin films that are much thicker than the thicknesses necessary for perturbing the length scale of cooperative rearrangements. These interface effects have led to a wealth of knowledge and understanding about glasses in their own right as well.

Enhanced mobility at the polymer-air free surface for instance helps us to understand the modifying effect that the extra mobility due to a lack of packing frustration has on the glass transition locally. While it is not a direct perturbation of the length scale for cooperative motion, examining these interfaces clearly holds some importance for better formulating and understanding ideas of bulk glasses that have been theorized but are hard to test.

Recently our lab has worked on exploring the changes to properties of glassy films under confinement and in the presence of interfaces. We have worked specifically on exploring the effects that interfaces have on both the average and local glass transition in polymer films. Several studies have built on the fluorescence method developed by Torkelson et al.²⁵ to measure the local glass transition in the presence of a particular interface, with Baglay et al.^{26,27} looking at polymer-polymer interfaces and Huang et al.²⁸ exploring the effects that end grafted chains have on the local T_g of the polymer films. Both studies saw large gradients in the local T_g in their systems over hundreds or tens of nanometers contrary to what would be expected based on long standing ideas in the literature. We also use spectroscopic ellipsometry to measure the physical aging behavior of thin films under different conditions. Pye et al.²⁹ noted that β was reduced at all temperatures for thin PS films and interpreted this as a layer or gradient of enhanced mobility at the polymer air interface contributing less or no physical aging to the thin films. Work by Rauscher et al.³⁰ studied the effect that a rubbery polymer layer of poly(n-butyl methacrylate) (PnBMA) would have on the physical aging rate and glass transition temperature of thin PS films, finding that the decrease in T_g observed for PS atop a rubbery PnBMA layer did not correspond to a similar decrease in the physical aging rate of the thin PS films. In this thesis I will be building on these works and techniques to address some new questions in the literature which have become topics of debate about polymer interfaces and glassy dynamics.

Interfacial interactions have been understood as enthalpic and local in nature, with the literature showing that for the glass transition there is largely no molecular weight effect to the T_g reduction reported. This viewpoint has been supported and confirmed by many studies which have primarily focused on the reduction in T_g in thin polymer films. However, recent works have shown molecular weight and chain connectivity may play a modifying role in the glassy dynamics at interface.³¹⁻³⁸ indicating chain architecture, and chain adsorption all could affect the glassy dynamics at the interface. We will aim to directly explore the effects that chain connectivity have on physical aging in thin polymer films by varying the molecular weight of polymer films and by exploring the effects that polymer adsorption have on the glassy dynamics at interfaces.

Some recent works in the field of confinement have claimed that polymer chains in the melt state can “irreversibly adsorb” to the substrate supposedly creating large changes in the dynamics of thin polymer films.³⁹⁻⁴⁴ Reports have claimed that these adsorbed layers are formed by annealing far above T_g for extended periods of time and then placing the films in a solution of good solvent for some amount of time to supposedly remove the unadsorbed chains. These measurements are often correlated with measurements done to measure properties of the glass such as T_g or dielectric relaxation in films similarly annealed for long times, but on separate samples which have not been washed in solvent to directly measure their adsorbed layers. These reports appear to be in conflict with the 25 years of reports about changes to dynamics in thin confined polymer films presented above where enhanced mobility from the free surface along with a largely neutral interaction between PS and the SiOx substrate create a decrease in the $T_g(h)$ behavior in thin films. We will therefore explore the effects of these adsorbed layers have on the average and local T_g of the polymer material as well as the physical aging rate in thin polymer films.

1.3 Outline

Chapter 2 will discuss direct evidence that chain connectivity alters glassy dynamics in confined polymer systems. Recently there were several groups who published works suggesting that entropy and chain connectivity may alter glassy dynamics in confined polymeric systems. We used physical aging measurements in thin PS films at high and ultra-high molecular weights as a means of testing if chain connectivity and molecular weight in these systems could alter the physical aging behavior in films of weight average molecular weight $M_w = 97$ to 10,100 kg/mol. We found that at ultra-high molecular weights, well above those previously studied, the physical aging behavior in thin ≈ 31 nm thick PS films is faster by as much as ~ 45 % at an aging temperature of 40 °C. However there was no corresponding dependence of M_w on the $T_g(h)$ seen in the these thin films. We also briefly examined if an exposed and capped adsorbed layer at the polymer-substrate interface could be altering the average chain dynamics with no such alteration observed. A version of this chapter was published as Michael F. Thees, and Connie B. Roth, Journal of Polymer Science, Part B: Polymer Physics 2019, 57, 1224–1238.

Chapter 3 will review the literature understanding of polymer adsorption in the cases where the adsorbed layer was both formed in solution and formed in the melt state. We will then discuss the reproducibility of the procedure used in the literature for isolating adsorbed layers supposedly formed in the melt state and discuss the contributions of each step in the procedure for measuring the adsorbed layers. Recent works have claimed that dynamics in confined polymeric glasses are dominated by the presence of adsorbed layers formed during annealing of melt film (above T_g). We will critically examine the underlying assumptions surrounding the experimental procedures used by these groups as presented in the literature and the resulting reproducibility of these procedures. We will present a series of measurements that characterizes the precision with which ultra thin polymeric films may be measured

via ellipsometry and discuss the various sources of error and uncertainty inherent in doing these adsorption experiments. We will then provide our best and most reproducible procedure for examining adsorbed layers and present the controlling factors in their formation. We also raise questions and concerns about the role of solvent washing in the procedure, a step that is often overlooked due to now longstanding assumptions about the irreversible nature of the adsorbed layer. These results are interpreted using the understanding that was historically developed for adsorbed layers grown in solution showing that in fact, many of the underlying assumptions made by people studying adsorbed layers supposedly grown in the melt are misguided. A version of this chapter was published as Michael F. Thees, Jennifer A. McGuire, and Connie B. Roth, *Soft Matter* 2020, DOI: 10.1039/D0SM00565G.

Chapter 4 will demonstrate the importance of solvent washing on the formation of adsorbed layers from the melt and the effect that adsorbed layers formed in both solution and by solvent washing of films annealed in the melt have on the local T_g of PS films. Following our work on determining the reproducibility of forming adsorbed layers in the melt and exposing them using solvent washing, we begin by showing that solvent washing is the critical step in formation of these adsorbed layers. We find that the adsorbed amount is determined primarily by the solution concentration when washing off of melt films. Furthermore, we show that these findings are in remarkable agreement with adsorbed layers grown directly in solutions of similar concentrations. We then conclude by addressing whether or not the adsorbed layers grown by solvent washing of melt films for various amounts of time and the adsorbed layers grown directly in solution have any effect on the local T_g using the local fluorescence label technique previously used by our lab.

Chapter 2

Unexpected Molecular Weight Dependence to the Physical Aging of Thin Polystyrene Films Present at Ultra High Molecular Weights

A version of this chapter was published as Michael F. Thees, and Connie B. Roth, *Journal of Polymer Science, Part B: Polymer Physics* 2019, 57, 1224–1238.

2.1 Introduction

For more than two decades the field has been struggling to understand the causes behind so-called ‘confinement’ effects in thin polymer films and other confined geometries, where large property changes occur in the material with decreasing system size, at size scales of tens to hundreds of nanometers.^{17,45–54} Understanding of this behavior would contribute to our knowledge of the glass transition and associated length scales^{55–64} and to surface effects and boundary phenomenon,^{65–73} but also has

important implications for understanding thin film applications,^{74,75} matrix reinforcement in nanocomposites,⁷⁶⁻⁸¹ rubber toughening,⁸² and nanostructured blend materials.^{26,83-88} At present, the property changes associated with confinement effects are primarily understood as being enthalpic in origin with ample evidence showing that interfacial interactions alter the local dynamics at the boundary,⁶⁵⁻⁷⁰ which sets up a local gradient in dynamics near the interface that propagates into the material over some depth before bulk-like dynamics are recovered.^{26,55,58,59,66,67} The depth or length scale of the gradient appears to depend on temperature, as well as the type of dynamics being investigated.^{55,57,58,89,90} Although the nature of the interfacial interactions are not fully understood, good correlations have been observed with interfacial energy of the substrate^{69,91,92} and specific hydrogen bonding interactions.^{65,68,93-95} Overall, the behavior, especially in supported films, has appeared to be predominantly independent of molecular weight^{17,19,96,97} (MW) suggesting a primarily enthalpic effect.

However, several recent studies have reported differences in confinement behavior associated with chain length,^{36,98-103} stiffness,^{104,105} entanglements,^{89,106-109} and chain architecture¹¹⁰⁻¹²² that are unexpected given the primarily enthalpic understanding developed over the years. This suggests that entropic effects may also play a modifying role in understanding confinement effects. For example, changes in dynamics due to tethering^{94,123-135} and adsorption^{39,41-43,136-144} of chains to substrates have been reported, as well as variations for different chain architectures such as stars^{110-114,116,117,119-121} and cyclic chains^{115,118,122} that otherwise have identical chemical composition, suggesting that the presence of a boundary or interface alters the available entropic conformations and influences the local dynamics, altering the nature of the dynamical gradient. Recent studies have also reported unexpected MW dependences^{36,99-102} and chain stiffness^{104,105} effects to the glass transition temperature (T_g) and surface dynamics^{89,98,106-108,145} that contradict the general understanding that had historically been formed. All these observations indicate that we need

to revisit our understanding of what factors control local dynamics near interfaces and consider how entropy and chain connectivity alter the gradient in dynamics near interfaces that result in large material property changes with decreasing system size (confinement).

Some of the largest and most confounding effects associated with confinement have been related with the glass transition and glassy dynamics, both of which are still not fully understood in bulk systems. Glasses are nonequilibrium materials characterized by the dramatic slowing down in dynamics, more than 12 decades in time over a modest temperature range of ~ 50 K,^{2,3} prior to the system vitrifying and effectively freezing into place. In polymers, these dynamics are associated with cooperative motions of segmental units¹⁴⁶ that become more tightly packed as the density is increased upon decreasing temperature. The many-body nature of the collective particle dynamics makes it complicated to understand, but there is believed to be a growing length scale with decreasing temperature that characterizes the number of units moving cooperatively together.^{147,148} Some studies suggest that the length scale of the dynamical gradient near the interface is related to cooperative length scales in glasses, primarily when considering gradients in local T_g values, cooperative α -relaxation times, and other glassy dynamics such as physical aging.^{55–64,66,149–153}

Physical aging represents the slow structural evolution of the nonequilibrium glassy material towards equilibrium and is characterized by a logarithmic time dependence of state-like variables such as density, volume, enthalpy, or other property changes.^{5,7,154,155} The speed of these glassy dynamics are often characterized by the physical aging rate $\beta = -\frac{d\delta}{d\log t}$, originally defined by Struik,⁵ where δ represents the departure from equilibrium (e.g., $\delta = \frac{V(t)-V_\infty}{V_\infty}$ for volume V). In 2010, Pye et al.⁵⁷ measured the temperature dependence of the physical aging rate $\beta(T)$ of thin polystyrene (PS) films supported on silicon using ellipsometry where, at a given temperature, β was determined from the time dependent decrease in film thickness $h(t)$

as $\beta = -\frac{d(h/h_0)}{d \log t}$, previously shown to provide an equivalent aging rate for bulk films compared with traditional volumetric measurements.¹⁴ By comparing the measured $\beta(T)$ for 30 nm thick films with those for bulk films, Pye et al.⁵⁷ found that the $\beta(T)$ values were reduced relative to bulk for all temperatures, not consistent with the average $T_g(h)$ decrease of these films, but consistent with a gradient in local $T_g(z)$ with depth z that had been previously measured⁶⁶ in these films. Analysis of the $\beta(T)$ data using both a gradient and simplified two-layer model, allowed Pye et al. to extract a characteristic length scale describing the depth to which local aging dynamics were perturbed from bulk, a measure of the size of the gradient in dynamics near the free surface.⁵⁷ The temperature dependence of this length scale was found to grow with decreasing temperature from a few nanometers near bulk T_g (T_g^{bulk}) to several tens of nanometers deep in the glassy state ($T_g^{\text{bulk}} - 60$ K), indicating that glassy dynamics are perturbed to greater depths further from T_g^{bulk} .

In the present work, we revisit these thin film physical aging measurements by Pye et al.⁵⁷ that had only been done with a single MW of PS ($M_w = 245$ kg/mol, $M_w/M_n = 2.0$), and demonstrate an unexpected MW-dependence to the physical aging response present only in thin films of very high MW polymer. Physical aging in bulk polymers is traditionally associated with local segmental motions as larger cooperative motions and certainly chain dynamics are frozen out below T_g . As such, physical aging in bulk is independent of chain length for MWs where $T_g(M_n)$ has saturated to its long chain-length limit.¹⁵⁶ This $T_g(M_n)$ saturation effect is attributed to when the chain is long enough to exhibit Gaussian chain statistics,^{157,158} and occurs at rather modest MWs ($M_n \gtrsim 20$ kg/mol for PS^{10,11,159,160}). As expected we confirm that bulk films show no MW-dependence to the physical aging behavior. However, to our surprise we have found an unexpected MW dependence to the physical aging rate $\beta(T)$ for thin, PS films that is not present in bulk films. Thin films with thicknesses $h < 80$ nm of exceedingly (ultra) high MWs $\geq 6,500$ kg/mol PS are observed to

exhibit an $\sim 45\%$ faster physical aging response than equivalent films of MWs $\leq 3,500$ kg/mol. Consistent with the Pye et al.⁵⁷ work, PS films with MWs $\leq 3,500$ kg/mol show a reduced physical aging rate relative to bulk indicative of the gradient in dynamics present in these films caused by the reduced T_g near the free surface. The faster physical aging we observe for the ultra-high MWs $\geq 6,500$ kg/mol thin films, which exhibit a more bulk-like aging response, suggests that the depth over which the gradient in dynamics propagates from the free surface is diminished relative to that in thin films of MWs $\leq 3,500$ kg/mol. These results strongly imply that chain connectivity plays some modifying role in controlling dynamical gradients in polymer glasses near interfaces. We demonstrate that this MW-dependent change in the physical aging response of thin films is not associated with a measurable change in the film-average $T_g(h)$ dependence or effective average film density (molecular packing).

2.2 Experimental Methods

Five different MWs of polystyrene were purchased as listed in Table 2.1, where all MWs were determined by the manufacturer using gel permeation chromatography (GPC). PS was dissolved in toluene (Aldrich) at different concentrations (0.4–8 wt %) and spin-coated onto (1,0,0) silicon substrates (2×2 cm in size) with native oxide layer (WaferNet), where films were made to desired thickness by varying both concentration and the spin speed. Prior to spin-coating, silicon wafers were washed with toluene. All films were then annealed under vacuum at 120°C ($T_g + 20^\circ\text{C}$) over night to remove residual solvent and produce films with a consistent thermal history. To examine whether sample preparation could be a contributing factor to the unexpected MW dependence of the physical aging rate, annealing time (2-72 h at 120°C) and spin-speed (750-3000 rpm) were varied, but no difference in physical

M_w (g/mol)	M_w/M_n	Supplier
97,400	1.01	Scientific Polymer Products
400,000	1.06	Pressure Chemical
1,444,000	1.04	Polymer Laboratories
3,239,000	1.05	Polymer Laboratories
6,793,000	1.09	Polymer Laboratories
10,100,000	1.09	Polymer Laboratories

Table 2.1: Polystyrenes used in the present study listing their weight average molecular weight M_w , polydispersity M_w/M_n , and supplier.

aging behavior was observed within experimental error. The reasoning behind these controls will be discussed in detail below.

Physical aging measurements were initiated by annealing films on the ellipsometer heat stage (Instec HSC 302) at 120 °C for 25 min in order to reset the thermal history. Films were then quenched from above T_g to the desired aging temperature of 40 °C at a constant rate of 55 °C/min using the liquid nitrogen cooling capability of the HSC 302 heater. Zero aging time is defined by when the heater temperature stabilizes at the desired aging temperature, where this was identified by following the quenching protocol using a 1000-nm SiOx–Si control, and is verified for each sample run. During aging, spectroscopic ellipsometry (J. A. Woollam M-2000) was used to measure film thickness every 2 min, averaging over a 45 s period, as previously described in Baker et al.¹⁴ Plots of normalized film thickness h/h_0 vs. log aging time were normalized with thickness h_0 corresponding to an aging time of 10 min, where h_0 is the average of thickness data over a 10 min period on either side of this value. In addition, the data were subsequently smoothed by doing a five-point adjacent average.

The glass transition temperature $T_g(h)$ values were also measured by ellipsometry on cooling, typically at 1 °C/min unless otherwise specified, while dry nitrogen gas was flowed (1.5 L/min) over the sample to prevent condensation. Following common convention in the literature, T_g was identified from the intersection of two linear fits above and below the transition. All ellipsometry $\Psi(\lambda)$ and $\Delta(\lambda)$ data were fit for

$\lambda = 400 - 1000$ nm to a layer model comprised of a Cauchy layer, $n(\lambda) = A + \frac{B}{\lambda^2} + \frac{C}{\lambda^4}$, for the PS layer, where A, B, and C were fit along with the PS film thickness h , atop a 2 nm thick native oxide layer as part of the silicon substrate. For the T_g runs on 20 nm thick films, the Cauchy C parameter was held constant at $0.00038 \mu\text{m}^4$ following our recent work by Huang and Roth.¹⁶⁰ In addition, for the thinnest films of ~ 10 nm, we found it necessary to hold the Cauchy B parameter constant at $0.00745 \mu\text{m}^2$, a value also determined from the average of bulk films. Holding these parameters constant for the thinnest films is reasonable because most of the change in polarization that the ellipsometer measures occurs upon reflection at the interfaces, and not via the wavelength-dependent dispersion of the material as the path length of the light through the film decreases. (Note we are following the common convention used within ellipsometry texts and the Woollam software where the values of A, B, and C for the Cauchy equation are quoted for the wavelength λ calculated in microns.)

2.3 Results and Discussion

2.3.1 Qualitative observations of differences in physical aging for thin films of ultra-high molecular weight polystyrene

Figure 2.1a plots the normalized film thickness h/h_0 versus log aging time for PS films on silicon substrates held at an aging temperature of 40°C , following a temperature quench at $55^\circ\text{C}/\text{min}$ from well above T_g . Data are shown for bulk (500-1200 nm) and thin films (31 ± 1 nm) for three different molecular weights $M_w = 97$ kg/mol, 400 kg/mol, and 3,240 kg/mol. No difference is observed in the aging behavior for this range of MWs, as one would expect. Previously, Pye et al.⁵⁷ characterized the temperature dependence of the physical aging rate $\beta(h, T)$ for thin supported PS films, where the aging rate of $h \approx 30$ nm thin films was observed to be reduced relative to bulk at all temperatures. This observation was understood as resulting

from the gradient in dynamics near the free surface previously demonstrated to be present in these films,⁶⁶ where the local aging rate $\beta(z)$ as a function of depth z could be considered to be correlated with the locally reduced $T_g(z)$.^{57,112} From the difference in the temperature-dependent aging rate $\beta(h, T)$ between the thin and thick (bulk) films, Pye et al.⁵⁷ chose to extract temperature-dependent length scales characterizing the breadth of the gradient in dynamics near the free surface. These measurements were done with a single, broad MW of $M_w = 245$ kg/mol, $M_w/M_n = 2.0$.⁵⁷ Figure 2.1a shows that the same results are obtained for a series of narrow, monodisperse MWs.

However, surprisingly, upon examination of higher MW films, we observe an anomalous behavior in the physical aging rate of the thin films. Figure 2.1b shows a second plot of h/h_0 vs. $\log(t)$, but this time for ultra-high MWs of $M_w = 6,790$ kg/mol and 10,100k g/mol, where we are again comparing data for bulk (500-1200 nm) and thin (31 ± 1 nm) films. Both of these two ultra-high MWs show the same aging behavior, but are distinctly different for thin films than the lower MWs $\leq 3,500$ kg/mol shown in Fig. 1a. Black lines have been added to Fig. 2.1b to represent the data from Fig. 2.1a: the two dashed lines represent the range of aging rates (standard deviation) measured for all the thin films with MWs $\leq 3,500$ kg/mol; the dotted curve representing the bulk data was created by combining and smoothing the bulk datasets shown in Fig. 2.1a. The bulk films show no MW dependence, even for these ultra-high MWs, as one would anticipate. However, unexpectedly, the aging rates for the thin (31 ± 1 nm) films of ultra-high MW $\geq 6,500$ kg/mol show a noticeably larger aging rate (higher slope) than the dashed lines representing the (merely) high MWs $\leq 3,500$ kg/mol. This difference in the 31-nm-film aging behavior between the high and ultra-high MW thin films are clearly outside of experimental error: $\beta = 3.4 \pm 0.6 \times 10^{-4}$ for MWs $\leq 3,500$ kg/mol shown in Fig. 2.1a vs. $\beta = 4.9 \pm 0.7 \times 10^{-4}$ MWs $\geq 6,500$ kg/mol in Fig. 2.1b.

We observe a noticeable and reproducible molecular weight dependence to the

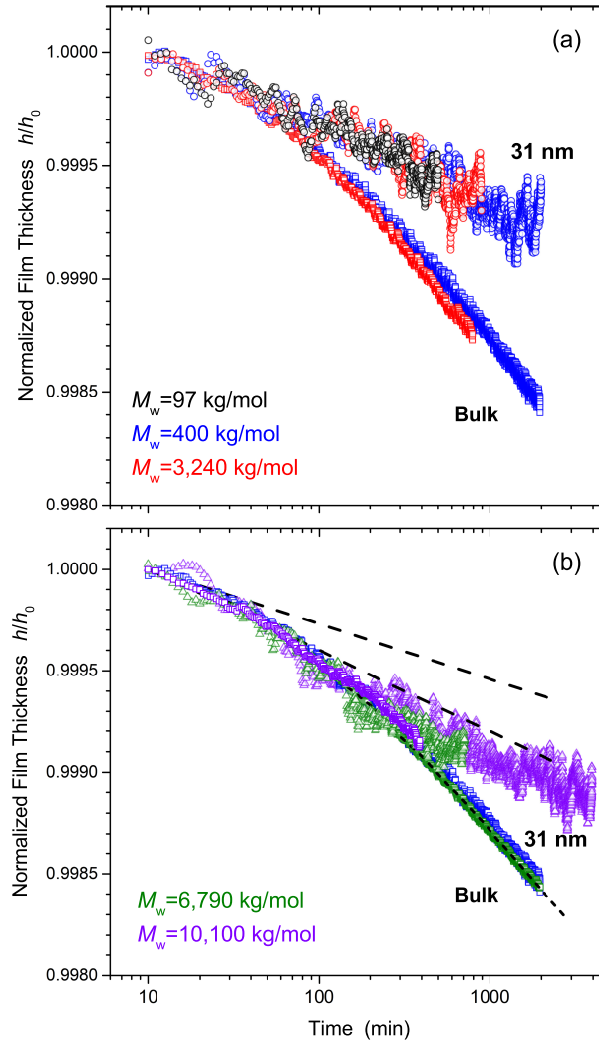


Figure 2.1: Plot of the normalized film thickness h/h_0 versus log aging time at 40 °C comparing the physical aging response of 31 ± 1 nm thick PS films with those of bulk (>500 nm thick) films. (a) Plots weight average molecular weights $M_w = 97$ kg/mol (black), $M_w = 400$ kg/mol (blue), and $M_w = 3,240$ kg/mol (red), while (b) plots $M_w = 6,790$ kg/mol (green) and $M_w = 10,100$ kg/mol (purple). The dashed lines in (b) identify the range of data for the 31 nm thick films (circles) with MWs $\leq 3,500$ kg/mol in (a), and the dotted line in (b) represents the bulk data (squares) from (a).

physical aging of polystyrene only present in thin films. This MW-dependent change in aging behavior is only occurring at extremely high MWs, somewhere between $M_w = 3,500$ kg/mol and $6,500$ kg/mol. In terms of chain size, the two bounds for where this MW-dependent change occurs both have radius of gyration R_g values much larger than the 31-nm film thickness: $R_g = 54$ nm for $M_w = 3,500$ kg/mol and $R_g = 74$

nm for $M_w = 6,500$ kg/mol.¹⁶¹ For both these high and ultra-high MWs, twice R_g is significantly larger than the film thickness ($2R_g \gg h$), implying that chains of these MWs must both be distorted in order to fit inside a 31-nm thick film. Yet, the range of MWs shown in Fig. 2.1a, which all exhibit the same physical aging response, encompasses both high ($M_w = 3,240$ kg/mol, $R_g = 52$ nm) and much lower ($M_w = 97.4$ kg/mol, $R_g = 8.7$ nm) MW chains, where the shortest chains likely experience no deformation to fit inside a 31-nm thick film. This reasoning suggests that the anomalous MW-dependent physical aging behavior observed for the ultra-high MW thin films is not simply due to changes in chain conformation associated with the finite size of the film, providing no immediate insight into the cause of this anomalous aging behavior. In Section 2.3.3, we will discuss, and in some cases negate, other possible causes.

How should we be interpreting this difference in physical aging response between the high and ultra-high MWs? We believe this MW dependence of the physical aging rate in thin films informs us about the breadth of the gradient in dynamics near the free surface. This follows from the analysis put forward by Pye et al.⁵⁷ to interpret the difference in the temperature dependence of the aging rate $\beta(h, T)$ between thin ($h \approx 30$ nm) and thick (bulk) films. Their analysis was based on the gradient in local T_g near the free surface of PS that was quantitatively established by Ellison and Torkelson demonstrating a depth of approximately 30-40 nm is required in thick films before bulk T_g is recovered,⁶⁶ in addition to several studies who have argued that the free surface itself may always be liquid-like.^{46,162} Given the significantly reduced local T_g near the free surface and its possible liquid-like nature, Pye et al.⁵⁷ reasoned that the physical aging rate must go to zero at the free surface, while a bulk physical aging rate $\beta_{\text{bulk}}(T)$ would likely be recovered at some depth deeper into the film. Experimentally only a single quantity is measured, $\beta(h, T)$ representing the film-average of the local aging rates $\beta(z)$ at that aging temperature; thus, the

explicit functional form for the depth-dependent local aging rate $\beta(z)$ is not known. For this reason, Pye et al.⁵⁷ interpreted their results using both a simple two-layer model and a more realistic gradient model, both of which assumed some correlation between the local $\beta(z)$ and the depth-dependent local glass transition temperature $T_g(z)$.^{57,112} Such assumptions are consistent with local fluorescence measurements of physical aging in poly(methyl methacrylate) (PMMA) films.⁶⁷ By quantitatively comparing the average aging rate of the thin films $\beta(h \approx 30 \text{ nm}, T)$ with what would be expected for thick (bulk) films $\beta_{\text{bulk}}(T)$ at each aging temperature, length scales characterizing the breadth of the gradient in dynamics near the free surface were extracted. Both analyses were quantitatively equivalent within experimental error and gave good agreement with the $\beta(h, T)$ data. These length scales were found to increase with decreasing temperature suggesting that deviations from bulk glassy dynamics propagate deeper into the film at lower temperatures further from bulk T_g .^{57,146} Based on this reasoning, we believe it is reasonable to interpret differences in the physical aging rate between thin (31 nm) and thick (bulk) films as indicative of the breadth of the gradient in local dynamics near free surfaces. Thus, the larger aging rate of the ultra-high MWs $\geq 6,500 \text{ kg/mol}$ thin films in Fig. 2.1b, which are closer to that of bulk aging, relative to the high MWs $\leq 3,500 \text{ kg/mol}$ thin films in Fig. 2.1a, suggests the depth over which the gradient in dynamics propagates near the free surface is diminished in the ultra-high MW films.

One additional qualitative observation we want to highlight before moving on to quantitative evaluation of the physical aging rates is the stark qualitative difference in the thin film physical aging behavior compared to that of bulk. Figure 2.2 plots h/h_0 vs. $\log(t)$ for the full range of MWs measured at 40 °C and includes a linear yellow-dashed line to separate the high MWs $\leq 3,500 \text{ kg/mol}$ from the ultra-high MWs $\geq 6,500 \text{ kg/mol}$ thin films. This yellow line also helps to highlight that all of the thin film data show a linear response in physical aging on this logarithmic time scale.

In contrast, the black-dotted curve, representing all the bulk data (same as shown in Fig.2.1b), exhibits the distinctive initial curvature typical of most bulk physical aging response at low aging temperatures far below T_g . This initial curvature in aging behavior at low temperatures is associated with the longest relaxation times of the glassy state becoming larger than the starting time of the aging measurement.^{7,163–165} Data for the thin films have been collected out to 4000 min (2.8 days) in aging time and still do not show any evidence of curvature. This suggests the thin film data do not exhibit any initial curvature because the all relaxation times are always shorter than the starting time of the aging measurement, presumably faster due to enhanced mobility near the free surface. The reduced aging rate in the thin films relative to bulk occurs because some near free-surface region that is effectively liquid-like at the aging temperature does not contribute to aging. We believe it is unlikely that the thin film data have an initial curvature (delay in aging) regime exceeding 4000 min, as this would imply that the longest relaxation times of the glassy state in the thin films exceeds those in the bulk by more than an order of magnitude. We also observe a progressive shortening of this initial curvature with decreasing film thickness below 80 nm (as shown in Fig. 2.4). Although the aging measurement is unable to differentiate between a lack of physical aging occurring because some fraction of the film is effectively liquid-like versus some immobile chains are present in the film, we simply believe the former is most likely given our data and existing literature studies.

2.3.2 Quantitative description of differences in physical aging for thin films of ultra-high molecular weight polystyrene

We proceed now with quantifying the physical aging rates for bulk and thin films to make quantitative comparisons between the high MWs $\leq 3,500$ kg/mol and ultra-high MWs $\geq 6,500$ kg/mol data. As just described at the end of Section I, measurements at low aging temperatures, where relaxation times are longer, typically exhibit an

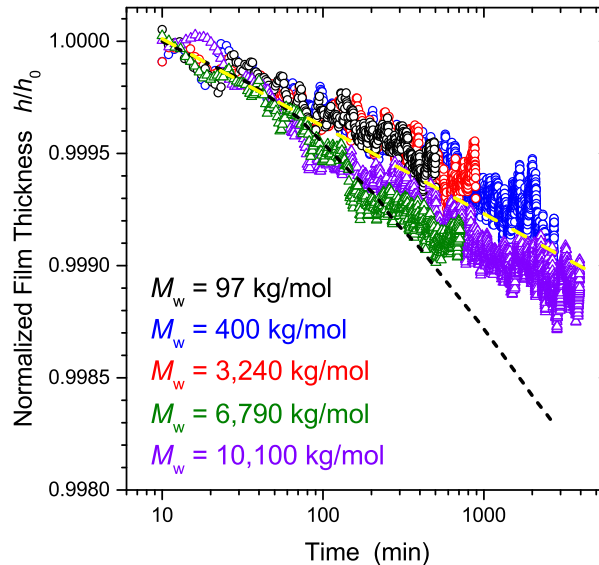


Figure 2.2: Comparison of 31 ± 1 nm thick PS films where the dashed yellow line delineates the slower aging response of MWs $\leq 3,500$ kg/mol (circles) from the faster aging observed for MWs $\geq 6,500$ kg/mol (triangles). All thin films exhibit a linear decrease in film thickness h/h_0 on this logarithmic scale, in contrast to the curvature exhibited by bulk films (dotted curve) at this low aging temperature of 40°C , suggesting that the distribution of relaxation times in thin films are shifted to shorter timescales.

initial curvature to the aging response associated with the onset of the distribution of relaxation times that contribute to physical aging in the glass. The linear decrease of h/h_0 in $\log(t)$ observed at long aging times that is characteristically used to quantify the aging rate β , as originally defined by Struik,⁵ begins once all the relaxation times are active. In contrast, for exceedingly short measurement times (less than those measured in the current study) before even the shortest relaxation times begin to age the sample, no physical aging will occur and the initial aging response would be flat. This initial flat regime has recently been robustly observed by Simon and coworkers¹⁶⁴⁻¹⁶⁶ using flash differential scanning calorimetry (Flash DSC) where they could begin aging measurements at aging times as short as 0.01 s.¹⁶⁴ In our present measurements, we do not directly observe this flat initial plateau seen in the Flash DSC work because the measurement time at which we begin collecting data (when the temperature stage has stabilized at the aging temperature) corresponds to when

the shortest, but not the longest, relaxation times have begun aging the sample. (Note, our new quench protocol performed directly on the ellipsometer allows us to begin measurements of the aging response earlier than our previous works,^{14,57,167} making the initial curvature more distinct.) This initial curvature has typically been quantified by what is called the induction time t_{ind} ,^{7,163,164,168} determined by the intersection of linear fits (on a log time scale) to the initial flat region and the long time aging behavior that is linear in $\log(t)$. Estimates of the induction time from our data appear to be consistent with literature values given differences in cooling rate and aging temperature.

Figure 2.3 shows the physical aging response of bulk films for several MWs where the normalized film thickness h/h_0 vs. \log aging time was measured at an aging temperature of 40 °C and 65 °C. As previously mentioned, we observe no MW dependence to the aging response for bulk films; those shown in Fig. 2.3 are representative of the aging behavior for all MWs. The initial curvature of the aging response is more prominent in the 40 °C data at low aging temperatures, as would be expected. To quantify the physical aging rate β for these data with the initial curvature associated with the delayed aging response, we introduce a functional form that allows us to fit the entire range of aging times to only three parameters. This empirical equation,

$$\frac{h(t)}{h_0} = 1 + A(1 - e^{-\frac{x}{\tau}}) - \beta x \quad \text{where, } x = \log\left(\frac{t}{10 \text{ min}}\right) \quad (\text{Eq:2.1})$$

was arrived at by treating the initial curvature as an exponential decay on a logarithmic time scale, recalling the thickness data $h(t)$ are normalized to h_0 , the thickness at an aging time of 10 min. The physical aging rate β comes from the long-time aging response that is linear in $\log(t)$, τ is a characteristic parameter that describes the range over which the initial curvatures dissipates, and A is the offset of the normalized film thickness h/h_0 representing where the slope of the long-

time aging response intercepts 10 min. Fitting Eq 2.1 to representative datasets determined from the compilation of multiple samples with different MWs, we obtain best fit parameters of $\beta_{\text{bulk}} = 10.8 \times 10^{-4}$, $A = 11.4 \times 10^{-4}$, $\tau = 1.3$ at 40 °C and $\beta_{\text{bulk}} = 10.4 \times 10^{-4}$, $A = 2.9 \times 10^{-4}$, $\tau = 0.4$ at 65 °C, shown as dashed curves in Fig. 2.3. Note these values of aging rate β could also be obtained by simply fitting the slope of the data at long aging times. When this is done, we do obtain comparable values of β ; however, this method is subject to a user-defined choice of which range of data to fit at long times.

Figure 2.4 shows a series of physical aging curves collected at 40 °C for samples at different film thicknesses for $M_w = 400$ kg/mol, a representative lower MW, and $M_w = 6,790$ kg/mol, a representative higher MW. All data are shown and fit for aging times out to 1000 min (16.7 h) to be consistent for comparison purposes. Although some of our longest data sets are out to aging times of 4000 min (2.8 days), it is not reasonable to collect data for multiple days on each sample because of limits in instrument time. The $M_w = 400$ kg/mol data in Fig. 2.4a show a clear progressive trend of decreasing aging rate with decreasing film thickness, while the $M_w = 6,790$ kg/mol data in Fig. 2.4b show a smaller decrease in aging response with decreasing film thickness. The fit parameters τ and A are found to decrease with decreasing film thickness, eventually reaching values near zero for the 31 nm thick films, consistent with the visual observation of these thinnest films exhibiting only a linear trend in h/h_0 with $\log(t)$. Note that we have specifically chosen to focus our comparisons between the thin film and bulk aging response in this study at an aging temperature of 40 °C because Pye et al.⁵⁷ demonstrated that lower temperatures showed the largest differences in aging behavior between bulk and thin films. We have also collected some data with different MWs at 65 °C, the peak in the temperature-dependent aging rate $\beta(T)$ for bulk PS,^{14,57} that appear to show similar trends, but are less conclusive because the overall difference between bulk and thin films is smaller.

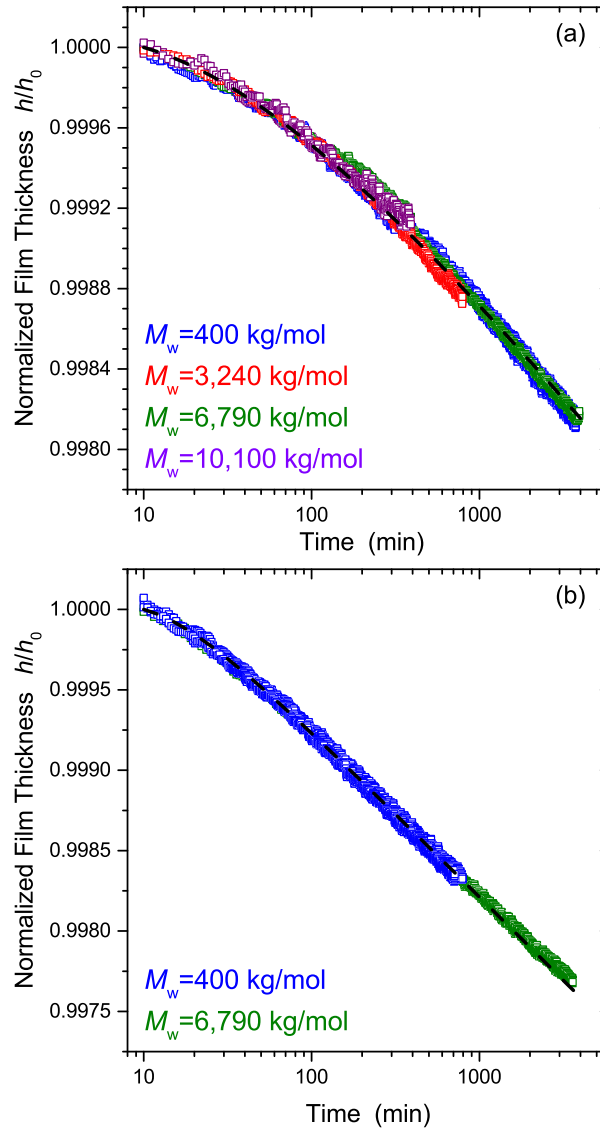


Figure 2.3: Comparison of bulk physical aging response measured at an aging temperature of 40 °C (a) and 65 °C (b) for representative molecular weights, where the black dashed curves are fits to Eq 2.1. The initial curvature in normalized thickness h/h_0 decrease is more prominent at lower aging temperatures as expected.

Figure 2.5 plots the physical aging rate β determined from fits of Eq 2.1 to datasets out to 1000 min in aging for all samples with $M_w = 400$ kg/mol and 6,790 kg/mol. For the thinnest films of 31 nm, the h/h_0 data are observed to be linear in $\log(t)$, as shown in Fig. 2.2; thus for these data, a simple linear fit to obtain β is used instead of Eq 2.1 to avoid overfitting. For bulk films with film thicknesses $h > 80$ nm, we observe no difference in physical aging response between the MWs (as was shown in

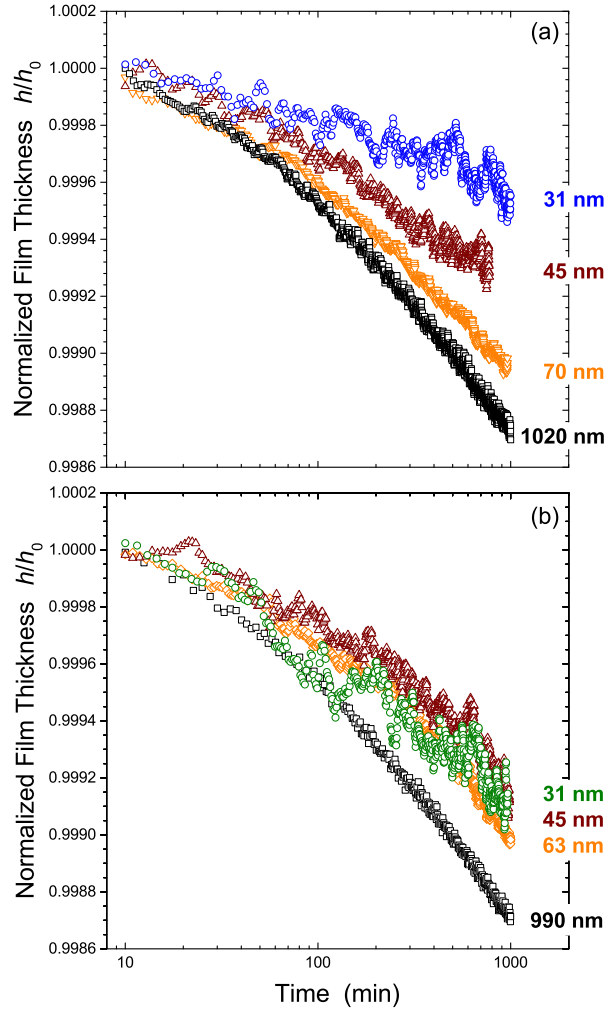


Figure 2.4: Plot of normalized film thickness h/h_0 versus log time for a series of samples with decreasing film thickness for (a) $M_w = 400$ kg/mol and (b) $M_w = 6,790$ kg/mol.

Fig. 2.3) with $\beta_{\text{bulk}} = 9.2 \pm 0.5 \times 10^{-4}$ for aging times fit out to 1000 min. However, below 80 nm in film thickness, the physical aging rate β decreases with decreasing thickness, with the aging rates for the two different MWs found to differ. For a given film thickness h , the aging rate $\beta(h)$ is observed to be consistently higher by $\sim 45\%$ for the $M_w = 6,790$ kg/mol films than the $M_w = 400$ kg/mol films. This faster physical aging for the ultra-high MW samples suggests that the ultra-high MW films are more bulk like, with a smaller region of the film not contributing to physical aging of the sample compared to the (merely) high MW films. We speculate that the extensive

chain connectivity of these ultra-high MW samples may be altering the dynamical gradient in these films. This transition around $h \approx 80$ nm is consistent with where changes in $T_g(h)$ begin to occur, as discussed below in Fig. 2.8. However, no difference in $T_g(h)$ with MW is observed outside of experimental variability suggesting that the changes in $\beta(h)$ we observe for thin films at a low aging temperature of 40 °C may be more sensitive to small differences in the dynamical gradient of these films.

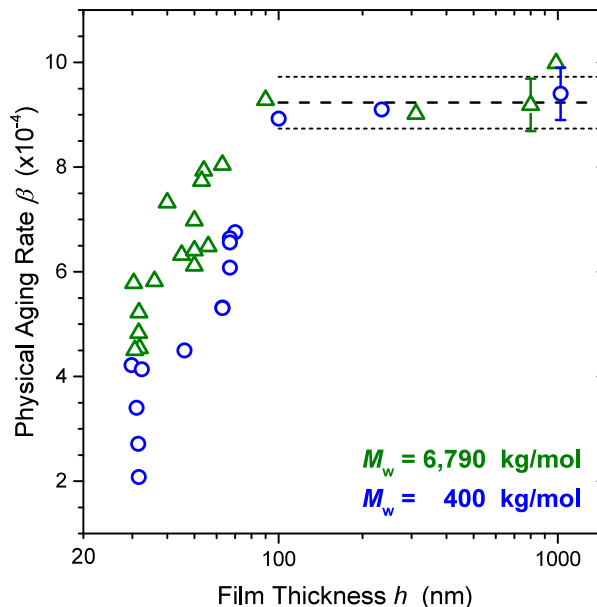


Figure 2.5: Thickness dependence of the physical aging rate measured at an aging temperature of 40 °C for two representative MWs: $M_w = 400$ kg/mol (blue circles) and ultra-high $M_w = 6,790$ kg/mol (green triangles). The horizontal dashed lines represent the average and standard deviation of the bulk physical aging rate $\beta_{\text{bulk}} = 9.2 \pm 0.5 \times 10^{-4}$ for aging times out to 1000 min.

We now examine more carefully the molecular weight dependence observed in the physical aging rate of these thin PS films. By comparing the physical aging rate β for thin (31 ± 1 nm) and thick (bulk) films we can quantify the magnitude of the reduced physical aging rate observed in these films. Figure 2.6 plots the physical aging rates (from typically an average of 4-7 samples) for the thin film data as a function of the logarithm of the weight average molecular weight M_w , while the range of aging rates for the bulk data ($\beta_{\text{bulk}} = 9.2 \pm 0.5 \times 10^{-4}$) are indicated by the horizontal gray bar.

The thin film data exhibit two distinct plateaus highlighted by the horizontal blue dashed lines that represent the average aging rate of all the runs within the given MW regime: $\beta = 3.4 \pm 0.6 \times 10^{-4}$ for the high MWs $\leq 3,500$ kg/mol and $\beta = 4.9 \pm 0.7 \times 10^{-4}$ for the ultra-high MWs $\geq 6,500$ kg/mol. These aging rates are both much lower than those observed for the bulk films, and are noticeably different from each other outside of experimental error.

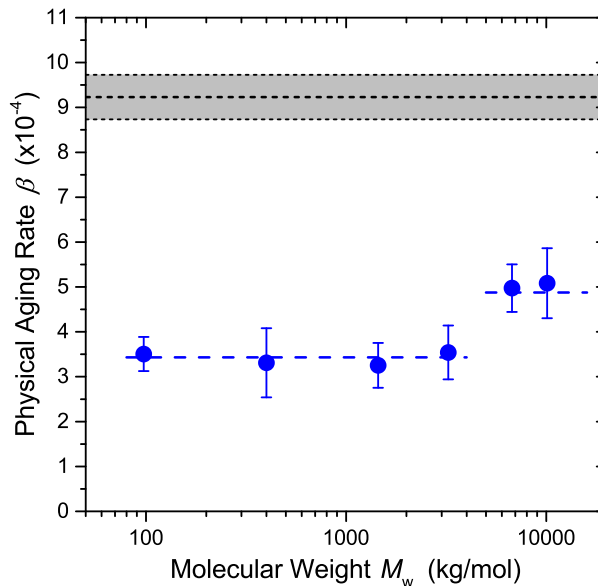


Figure 2.6: Average physical aging rate β for 31 ± 1 nm thick PS films measure at 40°C as a function of weight average molecular weight M_w on a logarithmic scale, where the error bars designate the standard deviation observed between multiple (typically 4-7) samples. MWs $\leq 3,500$ kg/mol give an average aging rate of $\beta = 3.4 \pm 0.6 \times 10^{-4}$, while ultra-high MWs $\geq 6,500$ kg/mol show a noticeably higher aging rate of $\beta = 4.9 \pm 0.7 \times 10^{-4}$ outside of experimental error. The horizontal gray bar designates the range of aging rates for the bulk data, $\beta_{\text{bulk}} = 9.2 \pm 0.5 \times 10^{-4}$.

As discussed qualitatively above, we believe the relative difference in aging rate between the thin and bulk films are indicative of the reduced physical aging response due to the presence of the free surface. This was previously interpreted as a length scale characterizing the breadth of the gradient in dynamics near the free surface,⁵⁷ such that the smaller difference in aging rates between thin and bulk films observed for the ultra-high MWs $\geq 6,500$ kg/mol suggests a diminished breadth to the en-

hanced dynamics emanating from the free surface in these films. Quantifying such length scales describing how deep into the film the effects of the free surface propagate presuppose some functional form for the depth-dependent local aging rate $\beta(z)$. Pye et al.⁵⁷ interpreted their data using two such possible $\beta(z)$ forms, as described above. Green and coworkers have noted that $\beta(z)$ could even be non-monotonic with depth depending on the aging temperature and local $T_g(z)$ profile because of the non-monotonic temperature dependence to the $\beta(T)$ aging curve.¹¹² In the present work, we choose to more conservatively characterize this relative difference in aging rate between thin and bulk films as a fractional loss of aging missing in the thin films relative to an equivalent material with bulk aging response. We define this fractional loss of aging as $F_\beta = \frac{\beta_{\text{bulk}} - \beta(h, T)}{\beta_{\text{bulk}}}$. Note, this is mathematically related to the $A(T)$ length scale previously used by Pye et al.⁵⁷ where $F_\beta = \frac{A(T)}{h}$, but this definition does not rely on any assumptions of how the reduced aging is distributed in the thin films. We observe the fractional loss of aging increases with decreasing film thickness as the impact of the free surface becomes more prominent in thinner films reducing physical aging. Figure 2.7 graphs this fractional loss of aging as a function of the logarithm of the weight average molecular weight M_w for the 31 ± 1 nm thick films measured in this study. The error bars are calculated via error propagation from those shown in Fig. 2.6, and represent the sample-to-sample variation in the measured aging rates. The decrease in the fractional loss of aging from 0.63 for the high MWs $\leq 3,500$ kg/mol to 0.47 for the ultra-high MWs $\geq 6,500$ kg/mol 31-nm thick films is indicative of the ultra-high MWs $\geq 6,500$ kg/mol films behaving more bulk like, suggesting the perturbing influence of the free surface to reduce the physical aging rate in these thin films is diminished. Given the current understanding in the literature, we interpret this as the ultra-high MWs $\geq 6,500$ kg/mol thin films having a diminished gradient in dynamics emanating from the free surface relative to the (merely) high MWs $\leq 3,500$ kg/mol thin films. What the possible causes are for this unexpected

difference will be discussed in the following subsection.

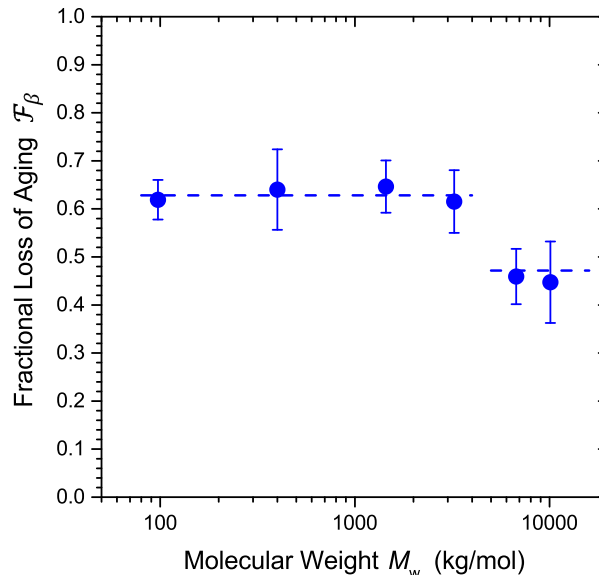


Figure 2.7: Fractional loss of aging F_β missing in 31 nm thin films relative to an equivalent material with bulk aging response, defined as $F_\beta = \frac{\beta_{\text{bulk}} - \beta(h, T)}{\beta_{\text{bulk}}}$ from the data shown in Fig. 2.6, as a function of weight average molecular weight M_w . We believe the difference in aging response between thin and bulk films results from the presence of the free surface and the extent to which the gradient in dynamics propagates into the film. The smaller fractional loss of aging for the ultra-high MWs $\geq 6,500$ kg/mol films suggest a diminished gradient in dynamics across the film.

2.3.3 Attempting to understanding differences in physical aging for thin films of ultra-high molecular weight polystyrene

We explore now what factors might be causing this unexpected MW dependence to the physical aging rate of thin ($h = 31$ nm) supported PS films between these high ($M_w \leq 3,500$ kg/mol) and ultra-high ($M_w \geq 6,500$ kg/mol) MWs. Since the physical aging rate is known to shift with depth below T_g , we start by investigating if the $T_g(h)$ values of these thin films are different for the ultra-high MWs. Note that previous studies that have examined the possible chain length dependence to the $T_g(h)$ of supported PS films, have only measured MWs up to $M_n = 3,000$ kg/mol.¹⁹ For $h = 31 \pm 1$ nm thick films, we have measured via ellipsometry on cooling at 1

$^{\circ}\text{C}/\text{min}$: $T_g(31 \text{ nm}) = 89.0 \pm 1.0 \text{ }^{\circ}\text{C}$ for $M_w = 400 \text{ kg/mol}$, $T_g(31 \text{ nm}) = 91.0 \pm 1.5 \text{ }^{\circ}\text{C}$ for $M_w = 3,240 \text{ kg/mol}$, and $T_g(31 \text{ nm}) = 91.0 \pm 1.5 \text{ }^{\circ}\text{C}$ for $M_w = 6,790 \text{ kg/mol}$ (based on an average of typically 5 runs on nominally identical samples), showing no difference in T_g with MW outside of experimental variability for 31 nm thick films. Bulk T_g was measured to be $96.4 \pm 0.7 \text{ }^{\circ}\text{C}$. However, one could argue that 31 nm thick films do not yet deviate substantially from bulk behavior in terms of $T_g(h)$ values, and that some more subtle difference with MW could perhaps be seen for thinner films, or within the temperature-dependent thickness $h(T)$ behavior. Thus, in Figure 2.8a we plot the film thickness h (normalized at $120 \text{ }^{\circ}\text{C}$ to overlap the liquid-line of each data set) as a function of temperature, comparing $h(T)$ for films with near equivalent thickness for two representative MWs: 10.5 and 23 nm thick films of $M_w = 400 \text{ kg/mol}$, 11.4 and 21 nm films of $M_w = 6,790 \text{ kg/mol}$, as well as bulk (200 nm) films of each. By examination of the curves in this manner, we see that the two MWs (high and ultra-high) collapse atop each other within typical experimental sample-to-sample variability, indicating no MW dependence to the $h(T)$ behavior, even for these very thin films out to these ultra-high MWs. In Figure 2.8b, we have compiled literature data from ellipsometry measurements to compare the film-thickness dependence of the measured average glass transition temperature $T_g(h)$ by various studies^{17,36,96,127,128,160,169–171}, and included our own data from this study. To facilitate comparison all data have been referenced to the bulk T_g value reported in that study. We have colored-code the data based on MW, grouping them into four categories: low $M_w < 300 \text{ kg/mol}$ (black), intermediate $350 \text{ kg/mol} < M_w < 1,000 \text{ kg/mol}$ (blue), high $1,500 \text{ kg/mol} < M_w < 3,500 \text{ kg/mol}$ (red), and ultra-high $M_w > 6,500 \text{ kg/mol}$ (green). Within the variability of the $T_g(h)$ values, no trend is observed with MW, consistent with previous reports.¹⁹ Thus, there is no evidence for a $T_g(h)$ change with MW in these films that can be used to explain the difference in physical aging rates observed.

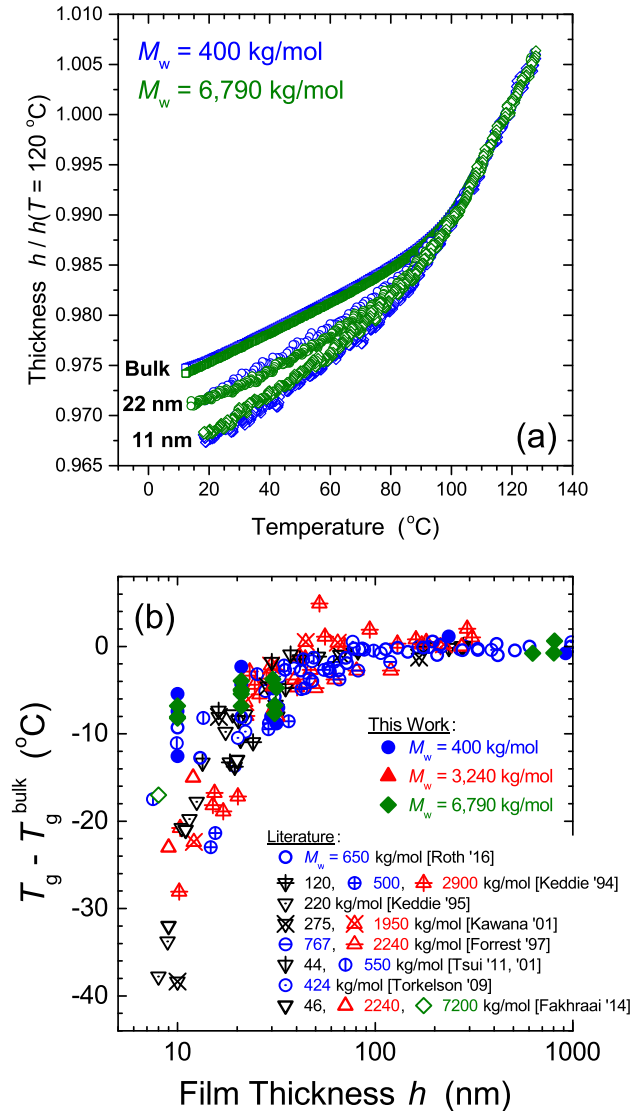


Figure 2.8: (a) Temperature dependence of the film thickness $h(T)$ collected on cooling at $1\text{ }^{\circ}\text{C}/\text{min}$, where the data of the liquid-line has been superimposed at $T = 120\text{ }^{\circ}\text{C}$. Films of near equivalent thicknesses of 11 nm, 22 nm, and 200 nm (bulk) are compared for a representative high $M_w = 400\text{ kg/mol}$ (blue data) and ultra-high $M_w = 6,790\text{ kg/mol}$ (green data). Collapse of the $h(T)$ data within sample-to-sample variability indicates no MW dependence to the glass transition behavior even in very thin films. (b) Compilation of the average $T_g(h)$ values measured by ellipsometry from the literature^{17,36,96,127,128,160,169–171} and this work, referenced to their given studies' T_g^{bulk} value. Data have been color-coded based on MW: low $M_w < 300\text{ kg/mol}$ (black), intermediate $350\text{ kg/mol} < M_w < 1,000\text{ kg/mol}$ (blue), high $1,500\text{ kg/mol} < M_w < 3,500\text{ kg/mol}$ (red), and ultra-high $M_w > 6,500\text{ kg/mol}$ (green).

We have also inspected more closely the cool rate dependence and thermal expansion coefficient $\alpha(T) = \frac{1}{h} \frac{dh(T)}{dT}$ looking for some systematic difference between the high and ultra-high MWs. Comparing 31 ± 1 nm thick films for a representative high $M_w = 400$ kg/mol and ultra-high $M_w = 6,790$ kg/mol, we find curves of normalized $h(T)$ overlap within typical sample-to-sample variability for the different MWs at all cooling rates inspected between $0.2 - 55$ °C/min, where 55 °C/min is the fastest our instrument can accomplish with liquid nitrogen cooling and the cooling rate used to initiate the aging measurements. For cooling rates of 5 °C/min or less we are able to collect enough data on cooling to meaningfully inspect $\alpha(T)$ and measure $T_g(h)$ as shown in Figure 2.9, but find no difference in the breadth or shape of the transition between the high and ultra-high MWs. The T_g ($h = 31$ nm) values are the same to within experimental error and demonstrate the slight increase of ~ 2 °C with increasing cooling rate one would expect. Even though we do not see a difference in the 31-nm thick films with MW, we note that there is a recent study by Glor and Fakhraai,³⁶ who examined the cooling rate dependence of very thin PS films for a range of MWs: $M_w = 22$ kg/mol to $7,200$ kg/mol. They also did not see a difference for ~ 30 nm thick films, however they did report a subtle, but systematic difference in cooling rate dependence with MW for 8 nm thick films (see their Figure 2.5). Their trends are consistent with our MW-dependent physical aging results that higher MWs exhibit a more bulk-like response with a slightly higher glass line, where the higher MW films have dynamics that appear to be less perturbed by the presence of the free surface. (Note that our previous study determined that it was not feasible to collect physical aging measurements on films much below ~ 30 nm.⁵⁷) These results on ultrathin films of ~ 8 nm support our conclusions and demonstrate that isothermal physical aging measurements are more sensitive to small differences in dynamical gradient across thin films than cooling rate measurements, where it appears that much thinner films are required to observe measurable differences between MWs.

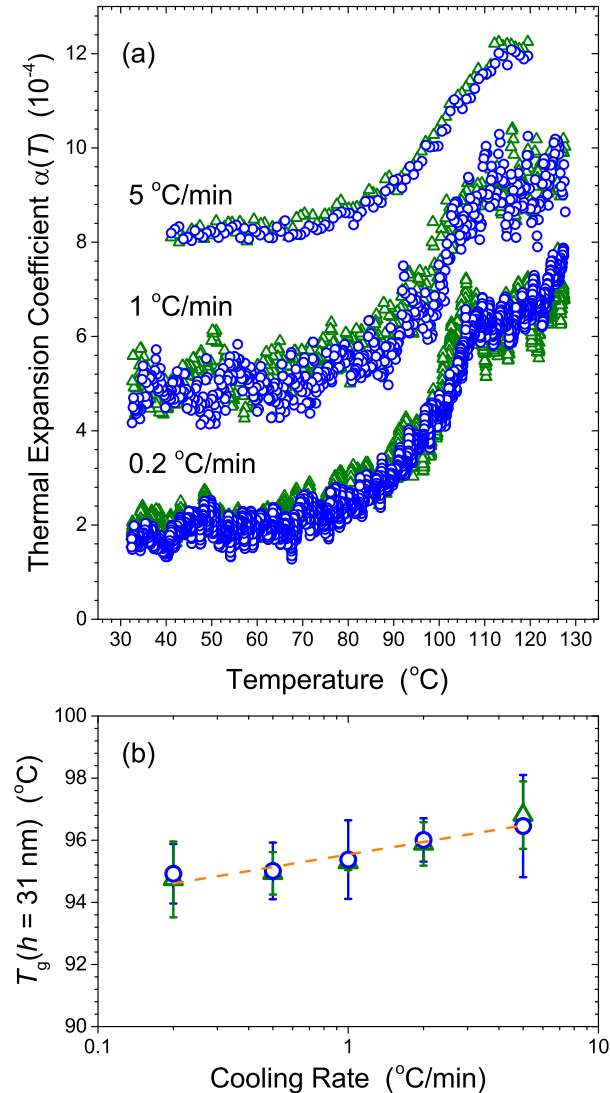


Figure 2.9: (a) Temperature dependence of the thermal expansion coefficient $\alpha(T)$ of 31-nm thick films collected on cooling at three different cooling rates, where the data for the higher cooling rates have been offset vertically for clarity: high $M_w = 400$ kg/mol (blue circles) and ultra-high $M_w = 6,790$ kg/mol (green triangles). (b) Cooling rate dependence of the glass transition temperature $T_g(h)$ for these 31 nm thick films.

Physical aging measures the slow densification of the glass on logarithmic timescales. Consequently, one could imagine that the measured aging behavior could be particularly sensitive to changes in packing frustration within the material. As the molecular weight increases, the global chain conformation must distort itself more to continue to be constrained in a thin film of a given thickness h . Typically confinement of

global chain conformations have not been associated with changes in film $T_g(h)$ or other local measures of mobility like physical aging, with relaxations of local chain conformations being sufficient to obtain reproducible measurements.^{45,172,173} However, rarely have experiments been carried out on thin films made of such high MWs of order 10 million g/mol. Thus, we have checked whether there is any measurable change in material packing with increasing MW by examining the index of refraction data collected simultaneously during the aging measurements. The Lorentz-Lorenz equation,

$$\frac{n^2 - 1}{n^2 + 2} = \frac{\alpha N_A}{3\varepsilon_0 M_0} \rho \quad , \quad (\text{Eq:2.2})$$

has routinely be used to obtain a measure of material density ρ from index of refraction n data as all other quantities are considered to be constants: monomer polarizability α , monomer molecular weight M_0 , Avogadro's number N_A , and permittivity of free space ε_0 .^{56,174,175} We have evaluated the index of refraction $n(\lambda)$ at a wavelength of 632.8 nm (corresponding to a HeNe laser) from the measured Cauchy parameters, in an analogous manner to which the initial thickness h_0 was defined at the start of the aging run, corresponding to an aging time of 10 min, averaged over a 10 min period, on either side of this value. This initial index of refraction value was used to calculate the quantity $\frac{n^2-1}{n^2+2}$ in the Lorentz-Lorenz equation that is directly proportional to the film density. Figure 2.10 plots the percent change in this measure of effective average film density as a function of molecular weight for the 31 nm thick films. The data show no measurable difference in average film density with increasing MW, outside of an experimental variability of $\pm 0.27\%$ indicated by the shaded gray region in Fig. 2.10. This suggests there is no strong change in molecular packing with increasing MW that could be the explanation for the observed change in physical aging response. Intuitively, this result does not seem surprising given how extended and diffuse three-dimensional random-walk chain conformations are; a significant amount of global chain confinement could easily occur without impacting

local segmental packing. We note that ellipsometry is only able to provide a measure of the effective average film density, and the data in Fig. 2.10 does not preclude there being a subtle depth-dependent change in local film density responsible for the observed changes in physical aging behavior. As dynamics in glasses are strongly dependent on density (free volume),¹⁷⁶ even a small unmeasurable change in local density could have a strong impact on local dynamics.

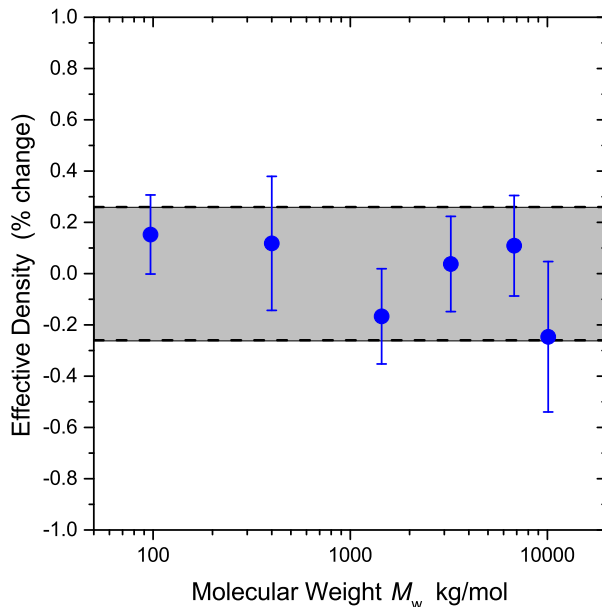


Figure 2.10: Percent change in the effective average film density as a function of molecular weight for 31 nm thick PS films. Effective density was determined from the index of refraction at an aging time of 10 min based on the Lorentz-Lorenz equation (Eq. 2).

Historically, there were a number of other factors that were considered possible concerns when studying very high molecular weight thin polymer films made by spin-coating. For example, initial studies expressed concerns that spin-coating high molecular weight chains could cause chain alignment within the film, especially at higher spin speeds.¹⁷⁷ The importance of annealing time and temperature necessary to relax chain conformations and get reproducible measurements was also debated.⁴⁵ These concerns have long since been addressed in the field, but since most studies have measured MWs only out to a few million g/mol, we revisit here some of these

arguments as they pertain to ultra-high MWs of order ten million. As such we have done a number of experimental checks to determine if any of these initial concerns are relevant at these much higher MWs, but do not find any evidence for differences with the ultra-high MWs. For example, we observe the same aging behavior for 31 nm thick films regardless of whether the spin-speed is varied during spin-coating, or whether the annealing time at 120 °C prior to the aging measurement is varied between 2 - 72 hours. Early on it was thought that annealing times should be longer than the reptation time in order to relax chain conformations.⁴⁵ However with high MW chains, it is frequently not possible to anneal longer than the reptation time. For the range of MWs used in this study, the reptation time τ_d at 120 °C varies between 50 seconds for $M_w = 97$ kg/mol to 11 years for $M_w = 10,100$ kg/mol.¹⁷⁸⁻¹⁸⁰ We typically anneal our samples for 15 h at 120 °C, which is comparable to the reptation time of a $M_w \approx 770$ kg/mol, while the change in physical aging behavior occurs somewhere between $M_w \leq 3,500$ kg/mol ($\tau_d \approx 3.5$ months) and $M_w \geq 6,500$ kg/mol ($\tau_d \approx 2.4$ years). Thus, the change in physical aging behavior observed in the ultra-high MWs is uncorrelated with reptation time. This is consistent with existing literature that has long since determined that annealing times relative to reptation are not relevant.⁴⁵ In contrast, studies have argued that only local chain relaxations via Rouse modes are likely necessary to achieve reproducible glass transition measurements, a relatively local chain property.^{45,172,173} Other annealing concerns have focused on residual stress relaxation from spin-coating or thermal expansion mismatch.^{53,173,181,182} Although Pye and Roth demonstrated that the physical aging rate of films are strongly dependent on stress imparted to the film from thermal expansion mismatch,⁵⁷ the thermal expansion coefficient is independent of MW, as is clear from the $h(T)$ and $\alpha(T)$ data plotted in Figures 2.8 and 2.9.

More recently, several studies have suggested that adsorption of polymer chains to the underlying substrate during annealing may influence the dynamics of thin

films.^{39,41–43,136–143} Chain adsorption of polymers to surfaces can occur readily because even weak favorable monomer-substrate interactions can be enough to overcome the free energy loss associated with non-ideal chain conformations when many monomers from a single chain are in contact with the interface.^{183–186} It has been suggested that higher MW chains can adsorb more readily,^{41,144} raising the possibility that the unusual MW dependence to the physical aging rate we observe in the thin films of ultra-high MWs could be associated with chain adsorption. We have done a series of different tests to ascertain whether changes in physical aging behavior of thin films are affected by sample preparation conditions that would, according to existing literature,^{41,141} lead to more or less chain adsorption. The physical aging rate of 31 nm thick films have been compared for samples of both $M_w = 400$ kg/mol and 6,790 kg/mol that were annealed for either only 2 h at 120 °C or for 72 h at 150 °C. The same physical aging response, to within normal experimental variability, was observed in these films regardless of annealing conditions, with the ultra-high MW samples always exhibiting a faster physical aging rate. We note a recent study by Napolitano et al. has found that the total amount of chain adsorption is reduced in thin films.¹⁸⁷ We have also spin-coated and annealed films on mica that were then floated off onto silicon substrates, presumably severing any adsorbed chains from the mica substrate. These samples, subsequently annealed for only 25 min at 120 °C to reset the thermal history and start the aging measurement, also give the same physical aging response as films directly spin-coated onto silicon wafers and annealed for different lengths of time. In addition, we have also created samples where an explicit adsorbed layer was made following literature protocols^{41,141} by annealing initially bulk (200 nm thick) films with $M_w = 400$ kg/mol and then washing them off with solvent (30 min in toluene) and measuring the resulting adsorbed layer thickness with ellipsometry. Films of near equivalent thickness ≈ 30 nm were then created by floating on a layer of thickness h_{float} to produce films with total thickness $h_{\text{total}} = h_{\text{ads}} + h_{\text{float}}$, where the capped films

were annealed for 2 h at 170 °C to heal the interface and ensure good interpenetration of the capped layer with the underlying adsorbed layer.^{123,188,189} Figure 2.11 compares the physical aging response of three different samples with total thickness $h_{\text{total}} \approx 30$ nm: (1) $h_{\text{total}} = 33.1$ nm with $h_{\text{ads}} = 3.2$ nm, (2) $h_{\text{total}} = 34.3$ nm with $h_{\text{ads}} = 6.9$ nm, and (3) a regular spin-coated film of thickness $h_{\text{total}} = 31.0$ nm. No difference in the physical aging response, decrease in normalized film thickness h/h_0 vs. logarithmic aging time, was observed between these three different types of samples with and without different amounts of explicit adsorbed layers. It does not appear to us that the presence or absence of an adsorbed layer has any impact on the measured average aging rate of thin polymer films. Thus, we conclude that the anomalous physical aging response observed for ultra-high MWs $\geq 6,500$ kg/mol thin films is not caused by differences in chain adsorption.

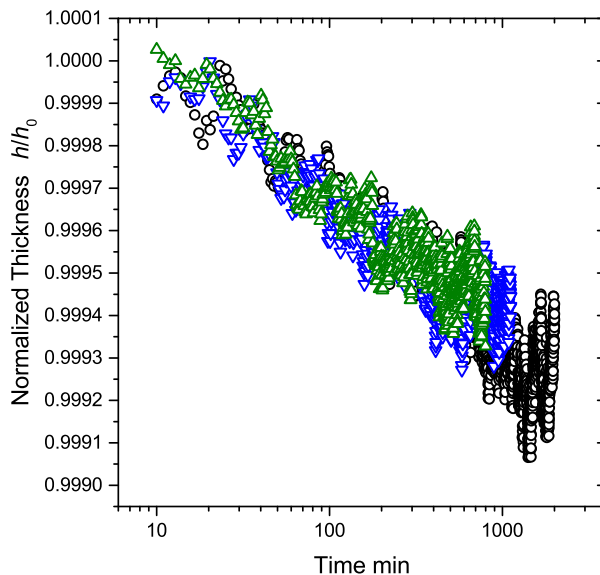


Figure 2.11: Plot of normalized film thickness h/h_0 vs. logarithmic aging time comparing the physical aging response of three different samples of $M_w = 400$ kg/mol with total thickness $h_{\text{total}} \approx 30\text{nm} = h_{\text{ads}} + h_{\text{float}}$: (blue down triangles) $h_{\text{total}} = 33.1$ nm with $h_{\text{ads}} = 3.2$ nm, (green up triangles) $h_{\text{total}} = 34.3$ nm with $h_{\text{ads}} = 6.9$ nm, and (black circles) a regular spin-coated film of thickness $h_{\text{total}} = 31.0$ nm.

2.4 Conclusions

We have observed an unexpected MW dependence to the physical aging behavior of thin ($h < 80$ nm thick) supported PS films that is only present for ultra-high MWs $\geq 6,500$ kg/mol. Physical aging in bulk polymers is traditionally associated with local segmental motions and as such does not exhibit any MW dependence above where $T_g(M_n)$ has saturated with chain length. Consistent with this, we do not observe any MW dependence to the physical aging response for thick bulk films for the entire range of molecular weights we have studied, $M_w = 97$ kg/mol to 10,100 kg/mol. In thin films, no molecular weight dependence is observed for MWs $\leq 3,500$ kg/mol as would be expected, only for ultra-high MWs $\geq 6,500$ kg/mol are differences observed with the ultra-high MWs consistently exhibiting an $\sim 45\%$ faster aging response.

In agreement with our previous work,⁵⁷ the physical aging rate for the thin ($h \approx 30$ nm) films is reduced from that of bulk, which has been attributed to the presence of the free surface and the enhanced mobility it imparts.^{57,112} This reduced physical aging rate in the thin films relative to bulk was interpreted⁵⁷ as providing a measure of the depth to which the glassy dynamics are perturbed by the free surface as a function of temperature, a distance much larger than similar measures of liquid-like dynamics, and found to be quantitatively consistent with the local glass transition temperature $T_g(z)$ reductions near the free surface expected for these films.⁶⁶ In the present work, we more conservatively interpret this reduced aging in the thin films as simply a fractional loss of aging $F_\beta = \frac{\beta_{\text{bulk}} - \beta(h,T)}{\beta_{\text{bulk}}}$ missing in the thin films relative to an equivalent material with bulk aging response. In contrast to thin films with MW $\leq 3,500$ kg/mol, we find that equivalent thin films with MWs $\geq 6,500$ kg/mol exhibit an $\sim 45\%$ faster physical aging rate, closer to that of bulk, but still reduced. We interpret this faster physical aging at ultra-high MWs $\geq 6,500$ kg/mol as a diminished breadth to the gradient in dynamics near the free surface relative to that in (merely) high MW $\leq 3,500$ kg/mol.

Differences in physical aging between the high MW $\leq 3,500$ kg/mol and ultra-high MWs $\geq 6,500$ kg/mol samples occur for film thicknesses $h < 80$ nm where the physical aging rate begins to deviate from a bulk MW-independent response. In this study, we primarily focused our ellipsometry measurements that characterize the time-dependent densification of the glassy films to an aging temperature of 40 °C as the aging response between thin and bulk films are largest at lower aging temperatures,⁵⁷ but we also observe a similar, weaker response at an aging temperature of 65 °C. As is common for glasses aged well below their glass transition temperature, an initial curvature is observed prior to the linear decrease in sample thickness h/h_0 with logarithmic time associated with the onset of physical aging by a distribution of relaxation times. We observe this initial curvature characteristic of the onset of physical aging in both bulk and thicker films, where we have introduced a three-parameter functional form that allows us to fit the complete h/h_0 vs. $\log(t)$ aging behavior. However, we find that the physical aging behavior of the thinnest (31 ± 1 nm thick) films always appears linear on a logarithmic scale and does not show the initial curvature at short aging times exhibited by bulk films at low aging temperatures. This observation is consistent with these thinnest films having faster relaxations than bulk such that all relaxation modes contributing to physical aging are active at the start of the aging measurement.

In an effort to ascertain the origin of this anomalous aging response present in ultra-high MWs $\geq 6,500$ kg/mol PS thin films, we have investigated a number of difference factors. The MW range over which the change in physical aging response occurs, between MWs of 3,500 kg/mol and 6,500 kg/mol, is very large and unrelated to the films' thickness in comparison to the radius of gyration R_g of the chains. We have tested, but do not find any change in the observed aging behavior in these thin films with varying annealing time, spin-speed, or the possible presence/absence of adsorbed layers. No measurable change is observed in the average film density (molecular

packing), as determined from the refractive index data through the Lorentz-Lorenz equation at the beginning of the aging run. For the range of film thicknesses studied by physical aging, we do not observe any change in the cooling rate dependence of the film-average glass transition temperature $T_g(h)$ or temperature-dependent thickness $h(T)$ behavior to within normal experimental variability even out to these ultra-high MWs. However, we note Glor and Fakhraai³⁶ have previously reported a slight MW difference to the cooling rate dependence of very thin films, where ~ 8 nm thick films show a slightly higher glass line for higher MWs consistent with the trends from our physical aging measurements. These observations suggest that the isothermal physical aging measurements are more sensitive to small differences in dynamical gradients across thin films. It is possible, although not testable experimentally at present, that the local, depth-dependent $T_g(z)$ may be altered slightly for thin films of ultra-high MWs. Based on our experimental investigations we attribute the ~ 45 % faster physical aging response of ultra-high MWs $\geq 6,500$ kg/mol thin PS films, relative to equivalent films of (merely) high MWs $\leq 3,500$ kg/mol, to a diminished gradient in dynamics near the free surface of these films. These results contribute to the growing reports in the literature^{36,89,98–108,110–122,145} that chain connectivity and entropy are additional factors influencing interfacial effects and dynamical gradients in thin films beyond the well-characterized enthalpic interactions.

Chapter 3

Review and Reproducibility of Forming Adsorbed Layers From Solvent Washing of Melt Annealed Films

A version of this chapter is in press to be published as Michael F. Thees, Jennifer A. McGuire, and Connie B. Roth, *Soft Matter* 2020, DOI: 10.1039/D0SM00565G

3.1 Introduction

In recent years a few groups have suggested that adsorption of chains to substrate interfaces occurs in melt films acting to modify the anomalous dynamics observed in ultrathin films and other ‘nanoconfined’ systems. These reports typically correlate some observed change in dynamics after prolonged annealing at an elevated temperature with parallel measurements of the thickness of a residual layer after a given solvent washing protocol on films that have been nominally annealed under equivalent condi-

tions.^{44,134,136,137,190–198} This residual adsorbed layer thickness $h_{\text{ads}}(t)$ as a function of annealing time at elevated temperature is frequently reported under the assumption that the solvent washing procedure used “reveals” the adsorbed layer structure formed in the melt (termed “Guiselin’s experiment” or approach).^{138,190,193,195,199–204} Thicker residual layers after solvent washing are found for films that have been annealed longer, from which authors have concluded that adsorbed layers are responsible for perturbations to the glass transition temperature $T_g(h)$ in thin films,^{137,190,193,205,206} increased viscosity of thin films,^{134,191} as well as other anomalous property changes observed in thin films spanning deviations to density,²⁰⁷ thermal expansion,²⁰¹ dewetting,^{44,204} crystallization,^{195,208} and water uptake.²⁰⁹ Given the prevalence of observations being attributed to chain adsorption in melt films, we believe it is imperative that the reliability and reproducibility of the experimental method used to ascertain such conclusions is evaluated.

In this work, we summarize this recent literature comparing the various results reported for the residual adsorbed layer thickness $h_{\text{ads}}(t)$ measured after solvent washing as a function of annealing time at 150 °C for polystyrene (PS) films on piranha cleaned silicon wafers, the most commonly reported case. We attempt to distill and test a coherent common protocol for the formation of adsorbed layers used in these various studies. In particular, we evaluate the impact of substrate cleaning method, solvent washing procedure used, ellipsometry measurement precision, and various other experimental protocol details on the reproducibility and reliability of forming adsorbed layers. We discuss these results in the context of the older, well-established 1950s–1990s literature on polymer adsorption in solution, and the two and a half decades of literature on anomalous dynamics in nanoconfined thin films. Our primary focus is to address the reliability and understanding associated with forming adsorbed layers $h_{\text{ads}}(t)$ from the melt, from which inferences have been made about the importance of chain adsorption for modifying dynamics in thin films. We do not review or eval-

uate the reported changes in dynamics attributed to adsorption themselves, which is beyond the scope of the present work.

3.1.1 Summary of Recent Investigations on Adsorbed Layers Formed from Melt Films

The recent reports in the literature that claim to correlate large changes in dynamics with the presence of an adsorbed layer utilize, in general, a common experimental protocol for obtaining adsorbed layers from melt films, but vary widely in the details of exactly how each step is performed. According to these studies, the basic procedure for creating an adsorbed layer involves cleaning the substrate, spin-coating a (typically bulk) polymer film on top, annealing the film at an elevated temperature for some extended length of time t , and then using a good solvent to wash away “unadsorbed chains”.^{192,199,200,206,210,211} The remaining residual adsorbed layer thickness $h_{\text{ads}}(t)$ left behind on the substrate after the solvent washing procedure is then measured, most often by ellipsometry.^{138,190,199,202,203,206,210,211} Although frequently not explicitly stated, the refractive index parameters for these ellipsometry measurements are typically held constant at the bulk value,^{201,202} because these films are very thin, frequently less than ~ 10 nm, and ellipsometry has difficulty independently resolving thickness and refractive index for such thin films.^{160,212} A couple of groups have also used atomic force microscopy (AFM) to confirm the h_{ads} values measured by ellipsometry match those obtained from a step-height measurement.^{199,211}

In studies of chain adsorption from the melt, silicon substrate cleaning has most frequently been done with piranha solution (7:3 $\text{H}_2\text{SO}_4:\text{H}_2\text{O}_2$),^{192,203,206,211} which strongly oxidizes organics allowing them to be rinsed away by water, leaving a highly hydrophilic SiOx surface. Other studies have used a hydrogen fluoride (HF) treatment of silicon substrates, which strips the native oxide layer, and usually shows higher amounts of chain adsorption.^{210,211} Alternately, some groups use a progressive series

of organic solvents to clean substrates.^{199,200,213} After cleaning, bulk polymer films are spin-coated onto the substrates, and the samples are then annealed at an elevated temperature, usually under vacuum^{192,203,206,210} or in some works on a hot plate.^{200,202,208,211} This annealing step is thought to facilitate the growth of the adsorbed layer as the measured residual thickness $h_{\text{ads}}(t)$ is found to increase with increasing annealing time t .^{44,138,190,192,194,199,202,203,206,210,213} A solvent washing procedure where the annealed films are immersed in a good solvent for some prolonged time, in some cases multiple times, is then used to “reveal” the adsorbed layer that was presumed to have formed in the melt.^{192,199,200,204,210,213} Most frequently the solvent is that used for spin coating the initial film (e.g., toluene),^{199,200,206,210,211} although occasionally a stronger solvent like chloroform is used instead.^{192,201,204}

This solvent washing step varies widely in the literature both in the length of time a film is washed and in the total number of washes conducted. As we will demonstrate that solvent washing is a defining step in the resulting $h_{\text{ads}}(t)$ measured, we summarize here the various washing procedures used by the existing studies. Napolitano et al. and Koga et al., two groups who have made significant claims in the recent literature on polymer adsorption from the melt, have developed similar, but distinctly different protocols for washing off unadsorbed chains. Napolitano et al. frequently report changes in film properties as a function of annealing time that are then correlated with separate measurements of the adsorbed layer thickness.^{136,137,190,194,197} For these experiments, they report using one 30 min wash in toluene¹⁹⁹ or one 30 min wash in chloroform²⁰¹ to remove the unadsorbed chains. However, several studies do not report details for their washing protocol, with some stating simply that “non-adsorbed chains were washed away in the same good solvent used for spin-coating (toluene)”,¹⁹⁰ or instead refer to a previous publications for experimental details.^{138,194,200,202} In contrast, Koga et al. report the most extensive and detailed washing procedure believing that extended solvent washing further reveals different structures of the adsorbed

layer in the melt. An initial series of washes, 3-5 times 30 min in toluene,^{203,204,210} is used to expose the “interfacial sublayer”.^{192,203,204} The more loosely bound chains can then also be removed by a “further prolonged leaching process (up to 150 days)” in toluene, exposing the more tightly bound “lone flattened higher density layer”.²¹⁰ More recent works have replaced the 150 days in toluene with only “a couple of days” in a stronger solvent, chloroform,¹⁹² or more recently three times 30 min in chloroform.²⁰⁴ Other groups have used three 10-minute washes in toluene to obtain the residual adsorbed layer.^{206,211}

Given the large differences in experimental protocol for producing residual adsorbed layer thicknesses, we directly compare in Figure 3.1 reported literature data for $h_{\text{ads}}(t)$ as a function of annealing time t at an elevated temperature above T_g from a number of different studies.^{192,199,206,210,211} For this comparison, we primarily chose $h_{\text{ads}}(t)$ data representing what appears to be the most common experimental protocol, PS films on piranha cleaned silicon substrates annealed at 150 °C under vacuum^{44,192,203,204,206} or in air.²¹¹ We also include the closest comparable data from Napolitano’s group of PS films on solvent cleaned silicon substrates annealed at 140 °C on a hot plate.¹⁹⁹ Solvent washing of these PS films were all done in toluene under roughly comparable conditions: three 10-min washes,^{206,211} one 30 min wash,¹⁹⁹ or 5+ (likely 10-min) washes.¹⁹² As shown in Figure 3.1a, the trends in $h_{\text{ads}}(t)$ typically show an initial rapid increase in h_{ads} that saturates at some long-time plateau $h_{\text{ads}}(t = \infty) = h_{\infty}$ after a few hours (5-10 h) of annealing,^{192,206,210,211} with larger h_{∞} values being observed at higher molecular weights.^{210,211} The $h_{\text{ads}}(t)$ data are most simply fit to a function having the general form of

$$h_{\text{ads}}(t) = h_{\infty}(1 - e^{-t/\tau}) \quad (3.1)$$

to determine the final long-time plateau h_{∞} value, where τ represents some charac-

teristic time.

The study from Tsui et al. provided only final long-time plateau h_∞ residual thickness values for a range of molecular weights spanning from $M_w = 13.7$ to 940 kg/mol,²¹¹ plotted to the far right side of the graph in Fig. 3.1a. They demonstrated that these h_∞ values scaled linearly with the radius of gyration R_g ($h_\infty = 0.47R_g$) as plotted in Figure 3.1b, where it was assumed that $R_g \sim N^{1/2}$ for melts.²¹¹ Similar data collected on HF treated silicon showed larger h_∞ values also scaling with R_g , $h_\infty = 0.81R_g$.²¹¹ These data, as well as complementary data by Koga et al.²¹⁰ are also plotted in Figure 3.1b. This scaling of the long-time plateau h_∞ residual thickness with the radius of gyration R_g of the chain was previously demonstrated by Durning et al.,²¹⁴ who appear to be the first to investigate the formation of residual polymer layers formed from solvent washed melt films. In their study 1 μm thick poly(methyl methacrylate) (PMMA) films were annealed at 165 °C for up to 120 h in an argon atmosphere on quartz substrates that were initially cleaned with a hydrochloric acid (HCl) based treatment. The annealed films were then washed three times for 3 h in benzene, the spin-coating solvent, followed by sonicating for 5-10 min, prior to measuring the dry residual layer thickness remaining (i.e., h_{ads}) with neutron reflectivity. Films were made from a range of molecular weights, $M_n = 13 - 1230$ kg/mol, with the final adsorbed layer thickness reached at long times scaling as $h_\infty \sim N^{0.47 \pm 0.05}$.

The $h_{\text{ads}}(t)$ data shown in Fig. 3.1a from Napolitano's group are for an annealing temperature of 140 °C. This study by Housmans et al. compared $M_w = 325$ kg/mol at three different annealing temperatures (140, 170, and 180 °C) finding that $h_{\text{ads}}(t)$ increases faster with increasing temperature.¹⁹⁹ Data for $M_w = 1460$ kg/mol at 140 °C showed that $h_{\text{ads}}(t)$ also increases faster for higher molecular weights. Not enough data is provided to estimate the final adsorbed amount h_∞ at long times, but as the data can be collapsed by scaling only the time axis, it appears that the final adsorbed amount would be independent of temperature. Koga et al. has also shown that h_∞

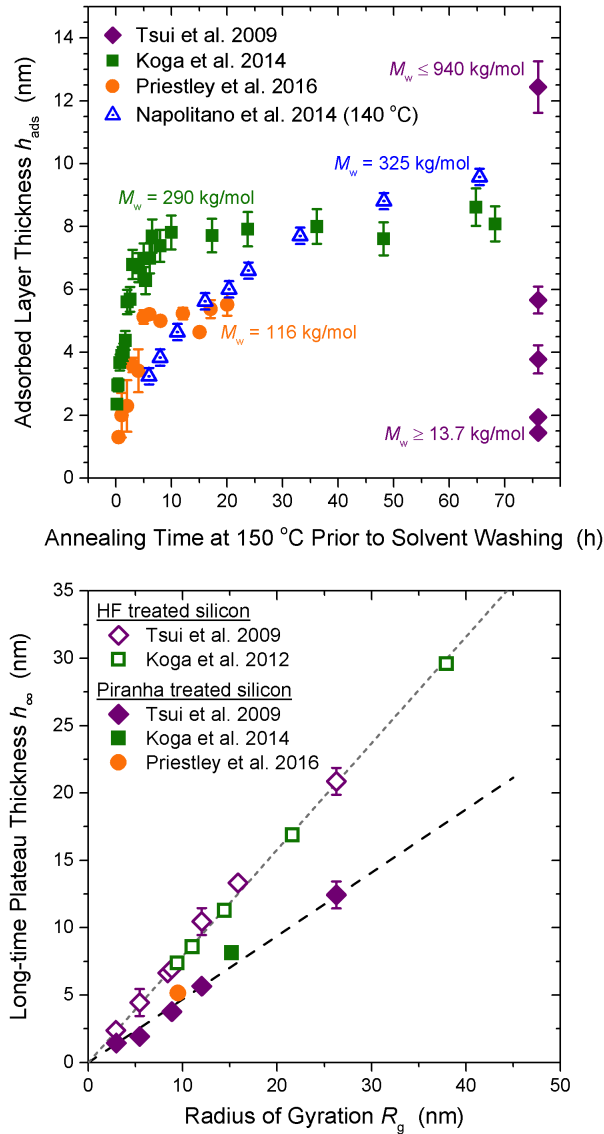


Figure 3.1: (a) Comparison of literature data for the residual adsorbed layer thickness $h_{\text{ads}}(t)$ remaining after solvent washing with toluene as a function of annealing time at 150 °C for PS films on piranha cleaned silicon wafers: data from Tsui et al.²¹¹ (purple diamonds at long annealing times for a range of molecular weights $M_w = 13.7 - 940$ kg/mol) and Priestley et al.²⁰⁶ (orange circles, $M_w = 116$ kg/mol) are for three 10 min washes, while that from Koga et al.¹⁹² (green squares, $M_w = 290$ kg/mol) are for three 30 min washes. Data from Napolitano et al. (blue triangles, $M_w = 325$ kg/mol) at 140 °C, the closest comparable temperature, are also included, where samples were washed once for 30 min.¹⁹⁹ (b) Final residual thickness plateau h_{∞} obtained at long annealing times on both piranha cleaned silicon (closed symbols) and HF treated silicon (open symbols) plotted as a function of radius of gyration, assuming $R_g \sim N^{1/2}$. Data are replotted from Tsui et al.,²¹¹ with additional data from Koga et al.²¹⁰ and estimated from Priestley et al.²⁰⁶ and Koga et al.'s 2014 study.¹⁹²

is independent of annealing temperature from 40-150 °C.²¹⁰ Napolitano et al. fit the slower growth of $h_{\text{ads}}(t)$ they observe to a two-stage functional form:

$$h_{\text{ads}}(t) = \begin{cases} h_0 + vt, & t < t_{\text{cross}} \\ h_{\text{cross}} + \Pi \log(t/t_{\text{cross}}), & t > t_{\text{cross}} \end{cases} \quad (3.2)$$

where h_0 is the initial adsorbed amount at $t = 0$, while t_{cross} and h_{cross} identify a transition point between a linear and logarithmic regime with respective growth rates v and Π .^{199,200,213}

This basic protocol of annealing and then solvent washing films as a method of obtaining adsorbed layers has been frequently referred to as following “Guiselin’s experiment”^{138,190,193,199–202} or “Guiselin’s approach”,^{195,203,204} citing the 1992 study by O. Guiselin.²¹⁵ This Guiselin work is a theoretical treatment using scaling analysis to determine the concentration profile of adsorbed chains in contact with a surface.²¹⁵ In particular, Guiselin proposes the thought experiment of starting with an equilibrated melt film in contact with a surface that is then washed with solvent to leave behind an adsorbed layer. In the theoretical treatment, Guiselin makes two critical assumptions:²¹⁵ (i) that the melt chains initially in contact with the substrate surface have an equilibrated Gaussian distribution, which is used to define the set of chain segments in contact with the surface, and (ii) that these contact points are then “irreversible” such that each polymer segment–surface contact remains permanently bound during the solvent washing step where all unadsorbed chains are removed. It is this thought experiment that drives the experimental procedure and interpretation of results described above, where the extended annealing time at elevated temperatures prior to solvent washing is thought to be required to reach the equilibrated melt state envisioned by Guiselin and that the solvent washing procedure merely “reveals” the structure of the adsorbed layer that was formed during this melt state annealing.^{190,192,199,200,203,205,210,213}

In the remainder of this work we address whether or not this interpretation is correct: first by summarizing the extensive body of literature and understanding that was developed from the study of polymer adsorption in solution, then second by experimentally evaluating the reproducibility and reliability of forming $h_{\text{ads}}(t)$ curves as shown in Figure 3.1. As we cannot possibly evaluate all permutations of the experimental protocols used in the literature, we instead investigate the most common procedure used and address the impact of varying what we believe are the most key factors. Figure 3.2 outlines the basic set of experimental steps we will follow and evaluate for producing and measuring adsorbed layers formed from solvent washing melt annealed films. Silicon wafer substrates with a native oxide layers will be rigorously cleaned with piranha solution, or later with an HCl solution found to produce equivalent results. Other common substrate cleaning methods using organic solvents will also be addressed. Bulk films with thicknesses $h > 200$ nm of PS ($M_w = 400$ kg/mol) will be spin-coated onto the freshly cleaned substrates and then annealed above T_g under vacuum for some period of time t , most typically at 150 °C for up to 60 hours. These samples will then be washed in toluene, a good solvent, most commonly for a single 30 min wash; however, we will also explore the impact of multiple solvent washes. The final dried films remaining after the solvent washing procedure will be measured using spectroscopic ellipsometry to determine the residual adsorbed layer thickness $h_{\text{ads}}(t)$. As the evaluation of all steps will rely on the accuracy of measuring the thickness of these very thin $h_{\text{ads}}(t)$ layers, typically less than ~ 10 nm, we will start by addressing the reliability of the spectroscopic ellipsometry measurement and the data analysis of fitting to the common optical layer model of a Cauchy layer with a fixed refractive index.

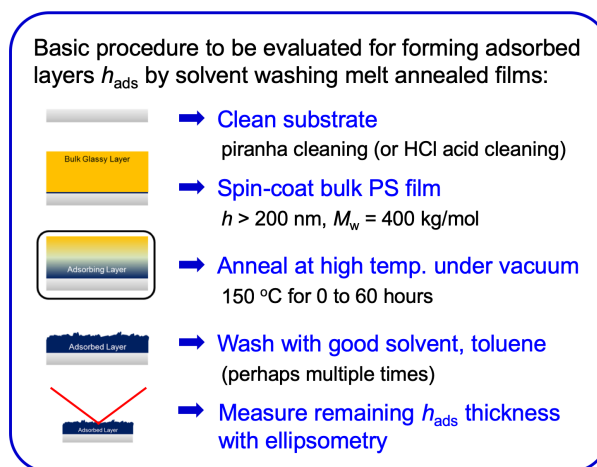


Figure 3.2: Illustration of the basic experimental steps to be evaluated for forming adsorbed layers $h_{\text{ads}}(t)$ by solvent washing films that were annealed at an elevated temperature for some length of time t .

3.1.2 Summary of the Understanding Developed of Chain Adsorption in Solution

The study of polymer adsorption has a long history with investigations dating back to the 1950s.²¹⁶ A great deal of work in the field was done from the 1970s-1990s, with major advances occurring in the experimental characterization and theoretical description of polymer adsorption in solution, culminating in the seminal 1993 book by Fler, Cohen Stuart, Scheutjens, Cosgrove, and Vincent.¹⁸⁶ There are also several excellent reviews by de Gennes,¹⁸³ Cohen Stuart and Fler,^{184,217} Granick,^{185,218} Douglas et al.,²¹⁹ and an excellent pedagogical chapter in Jones and Richards book, *Polymer Surfaces and Interfaces*.²²⁰ These early efforts on chains in solution set the stage for studies on protein adsorption where additional electrostatic interactions need to be incorporated to account for charges on both the chain and in solution.^{221,222} Surface science textbooks^{223,224} also describe numerous types of adsorption behavior for a range of different systems, with extensive work on gases demonstrating complex isotherms depending on neighboring interactions and other factors, having long since expanded beyond the original simple Langmuir adsorption model.²²⁵ In contrast, ad-

sorption isotherms for polymers are usually so steep that there is little ability to characterize features. In the present review, we focus on summarizing the understanding developed for polymer adsorption in solution that would be relevant to interpreting the experimental studies of polymer adsorption in melts. Most of this comes from the earlier literature on uncharged systems.

The basic adsorption mechanism results from a favorable energy gain for polymer segments to be in contact with the surface over a solvent molecule. This is despite an entropic conformational energy penalty for partially unfolding the chain to make these polymer segment–surface contacts. There is also translational entropy lost by an adsorbed species in contact with the surface where larger molecules can make more surface contacts per molecule for the same translational entropy loss. However this is not the primary reason why high molecular weight chains adsorb preferentially in solution; instead, the main driving force comes from the strongly reduced entropy of mixing for large chains in solution.¹⁸⁶ Overall it is the free energy balance of the entire system that makes it entropically more advantageous to have small solvent molecules free in solution with larger polymer chains at the surface, unless there is a much stronger favorable interaction between the solvent molecule and the surface.

There have been numerous theoretical approaches over the years for treating polymer adsorption to surfaces.^{186,220} The main approaches have been a self-consistent mean field theory (SCFT) treatment extensively developed by Scheutjens and Fleer,^{226,227} based on a lattice theory similar to the standard Flory-Huggins formulation for blends, and a scaling theory formulation with an initial treatment by de Gennes²²⁸ and then subsequent work by Guiselin and Aubouy.^{215,229} The scaling approach is considered better for diffuse adsorbed layers found in dilute solutions, technically only rigorously valid in the limit of long chains at very low solution concentrations.^{183,220} The concern with mean-field treatments like SCFT is that they tend to only work well for systems with weak fluctuations as in concentrated solutions and melts. However, as polymer

concentration within the adsorbed layer near the surface is usually high this may be less of a concern; mean field treatments also have the advantage of being readily adaptable computationally.²²⁰

Initially developed to explain classic adsorption experiments in solution, these models provide statistical descriptions of adsorption isotherms and segment density distributions as a function of distance from the surface for adsorbed layers in equilibrium. Chain conformations of surface attached chains are typically characterized in terms of trains, loops, and tails; terminology dating back to Jenkel and Rumbach in 1951.²¹⁶ The loop-train-tail model classifies segments of an adsorbed chain as being part of either a *train*, series of segments in direct contact with the surface, a *loop*, set of segments tethered between two adsorption points, or a *tail*, chain ends dangling into the solution (see depiction in Figure 3.3a). The classic adsorption experiments in solution characterized the amount of polymer adsorbed to a surface in the equilibrium limit for solutions of different concentration.^{186,216} Figure 3.3b depicts the typical shape of such an adsorption isotherm where the axes usually correspond to the adsorbed amount Γ as a function of bulk solution concentration c . The thickness of the resulting adsorbed layer has been experimentally found to scale with chain length as $\sim N^{0.4-0.8}$,¹⁸⁶ depending on solvent quality and the extent to which the chains stretch out into solution. For a dried film where all solvent has been removed, the resulting adsorbed layer thickness would be expected to scale as $h_{\text{ads}} \sim N^{0.5}$, as was shown in Fig. 3.1b. The adsorbed amount Γ (mass per unit area) can be determined for a dry film from its residual thickness h_{ads} based on $\Gamma = \rho h_{\text{ads}}$, where bulk density is usually assumed for ρ .^{28,202,230} One can also calculate an effective number density of chains per unit area σ_{ads} by dividing Γ by the mass of a single chain leading to $\sigma_{\text{ads}} = \rho N_A h_{\text{ads}} / M_n$, equivalent to the standard formula used for grafted chains.²²⁰

The key parameter that underpins essentially all theoretical formulations of polymer adsorption to interfaces is the adsorption energy parameter χ_s , often thought

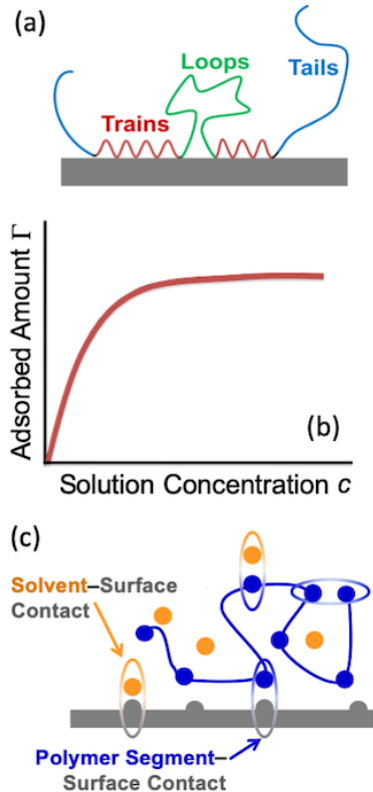


Figure 3.3: (a) Cartoon of an adsorbed chain depicting trains, loops, and tails. (b) Schematic of a classic adsorption isotherm in solution, equilibrium adsorbed amount Γ as a function of solution concentration c . (c) Diagram illustrating the different interaction energies in the system, where the segmental “sticking” energy χ_s , eq. 3.3, is defined as the difference in interaction energy between a polymer segment–surface contact and solvent–surface contact.

of as a segmental “sticking” energy for a given polymer segment to the substrate surface. Although often obscurely or abstractly defined, almost all studies cite the original definition formulated by Silberberg in 1968:^{226,231,232}

$$\chi_s = -(u_s - u_s^0)/kT, \quad (3.3)$$

where u_s and u_s^0 are the interaction energies for a polymer segment–surface contact and a solvent–surface contact, respectively. Eq. 3.3 expresses χ_s in terms of the thermal energy kT to make it unitless, similar to how the Flory-Huggins interaction parameter is defined. For polymer solution studies, the thermal energy reference

temperature was almost always room temperature, and used simply to define the energy scale, where “weak adsorption” was considered to mean χ_s is comparable to kT , while “strong adsorption” implied χ_s is several times kT .²²⁸ Granick pointed out in his 2002 Perspective¹⁸⁵ that this customary definition “implies that it [χ_s] scales with temperature, which is unlikely; it is a misleading convention, because these values are usually determined near room temperature.” In fact, the equilibrium adsorbed amount Γ is observed to decrease with increasing temperature as more thermal energy is available to overcome the likely temperature-independent χ_s adsorption energy, as was shown by Granick et al. measuring at 35 °C only 40% of the surface coverage present at 25 °C.²³³

The second issue with the χ_s definition that is frequently obscured is that the adsorption energy parameter χ_s corresponds to the *difference* in free energy to transfer a polymer segment from the bulk to the surface relative to transferring a solvent molecule from the surface to the bulk (see depiction in Figure 3.3c). In eq. 3.3, this exchange of surface contacts is written as the difference ($u_s - u_s^0$) in interaction energy between a polymer segment–surface contact u_s and a solvent–surface contact u_s^0 , with a positive χ_s corresponding to preferential adsorption of polymer segments.^{217,226,231,234} The meaning of this exchange energy is especially unclear when some texts simply define some abstract interaction parameter (e.g., δkT) to represent the “sticking” energy of the polymer chain to the substrate surface,^{228,235} frequently citing the original Silberberg paper[231] in the process.

Reference to theoretical works of polymer adsorption in solution that are formulated based on Silberberg’s definition for the adsorption energy parameter χ_s is often cited to justify adsorption in melts,^{44,192,210} even though no solvent is present in the system. Alternatively, others just assume some favorable polymer segment–surface interaction energy of $\sim kT$ without justification for there even being attractive interactions.^{138,213} However, by Silberberg’s definition for χ_s (eq. 3.3), the adsorption

energy parameter χ_s for melts with no solvent would be strictly zero as the difference in free energy would be to exchange one polymer segment–surface contact with another equivalent polymer segment–surface contact. A more proper definition of some “sticking” energy parameter χ_s for a melt system would likely benchmark the difference in interaction energy between a polymer segment–surface contact u_s with a polymer segment–segment contact in the bulk u_b^0 , although the theoretical framework would need to be revised because this does not correspond to an equivalent definition in the way eq. 3.3 is used. We also note that the main driving force for polymer segregation to surfaces in solution, the reduced miscibility of large chains in solution,¹⁸⁶ would not be applicable in melts. Leaving only this, likely weak, “sticking” energy to drive adsorption in melts against the entropy cost of unfolding the chain near the surface. Thus, unless there is some strongly favorable interaction like hydrogen bonding between the polymer segments and substrate surface, it is unclear if sufficient driving force for chain adsorption even exists in melts.

The kinetics of chain adsorption to a surface in solution has also been extensively studied.^{184,186,218} The complete adsorption process involves a number of steps: starting with bulk mass transfer of chains diffusing to the surface; the “sticking” of chains to the surface, a largely unknown process, but assumed to be very fast; subsequent changes in chain conformation of surface attached chains; and finally the exchange of surface chains with those in solution. Migration and detachment of surface attached chains are considered the slowest processes such that significant non-equilibrium effects are often observed experimentally. Initial chain adsorption to a bare surface is often treated as a “parking problem” where the first chains impinging on the surface are thought to spread out and maximize the number of segment–surface contacts made, while subsequent chains are left to occupy smaller “footprints” on the surface, filling in the remaining adsorption sites.^{185,219,236,237} This has led to the view that there can be two populations of surface attached chains, one “tightly” bound with

many surface contact points per chain and the other more “loosely” bound.^{218,236} Some experimental evidence supports this view where exchange experiments have observed two stages to desorption, an initial rapid decrease in the population of surface attached chains followed by a slower decrease at longer times, interpreted as an initial desorption of more “loosely” bound chains followed by a slower desorption of the more “tightly” bound population.^{218,234,238} However, extensive studies by Granick et al. have found that this desorption rate can depend substantially on how long after the newly adsorbed layer was formed that the exchange experiment was started.^{234,239} It appears that an extensive surface residence time of many hours can be required to equilibrate adsorbed layers in solution,²³⁹ substantially longer than the rapid time to reach constant adsorbed amount Γ ,²¹⁸ during which the number of contact points per chain will evolve. These experimental challenges of determining whether the system is in equilibrium or not substantially complicate comparisons with theory that typically assume equilibrium conditions.²¹⁸

A related conundrum has been the question of whether adsorption is reversible or irreversible, which was already deemed a long-standing dispute more than 30 years ago.¹⁸³ The classic argument for irreversibility is based on a Boltzmann factor and has the following reasoning:¹⁸³ For a given adsorbed chain with N segments, some fraction f of these segments will be in contact with the surface. Even if this fraction is small ($f \sim 0.1$), the probability of all fN segments detaching from the surface at once is exponentially small, $\sim e^{-fNU_b/kT}$, where U_b represent the appropriate sticking energy per segment. As de Gennes stated in his 1987 review,¹⁸³ “this argument is utterly wrong”, as it assumes that chain desorption must occur with all segments detaching simultaneously. However, there is nothing preventing chains from desorbing piecemeal, by unzipping from the surface with the fN bound chain segments being slowly replaced by segments from different chains.^{239,240} By no means would the displacement of all fN bound segments occur quickly, and certainly some segments will

detach and reattach multiple times, but as individual segments exchange readily over time, an adsorbed chain could easily detach from the surface and drift away into the solution. Studies by Douglas and Granick have shown that the rate limiting step is frequently diffusion of the chain away from the surface and not the energetics of surface detachment.^{241,242}

This view of reversible adsorption is supported by numerous experiments.^{184,186,238,240,243} Some of the most compelling are exchange experiments with isotopically labeled chains of equivalent molecular weight, where the concentration of radioactive chains on the surface decreases with time as equivalent, but non-radioactive chains in solution exchange with those on the surface.^{238,243} The original experimental support for the concept of irreversible adsorption was based on observations that the total adsorbed amount Γ at the surface is strongly conserved and does not decrease when adsorbed layers are rinsed with pure solvent. However, as explained by de Gennes,¹⁸³ this constancy of Γ does not represent irreversibility of adsorbed chains, but instead a strong driving force to maintain the saturation of chains at the surface in equilibrium. Even though the total adsorbed amount Γ is strongly conserved, individual chains can readily exchange.^{218,240} Experiments by van der Beek et al.^{244,245} have demonstrated that the displacement of surface bound chains can even be driven by small molecules if the “displacer” has a stronger binding energy u_s^0 to the surface than the bound polymer segment u_s , thereby reducing the adsorption energy parameter χ_s representing the difference in binding energy between the polymer segment and solvent molecule.²¹⁷

Granick’s group has done some of the most extensive characterization of the surface mobility of adsorbed chains. Direct measurements of the surface diffusion of adsorbed chains have demonstrated that surface bound chains in solution are extremely mobile.^{233,240,246–248} As would be expected, surface rearrangements occur more readily for weakly bound chains, compared to more strongly adsorbed chains.²¹⁹ The surface

mobility of chains also depends on surface coverage where molecular crowding of chains on the surface can strongly reduce the measured diffusion constant.²⁴⁶ Surface hopping of chains that detach and reattach to the surface some distance away has been directly observed with weakly bound chains.^{247,249} Even for strongly adsorbed chains with sticking energies greater than kT , chain diffusion across the surface can be readily measured.^{233,248} These strongly adsorbed systems demonstrate crawling of surface bound chains with a heterogeneous distribution of diffusion coefficients reflecting a range of chain mobilities associated with varying fractions of bound segments per chain. A given bound chain “may be adsorbed firmly even though the individual repeat units are in thermal equilibrium between the adsorbed and unadsorbed states”, meaning even strongly bound chains change conformation readily.²⁴⁰ The picture that emerges from all these experiments is that individual repeat units are not irreversibly attached, but instead, taken as a whole, the adsorbed layer in equilibrium is in essence “irreversibly” present on the surface because of the strong driving force to maintain a constant surface coverage Γ .¹⁸³

As is evident, there is a disconnect in conceptual understanding and interpretation between this older literature on chain adsorption in solution and the more recent literature on forming adsorbed layers by solvent washing melt films. We find that there is much experimental evidence from this older literature of how mobile adsorbed chains are in solution that invalidates the Guiselin assumptions in his proposed thought experiment. In particular, chains are not irreversibly adsorbed at the polymer segment level, but change conformation readily in solution even for strongly bound chains.

3.2 Experimental Methods

Silicon wafers were cleaned with one of three different procedures, all commonly used in the literature. Following most studies on chain adsorption,^{192,203,204,206,211}

piranha cleaning was done by submerging silicon wafers in a mixture of 70% by volume H_2SO_4 and 30% by volume H_2O_2 (which is itself 30 vol% H_2O_2) for 30 min, with the temperature of the solution kept between 100-120 °C. Piranha solution is a strong oxidizer commonly used to remove organics and hydroxylate the surface. After removal from the solution, the substrates were rinsed liberally in hot deionized (DI) water, then dried with N_2 gas and placed in a closed clean container. Efforts were made to spin-coat polymer films onto these substrates within 10 min to minimize substrate recontamination. Alternatively, silicon wafers were cleaned with 10 vol% hydrochloric acid (HCl) for 30 min,²⁸ before being rinsed liberally and sonicated in DI water for 5 min, then dried with N_2 gas and spin-coated within ~ 1 min. This acid cleaning procedure also removes organics and hydroxylates the surface, but is safer and logistically easier than piranha cleaning. As we demonstrate, both these acid cleaning procedures give comparable results of $h_{\text{ads}}(t)$. Some samples were also simply cleaned using toluene by dropping the solvent onto the spinning silicon wafer immediately prior to spin-coating to remove organic contaminants and dust from the surface. This limited toluene cleaning procedure is common to much of the literature on T_g confinement and other property changes in thin films when no cleaning procedure of silicon wafers is specified. It effectively recognizes that silicon wafers from the manufacturer come extremely clean, in most cases packaged in a cleanroom environment.

Polystyrene ($M_w = 400$ kg/mol, $M_w/M_n = 1.06$, Pressure Chemical) was dissolved in toluene and spin-coated onto the cleaned (2 cm \times 2 cm) Si wafers to create 200+ nm thick films. To be consistent, all samples were spin-coated at 800 rpm from 2.5 wt% solutions. However, we do not believe that differences in spin-speed or solution concentration would have a big impact on the measured adsorbed layer thickness h_{ads} formed after solvent washing because the compilation of $h_{\text{ads}}(t)$ results shown in Figure 3.1 are rather consistent (especially Fig. 3.1b) and come from a number of

different groups who would not have all used the same spin-speed and concentration. We do note that a recent study by Napolitano et al.²⁰² has shown that $h_{\text{ads}}(t)$ values do decrease with decreasing film thickness for very thin films, $h < 5\text{-}10R_g$, which is why we have consistently started with bulk 200+ nm thick films, which are $> 10R_g$ for our 400 kg/mol M_w . Samples were then annealed for 0-50+ h at 150 °C or 120 °C under vacuum, or stored at room temperature. To remove the PS film and create adsorbed layers, annealed samples were then subjected to an iterative washing procedure,^{192,203,204,210,211} with one to three toluene washings, each performed by submersing samples individually in 50 or 100 mL of toluene for 30 min in covered glass containers. After washing, samples were blown dry with N₂ gas prior to being measured by ellipsometry.

Spectroscopic ellipsometry (Woollam M-2000) was used to determine the film thickness h_{ads} of adsorbed layers. Measurements were done at three angles of incidence from 55° to 65° every 5°, after being aligned at 65°, where data at different angles were fit simultaneously. The $\Psi(\lambda)$ and $\Delta(\lambda)$ data for $\lambda = 400 - 1000$ nm were modeled using a standard three layer optical model comprised of a Cauchy layer, $n(\lambda) = A + B/\lambda^2 + C/\lambda^4$, for the polymer film atop a Si substrate with a 1.32 nm native oxide layer, where this native oxide thickness was determined from the average of measurements on three 4-inch diameter wafers at five different points. Because ellipsometry has difficulty independently resolving thickness and index of refraction for very thin films less than ~ 10 nm,^{212,250} the index of refraction was held constant at values of $A = 1.563$, $B = 0.0079$, and $C = 0.00038$, based on an average over multiple PS films of bulk thickness.¹⁶⁰ Note, these Cauchy parameter values of A , B , and C are quoted for the wavelength λ in microns following the common convention used within the Woollam software.

3.3 Results and Discussion

We now evaluate experimentally the reproducibility and reliability of forming adsorbed layers by solvent washing melt films, following the most commonly used protocol in the literature (depicted in Fig. 3.2). Section 3.3.1 starts with ascertaining the reliability of using ellipsometry to accurately measure the absolute thickness of h_{ads} corresponding to very thin films $\lesssim 10$ nm, as well as the accuracy with which zero thickness of h_{ads} can be verifiably established. From these control tests we determined that a single measurement of h_{ads} is accurate to within ± 0.2 nm (which defines the symbol size used for h_{ads} in all subsequent figures), and that an adsorbed layer thickness h_{ads} below 0.24 nm is impossible to distinguish from zero. This minimum adsorbed amount we find reliably measurable is represented by a gray bar at a level of $h_{\text{ads}} = 0.24$ nm in Figures 3.4, 3.5, 3.7 and 3.8. Section 3.3.2 then addresses the reproducibility and reliability of creating $h_{\text{ads}}(t)$ curves as depicted in Fig. 3.1a following the experimental protocols outlined in the literature. We discuss the various experimental factors found to affect this process and provide some interpretation for the unexpected variability. Section 3.3.3 continues with addressing the impact of multiple solvent washing stages, as well as the initial substrate preparation and cleaning method. Section 3.3.4 evaluates the film average glass transition temperature $T_g(h)$ and physical aging rate β for $h \approx 30$ nm thick films made with and without varying h_{ads} layers. We end with a summary and discussion of the implications of our findings with respect to the existing literature in thin films and polymer nanocomposites, and provide an outline of open questions still remaining to be addressed.

3.3.1 Reliability of Measuring Adsorbed Layer Thickness h_{ads} with Ellipsometry

As we are interested in investigating the reproducibility of forming adsorbed layers, we start by determining the accuracy and error with which ellipsometry can reliably measure the absolute thickness h_{ads} of such thin films. It is well known that ellipsometry has difficulty accurately measuring very thin films $\lesssim 10$ nm because the signal becomes primarily determined by the reflection at the interfaces when the path length of the light through the film becomes much less than the wavelength λ , minimizing the dispersion (wavelength dependence) contribution to the change in polarization.^{212,250} This is often illustrated using Δ vs. Ψ plots where, for a given angle of incidence, the trajectories of different curves, corresponding to different refractive index values of the film, converge to the same film-free point as the film thickness decreases to zero.²⁵⁰ We address this limitation by measuring three different angles of incidence (55° , 60° , 65°) for each sample, and globally fitting $\Psi(\lambda)$ and $\Delta(\lambda)$ values at all three angles for the wavelength range $\lambda = 400 - 1000$ nm to an optical layer model of a PS film on silicon. Following what is typically done for very thin films ($h \lesssim 10$ nm), we hold the index of refraction $n(\lambda)$ Cauchy parameters fixed at the bulk value.

Since there is always some uncertainty with which bulk refractive index values can be known, one could ask how sensitive the measured h_{ads} values are to the particular bulk value used. The Cauchy parameter values we determined from an average of multiple bulk samples have average and standard deviations of $A \pm \Delta A = 1.563 \pm 0.004$ and $B \pm \Delta B = 0.0079 \pm 0.0004$. (As the fitting is quite insensitive to the Cauchy C parameter, it was simply held fixed at the bulk value, $C = 0.00038$, although it quite reasonably could have been held fixed at zero too.) When we vary the Cauchy A and B parameters within one standard deviation of their bulk values ($\pm \Delta A, \pm \Delta B$), we find the measured values of h_{ads} vary by less than ± 0.01 nm. This demonstrates that the best fit values for h_{ads} are not particularly sensitive to the specific refractive index

values chosen, assuming they are appropriate bulk values. We note that some works have suggested that adsorbed layers could have different properties from bulk, e.g., increased density,^{136,192,194,204,210,251} such that the choice of using bulk values for $n(\lambda)$ parameters may not be the most appropriate. However, given that these suggested property differences are still uncertain, bulk refractive index parameters seem to be the most reasonable to use. The choice of bulk parameters is supported by the works of Napolitano et al.^{199,202} and Tsui et al.²¹¹, which demonstrated film thickness values for adsorbed layers measured by AFM gave the same results to those measured by ellipsometry using a fixed *bulk* value for $n(\lambda)$ during their layer model fitting. We have also done some AFM measurements verifying that h_{ads} thickness values by ellipsometry match. However, with its larger spot size, ellipsometry does a better job of characterizing the adsorbed layer thickness across the sample surface than AFM which is restricted to a small area. We do note that similar to previous reports we observe some dewetting of the h_{ads} layers after solvent washing.^{204,206,252} All together these holes make up less than 10 % of the total surface area for very thin films < 4 nm, and less than 1 % of the total surface area for thicker films. The ellipsometer beam size on the sample spans a few mm by few mm thus easily averaging over these small holes.

It is well known that the largest instrument error associated with measuring the absolute film thickness with ellipsometry is often associated with the precision with which the angle of incidence to the sample is known.^{212,253} As this angle can be readily affected by sample tilt and alignment that can easily vary slightly from measurement-to-measurement or sample-to-sample due to anything from dust on the back of the sample to an individual researcher's alignment protocol, a series of different samples were measured repeatedly under varying conditions. We found that the error associated with measuring the thickness of a single sample is ± 0.13 nm on average with a maximum value of ± 0.17 nm. Thus, we conservatively conclude that the error in h_{ads}

for any given measurement of a sample is ± 0.2 nm, and have consequently chosen to depict the size of the symbols (error bars) associated with any single measurement of h_{ads} as this value on the figures in this study.

Another point of consideration is the uncertainty associated with measuring zero h_{ads} adsorbed layer thickness, particularly because we aim to characterize the presence or absence of adsorbed layers. All silicon wafers have a native oxide layer that naturally forms when the silicon is exposed to oxygen in the atmosphere. Although technically this native oxide layer has a gradient composition, it is typically fit in ellipsometer optical layer models as a homogeneous SiOx layer atop the silicon with a thickness varying between 1-2 nm in the literature. We specifically measured the thickness of the native oxide layer of our silicon wafers to be $h_{\text{SiOx}} = 1.32 \pm 0.03$ nm (based on an average of five measurements each at different locations on three different 4-inch diameter wafers) using a homogeneous SiOx layer with standard optical constants from Ref. 254 provided by Woollam in our ellipsometer software. This h_{SiOx} value was for a single batch of silicon wafers at one point in time. Our lab has also previously done this test a few years prior finding¹⁶⁰ $h_{\text{SiOx}} = 1.25$ nm and several years before that measuring²⁹ $h_{\text{SiOx}} = 2$ nm. Thus, for any given batch of silicon wafers (all purchased from the same supplier), it would not be unusual for the SiOx native oxide layer thickness h_{SiOx} to vary between 1.25-2 nm. As the refractive index parameters for SiOx are not that distinct from that for the polymer, a variation in the native oxide layer thickness h_{SiOx} will affect the measured adsorbed layer thickness h_{ads} , especially influencing the thickness of h_{ads} that would be considered zero. If we take a bare silicon wafer, for which we know there is no adsorbed polymer, and vary the h_{SiOx} layer thickness in the optical model between 1.25-2 nm, we find that the optical model fit returns an adsorbed layer thickness h_{ads} of up to 0.24 nm. Thus, we conclude that any adsorbed layer thickness h_{ads} below 0.24 nm is impossible to distinguish from natural variations in the native oxide layer thickness. We note that

this value is close to, but above the ± 0.2 nm error we determined above for a single ellipsometry measurement of h_{ads} . To indicate this uncertainty in measuring zero h_{ads} adsorbed layer thickness, we have added a gray bar to Figures 3.4, 3.5, 3.7 and 3.8 at a level of $h_{\text{ads}} = 0.24$ nm, which represents the minimum adsorbed amount we find reliably measurable.

3.3.2 Reproducibility of Measuring Adsorbed Layer Thickness h_{ads}

With a solid foundation from Section 3.3.1 of how reliable a single ellipsometry measurement of h_{ads} is and how accurate zero thickness can be determined, we proceed now with evaluating the reproducibility of forming adsorbed layers by solvent washing melt films. We follow the sample preparation protocol depicted in Figure 3.2 representing that most commonly used in the literature with h_{ads} evaluated as a function of annealing time at an elevated temperature above T_g . Figure 3.4 shows a plot of adsorbed layer thickness h_{ads} versus annealing time at 150 °C under vacuum for PS films (>200 nm thick, $M_w = 400$ kg/mol, $M_w/M_n = 1.06$) spin-coated onto piranha cleaned silicon wafers. Each open symbol in the graph represents an individual sample where the value h_{ads} measured by ellipsometry was determined after a single wash of the sample for 30 min in 100 mL of toluene (a good solvent). This corresponds to the solvent washing procedure most frequently used in the literature that uses either one 30-min wash or 3+ 10-min washes in toluene.^{192,199,201,206,210,211} We have verified that a single 30 min wash gives the same final adsorbed layer thickness h_{ads} as three repeated washings of 10 min each.

Because of experimental limitations in the number of 2 cm \times 2 cm silicon wafer pieces that can be piranha cleaned at one time, samples were prepared in batches with a maximum of 15 samples at a time. The maximum batch size was dictated by safety concerns about the amount of acid being used, as well as the logistics of

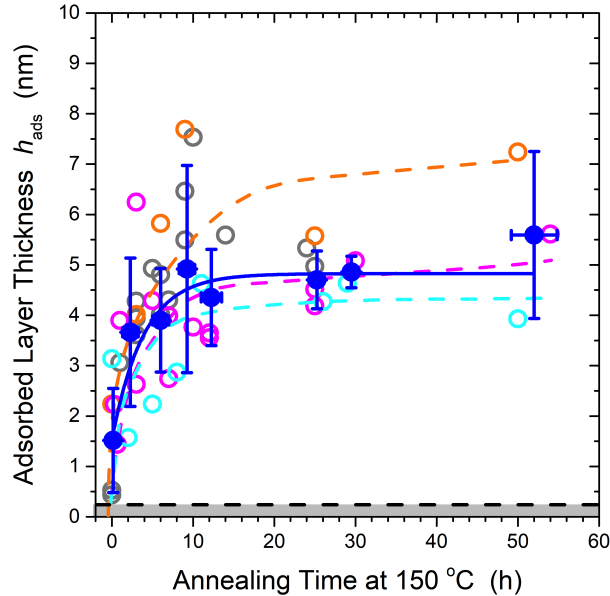


Figure 3.4: Reproducibility of the measured adsorbed layer thickness h_{ads} as a function of time the film was annealed at 150 °C under vacuum prior to solvent washing for 30 min in toluene. Data are for PS films (>200 nm thick, $M_w = 400$ kg/mol) spin-coated onto piranha cleaned silicon wafers, where the symbol size represents the error of ± 0.2 nm for an individual ellipsometry measurement of h_{ads} , while the gray bar and dashed line across the bottom of the graph represent the uncertainty in measuring zero adsorbed layer thickness, $h_{\text{ads}} \leq 0.24$ nm. Open symbols highlighted in orange, cyan, and magenta are for individual batches of samples that were piranha cleaned and measured together, where dashed curves are drawn to guide the eye through the trends in the individual batches. Gray open symbols represent data from other batches collected. Solid blue symbols and associated error bars are the average and standard deviation for all batches binned together where the solid blue curve is a fit to eq. 3.4, the most simple functional form used in the literature for $h_{\text{ads}}(t)$.

minimizing the time between cleaning and spin-coating in order to prevent possible contamination of the freshly cleaned substrates. Batch sizes were also frequently smaller than the maximum batch size to help better control the quality of samples. In Figure 3.4, three batches have been highlighted in orange, cyan, and magenta, where data from additional batches are simply shown in gray. Dashed curves have been drawn to guide the eye through the trends of each highlighted batch. Although all batches show a similar trend, there is considerable variability from batch to batch, even though all were collected under nominally identical conditions. This batch-to-batch variability is noticeably larger than the ± 0.6 nm error in sample-to-sample

reproducibility within a batch (see discussion below of Fig. 3.8) and the ± 0.2 nm single measurement error described above. Although the different batches in Figure 3.4 show qualitatively similar trends, there are significant quantitative differences such that a quantified $h_{\text{ads}}(t)$ trend determined from an analysis of the data would be highly dependent on the amount of data and, in particular, the number of batches collected.

To overcome this batch-to-batch variability in order to quantify trends in $h_{\text{ads}}(t)$, we bin together the data for similar annealing times from different batches, where the solid blue data in Figure 3.4 represent the average and standard deviation of this binned data. The binned data show that the adsorbed layer thickness h_{ads} increases with increasing annealing time and saturates out at some long time value, consistent with literature reports as depicted in Figure 3.1.^{192,199,200,206,210,211} Following what seems most reasonable from other studies,^{190,192,200,206,210,211,213} we fit the solid blue binned data to a function of the form

$$h_{\text{ads}}(t) = \Delta h(1 - e^{-t/\tau}) + h_0 \quad (3.4)$$

to describe the increase in h_{ads} observed with increasing annealing time, where the long-term plateau $h_{\text{ads}}(t = \infty) = \Delta h + h_0$ is given by two constants. The initial thickness at zero annealing time, $h_{\text{ads}}(t = 0) = h_0$, accounts for the uncertainty in measuring zero adsorbed layer thickness as described above, and that not all polymer chains may be completely washed off even for films that were never annealed (as demonstrated below in Fig. 3.8). The best fit parameters for the blue curve shown in Figure 3.4 are $h_0 = 1.5 \pm 0.4$ nm, $\Delta h = 3.3 \pm 0.4$ nm, and $\tau = 4 \pm 1$ h, with the long-term plateau corresponding to $h_{\text{ads}}(t = \infty) = \Delta h + h_0 = 4.8 \pm 0.8$ nm. Note that if the individual batches are fit separately to eq. 3.4, the variability in the parameters would be significant, with τ varying by more than an order of magnitude.

When we first started to reproduce curves of $h_{\text{ads}}(t)$ following the basic litera-

ture protocol outlined in Figure 3.2, we did not get as reproducible data as shown in Figure 3.4. Figure 3.5 shows a second graph of adsorbed layer thickness h_{ads} versus annealing time at 150 °C where the black open symbols are data collected by two separate people following the Fig. 3.2 literature protocol, but without particular attention paid to collecting data in consistent batches with progressively increasing annealing time within the batch. The data shown in Figure 3.5 were often collected under conditions where several samples within a batch were intended to fill-in data on the graph at particular annealing times. For efficiency, it was common to solvent wash a group of samples at the same time resulting in samples frequently being left in a drawer overnight (or even a weekend) after or even prior to annealing at 150 °C for a few hours. As can be seen in Figure 3.5, this produces $h_{\text{ads}}(t)$ values with considerably more scatter than that shown in Figure 3.4. (For reference, the blue binned data of Fig. 3.4 are also plotted on Fig. 3.5.) After considerable sleuthing, we determined that time spent by samples ‘sitting in a drawer’ either prior to or after annealing at 150 °C, before solvent washing, have a large and reproducible impact on the measured h_{ads} thickness after solvent washing. Figure 3.5 highlights purple data for which the time spent by the samples ‘sitting in a drawer’ prior to annealing at 150 °C was systematically increased from zero to 3, 6, 9, 24 hours (open-crossed diamonds) and 48 hours (solid diamonds), where the data clearly show a progressive increase in h_{ads} thickness with increasing time ‘sitting in a drawer’. For these samples, we specifically ensured that the samples were solvent washed immediately after annealing at 150 °C. We separately found that time ‘sitting in a drawer’ after annealing at 150 °C also tended to increase the measured h_{ads} thickness after solvent washing. In contrast, the data shown in Figure 3.4 are for samples where we specifically ensured that the samples were not left ‘sitting in a drawer’ either prior to or after annealing at 150 °C.

What is particularly perplexing about the purple data highlighted in Figure 3.5 where the samples were simply left in a drawer prior to annealing at 150 °C, is that

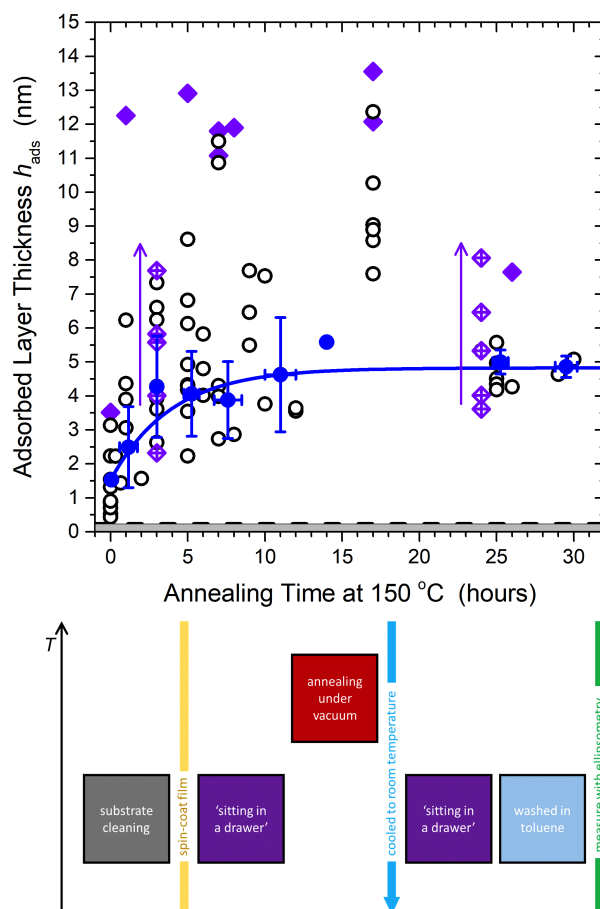


Figure 3.5: Wider range of adsorbed layer thickness h_{ads} data (black open circles) plotted as a function of time the film was annealed at 150 °C under vacuum prior to solvent washing for 30 min in toluene, where no particular effort was done to make the samples in batches or minimized the time between steps in the experimental protocol outlined in Fig. 3.2. In contrast, the solid blue data and error bars are the binned data from Fig. 3.4 where effort was made to minimize the time samples spent ‘sitting in a drawer’ either prior to or after the annealing step at 150 °C. Purple data highlight the increase in h_{ads} observed when the time spent ‘sitting in a drawer’ prior to the thermal annealing step is systematically increase from zero to 3, 6, 9, 24 hours (open crossed diamonds) and at 48 hours (solid purple diamonds). Again data are for PS films (>200 nm thick, $M_w = 400$ kg/mol) spin-coated onto piranha cleaned silicon wafers, where the symbol size represents the error of ± 0.2 nm for an individual ellipsometry measurement of h_{ads} , while the gray bar and dashed line across the bottom of the graph represent the uncertainty in measuring zero adsorbed layer thickness, $h_{\text{ads}} \leq 0.24$ nm.

one would expect that the extended annealing at 150 °C, a temperature well above T_g , would erase all thermal history of the sample. It is well known that glassy poly-

mer films undergo physical aging (densification) as a function of time, even at room temperature ‘sitting in a drawer’. Typically in experimental studies we do not pay particular attention to this because the amount of aging that occurs is minimal and most experiments start with an annealing step immediately prior to data collection to reset the thermal history of the sample. However, in this case, we find that this aging at room temperature has an impact on the ability of the solvent to wash away the film. We can rationalize this observation by recognizing that the ability of the solvent washing step to remove chains from the glassy polymer film will depend on how much the film has densified.

Dissolving of glassy polymer films with solvent typically occurs through a Case-II diffusion process^{220,255–257} where the solvent must first penetrate and swell the glassy material through a diffusion front before there is sufficient mobility of the chains to be dissolved away. The speed of this dissolution process will be reduced for films that have undergone densification due to physical aging of the glassy film.^{258,259} For the purple data shown in Fig. 3.5, the time ‘sitting in a drawer’ prior to annealing at 150 °C occurs after spin-coating. These glassy films formed by a solvent quench initially contain a significantly reduced density as the glassy film solidified during spin-coating when solvent was still present in the film, after which the solvent evaporated leaving behind voids. Thus, these solvent-quenched glassy films would be expected to undergo a significant amount of densification over time ‘sitting in a drawer’. Similarly, films stored in a drawer after the annealing step at 150 °C will undergo physical aging after their thermal quench to room temperature, also densifying over time.

Figure 3.6 compares the densification of bulk PS films after a solvent and thermal quench into the glassy state by plotting normalized film thickness h/h_0 as a function of aging time on a logarithmic axis. The solvent quenched data are for a sample placed on the ellipsometer at near room temperature (30 °C) immediately after spin-coating, while the thermally quenched data show a traditional physical aging curve at

an aging temperature of 40 °C, a near room temperature value, and at 65 °C, where the maximum in aging rate occurs.^{38,253} Both curves in Figure 3.6 were normalized to their respective film thicknesses at 10 min after the quench process such that the y -axis provides a measure of the film's percentage decrease in thickness. Freshly spin-coated films show a large ~ 3.5 % decrease in film thickness immediately after spin-coating, which is significantly larger than the ~ 0.5 % decrease for film that undergo a thermal quench from the equilibrium liquid state. This is because spin-coated films undergo vitrification into the glassy state via a solvent quench while some solvent is still present in the film, which then evaporates out of the film leaving behind voids that then collapse over time. The thermally quenched film, in contrast, has no such voids and thus the resulting time-dependent densification after vitrification is much less. A similar comparison was published previously by Keddie et al.^{260,261} for solvent and thermally quenched PMMA films also demonstrating a much larger densification for solvent-quenched vs. temperature quenched films. Note that we chose to normalize the data in Fig. 3.6 at the $h(t)$ curve's initial value h_0 because this value is well defined. However, in the long time limit $h(t \rightarrow \infty)$ all curves tend towards the same equilibrium value for a given temperature,^{260,262} but as this long time equilibrium limit cannot be reached experimentally, it is less well defined.²⁵³ The data in Fig. 3.6 should not be misinterpreted to imply that solvent quenched films are denser than thermally quenched films; in fact, the opposite is true.²⁶⁰

We believe this densification of solvent-quenched films at room temperature explains why films with zero hours of annealing at 150 °C show a larger h_{ads} thickness if left 'sitting in a drawer' for some length of time. Such densification would significantly slow solvent penetration and swelling of the glassy film, making it harder to wash off. For a given 30-min solvent washing procedure, a larger h_{ads} layer would remain. This interpretation is consistent with data by Koga et al. (inset of Fig. 1 in Ref. 210) showing that the maximum adsorbed layer thickness reached at long times

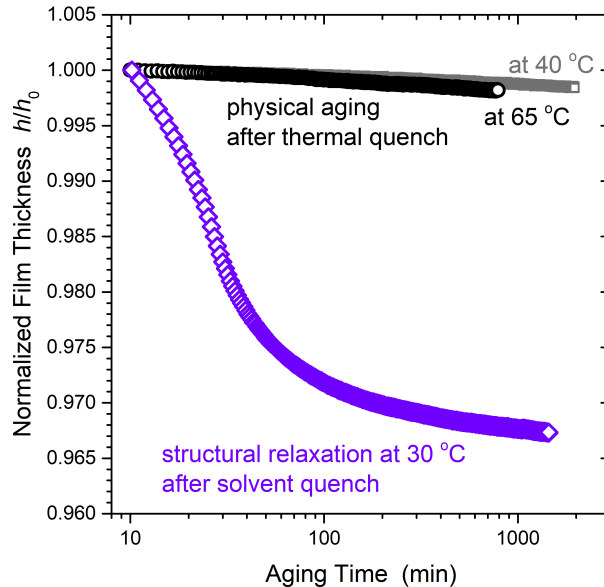


Figure 3.6: Decrease in film thickness h , normalized to the initial thickness h_0 , observed for bulk PS films ($M_w = 400$ kg/mol) as a function of aging time demonstrating the densification of the film that occurs following a solvent quench (purple diamonds) where the film immediately after spin-coating was placed on the ellipsometer hot stage held at 30 °C, compared to an equivalent film that underwent a thermal quench from 120 °C to an aging temperature of either 40 °C (gray squares) or 65 °C (black circles), the temperature at which the physical aging rate is maximum.

$h_{\text{ads}}(t = \infty)$ is independent of annealing temperature from 140 °C all the way down to 40 °C (near room temperature). These data demonstrate that annealing above T_g is clearly unnecessary to form adsorbed layers by solvent washing films off substrates.

The interpretation of why densification of solvent-quenched films when ‘sitting in a drawer’ *prior to* annealing at 150 °C also leads to larger h_{ads} thicknesses is less clear. By examining the data in Fig. 3.5, it appears that extended annealing of films at elevated temperatures above T_g (>20 h at 150 °C) leads to less variation in the residual $h_{\text{ads}}(t)$ thickness remaining after solvent washing, where perhaps the sample history of ‘sitting in a drawer’ prior to annealing is slowly erased. This slow evolution of the $h_{\text{ads}}(t)$ data at long annealing times is suggestive of a slow restructuring of chains within the film that may be occurring near the substrate interface, where perhaps the fraction of chains with monomers in contact with the substrate interface

may be changing. It would be reasonable to conclude that films which were densified significantly after solvent quenching by ‘sitting in a drawer’ prior to being thermally annealed may have considerably slower exchange kinetics of monomers in contact with the substrate. Studies of chain diffusion near substrates have reported slower than bulk dynamics,^{263–265} which would be consistent with this interpretation. However, these $h_{\text{ads}}(t)$ values are for films that were rinsed with a specific solvent washing protocol (30 min in toluene), which makes the interpretation of any restructuring of chain conformations that could be occurring in the film during annealing indirect as what is actually being measured is the ability of this solvent washing protocol to swell and rinse off the glassy film resulting from this sample history and annealing protocol. A more direct approach to investigating such questions would be to directly measure the exchange kinetics at elevated temperatures with something like neutron scattering, an experiment which has been done recently by Kumar et al. for poly(2-vinyl pyridine) (P2VP) chains bound to silica nanoparticles.²⁶⁶ For this strongly attractive hydrogen bonding system, they observed a strong temperature dependence where surface bound $d3$ -P2VP chains slowly exchanged with h -P2VP chains in the matrix over ~ 10 hours at 175 °C, but not after 1000 h at only 150 °C.

We recognize that our Figures 3.4 and 3.5 look substantially different from the $h_{\text{ads}}(t)$ curves previously shown in the literature, as summarized in Figure 3.1. This may be because other studies likely only collect one batch of data^{192,210,211,267} or only graph binned data.^{199,200,206} The only statement we have found in the existing literature that acknowledges that some samples may not infrequently have much larger or different h_{ads} values is in a recent paper by Napolitano et al. that specifically discussed sample preparation and analysis details with a section on data handling stating:²⁰⁰

“In order to consistently obtain the adsorption kinetic parameters in Equation 1 [eq. 3.2 in Section 3.1.1], a number of steps is necessary for a proper

analysis of the data sets (h_{ads} as a function of annealing time) experimentally determined. First, the quality of the data is significantly improved by averaging several measurements of samples prepared within identical conditions (annealing temperature, type of substrate) and history (same annealing times). When averaging, dataset clear outliers, e.g. resulting from improper handling of a sample, must be discarded. This can be achieved by fitting a single saturating exponential to the data (i.e. $h_{\text{ads}} = h_0 + \Delta h[1 - \exp(-t/t_{\text{ads}})]$ where $h_\infty = h_0 + \Delta h$ and t_{ads} is the characteristic time of the process) [eq. 3.4 above]. This fit can be used to eliminate outliers in the data set (i.e. $|h_{\text{ads}} - h_{\text{fit}}| > 3\sigma$), in addition to provide a good estimate of the equilibrium adsorbed thickness h_∞ . The uncertainty in the fit for h_∞ can be used to discard data-sets in which the annealing time was insufficient to achieve an equilibrium saturated value.”

This suggests to us that others have also observed considerable variability in the measured $h_{\text{ads}}(t)$ values after solvent washing, perhaps from similar variables we have described in this section, but have instead chosen to interpret it in a different manner. In our view, we would be concerned with this data analysis procedure described in the quoted text where $h_{\text{ads}}(t)$ data, perhaps comparable to those shown in Figures 3.4 or 3.5, were first fit to eq. 3.4 (a three parameter fit) and used to discard data which fall outside of 3σ , prior to performing a second fit on the remaining data to a more complicated two-stage functional form, eq. 3.2 with five fitting parameters.

From our experimental investigations, we find that the $h_{\text{ads}}(t)$ results are strongly impacted by the solvent washing protocol used and the prior history of the sample, consistent with the interpretation that denser films require longer for a given solvent to swell and wash off the glassy polymer film. Even though averaging and binning of data do result in much nicer looking $h_{\text{ads}}(t)$ curves closer to those compiled in Figure 3.1a, we question whether this protocol meaningfully reveals information about the state

of the melt film prior to solvent washing. As we will demonstrate in the next section, continued solvent washing also further alters the measured $h_{\text{ads}}(t)$ values consistent with restructuring of the adsorbed polymer chains in solution as previously reported in the earlier literature.

3.3.3 Impact of Multiple of Washings and Substrate Cleaning Method on Adsorbed Layer Thickness h_{ads}

We look now at the impact of multiple solvent washings on the $h_{\text{ads}}(t)$ trends given that several studies,^{192,203,204,206,210,211} especially those by Koga et al.,^{192,203,204,210} have done multiple washing believing these procedures to provide more information about the adsorbed layer structure. As it is logistically cumbersome to collect multiple batches of data each time, we proceed now with our discussion using only a single batch of data to represent the trends we observe recognizing that trends will be qualitatively similar if another batch were collected, but likely have quantitative differences. We also return now to the experimental protocol used in the collection of data for Figure 3.4 where we ensure samples were annealed and washed immediately after each step, without any time spent ‘sitting in a drawer’, the protocol which we believe produces data that most closely resembles that shown in the literature. Figure 3.7 shows the $h_{\text{ads}}(t)$ trend for a single batch of data upon repetitive washing, with the open, half-filled, and filled symbols representing the first, second, and third 30-min wash in 100 mL of fresh toluene, respectively. The curves shown, included as guides to the eye through each dataset, demonstrate that $h_{\text{ads}}(t)$ decreases progressively with each subsequent washing. This decrease in the adsorbed layer thickness with only a few increasing repetitions of washing indicates that the continued washing of annealed samples affects the final adsorbed layer amount, even those samples annealed for long times. However, the overall trend of increasing adsorbed layer thickness with increasing annealing time remains unchanged, indicating that at longer annealing times the

removal of the polymer film by solvent washing is more challenging.

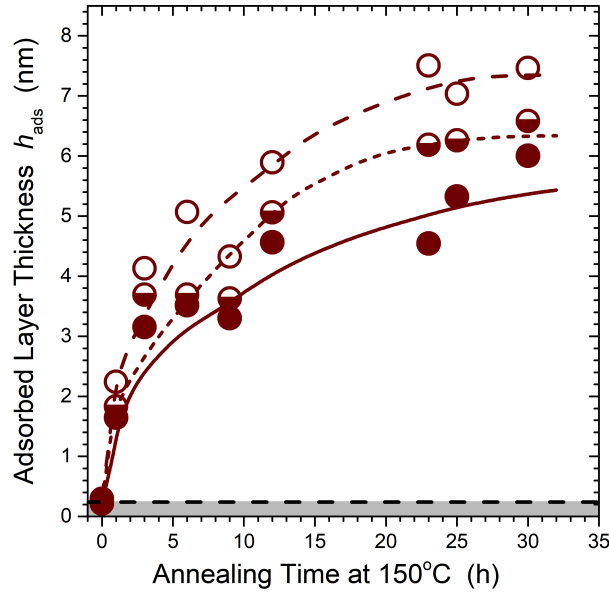


Figure 3.7: Plots of the adsorbed layer thickness $h_{\text{ads}}(t)$ as a function of annealing time at 150 °C under vacuum for PS films (>200 nm thick, $M_w = 400$ kg/mol) on HCl acid cleaned silicon wafers (made as a single batch) where the films were subsequently solvent washed in 100 mL toluene for 30 min once (open circles), twice (half-filled circles), or three times (filled circles). The curves through the data are guides to the eye indicating the general trend of a progressive decrease in the $h_{\text{ads}}(t)$ curve with increasing number of washes. Again the symbol size represents the error of ± 0.2 nm for an individual ellipsometry measurement of h_{ads} , while the gray bar and dashed line across the bottom of the graph represent the uncertainty in measuring zero adsorbed layer thickness, $h_{\text{ads}} \leq 0.24$ nm.

These data naturally lead to the question that if only a few repetitive washings have such a significant impact on the measured $h_{\text{ads}}(t)$ adsorbed layer thickness, what does this procedure inform us about the state of the melt film prior to solvent washing? Proponents of chain adsorption in the melt argue that solvent washing films in a good solvent like toluene removes the unattached chains leaving behind only the “irreversibly adsorbed” chains.^{138,190,193,195,199–204} This is a procedure that has been termed “Guiselin’s experiment” or “Guiselin’s approach”, based on Guiselin’s theoretical assumption²¹⁵ that chain segments in contact with the substrate interface in a film are irreversibly adsorbed and his proposition that solvent washing could remove unattached chains to access this adsorbed layer from the melt. Koga et al.

argues that further solvent washing (150 days in toluene²¹⁰ or a couple of days in a stronger solvent such as chloroform¹⁹²) “reveals” additional buried structure of the adsorbed layer in the melt that they have termed “flattened layers”.^{192,203,210}

The Guiselin paper cited²¹⁵ is a theoretical study following the scaling analysis methods of Alexander²⁶⁸ and de Gennes²⁶⁹ for grafted chains in solution, where Guiselin uses similar scaling arguments to calculate the concentration profile of irreversibly adsorbed chains in a good solvent. To make the theoretical analysis possible, Guiselin assumes there are a set of chain segments permanently fixed to the surface, the set of which is determined by the random walk (Gaussian) statistics of chains in an initially concentrated solution or melt. The analysis relies on the theoretical assumption that all points in contact with the surface become permanently (or irreversibly) adsorbed, while all other chains not in direct contact with the surface can be removed without changing the initial permanent set of contact points. Guiselin proposes that this could potentially be achieved experimentally by washing out unattached chains with pure solvent, arguing this would be valid in the limit of strong adsorption sites.²¹⁵ However, this theoretical case treated by Guiselin requires chains be sufficiently *mobile* in the initial concentrated solution or melt state to allow equilibrium Gaussian random walk chain conformations to be achieved, yet then be subsequently sufficiently *immobile* in the good solvent state to produce permanent, irreversibly adsorbed chain segments. Experimentally such a mobile-then-immobile situation could only be realistically achieved with some form of chemical bonding or grafting, as in the case of polydimethylsiloxane (PDMS) that can crosslink with silica substrates when heated to elevated temperatures, producing what is known as a “pseudobrush”.²⁷⁰

Durning and O’Shaughnessy²¹⁴ appear to be the first to attempt an experimental realization of Guiselin’s mobile-then-immobile thought experiment, which they recognized would be “difficult to achieve in practice”. They stated:²¹⁴ “In principle, one has

to equilibrate the melt or dense solution against an inert solid surface and then, by some means, suddenly and permanently fix only the segments currently adsorbed.” For their experiments they selected a PMMA/quartz/benzene system because the segmental sticking energy would be of order several kT . PMMA films on quartz were annealed at 165 °C for up to 120 h in an argon atmosphere, and subsequently washed with benzene three times for 3 h, followed by sonicating for 5-10 min. The extended annealing at 165 °C was believed to be necessary and sufficient to obtain reflected random walk statistics of chain conformations in the melt prior to solvent washing, with the hydrogen bonding between PMMA and the quartz surface then strong enough to prevent rearrangement of bound chains during solvent washing. A later review by O’Shaughnessy and Vavylonis²⁷¹ cautioned that these “experiments raise two important issues which deserve further study: (1) Guiselin’s thought experiment which envisions the instantaneous freezing-in of equilibrium melt configurations in practice may require annealing over large timescales for many experimental realizations. If the Guiselin predictions are to apply, this timescale, which depends on these unknown chain dynamics, must be large enough for any non-equilibrium configurations generated at the interface during melt deposition to have disappeared. (2) After swelling by solvent, one expects desorption–readsorption events and slow chain movements.”

Experimental works have shown that these two mobile-then-immobile requirements for Guiselin’s thought experiment are mutually exclusive, and appear to be experimentally unviable. The polymer solution literature summarized in Section 3.1.2 has extensively demonstrated that polymer chain segments adsorbed on a surface are extremely mobile, readily desorbing and readsorbing, even for the case of strong adsorption where the segment-substrate interaction strengths are several kT .²³³ Experiments have measured the surface diffusion of adsorbed chains in solution translating across the surface via crawling and hopping mechanisms,^{233,246–249} and readily exchanging with other species in solution.^{184,186,217–219,238,240,243–245} Thus, it is well

documented that the structure of surface bound chains and their segment–surface contacts change quickly in solution.

Rearrangement of segment–surface contacts in a melt state is more challenging to interrogate experimentally and many open questions remain. As argued in Section 3.1.2, the adsorption energy parameter χ_s as defined in most adsorption theories, eq. 3.3, would be strictly zero in a melt system with no solvent present; thus, simple analogies with solution treatments cannot be made. Certainly dynamics in a melt will be slower than that in solution. Several studies have demonstrated slower than bulk diffusion for PS chains near silica substrates,^{134,191,263–265} attributed to segment–surface contacts increasing the friction for reptation,^{263,264} with effects reaching extended distances from the interface.^{134,264} Most recently, Kumar et al. have investigated the exchange lifetime of surface bound P2VP chains to silica nanoparticles at elevated temperatures, with results suggesting that in such strongly favorable systems, surface bound chains can persist for weeks at 150 °C.²⁶⁶ Dielectric measurements by Sokolov et al. have also found that the segmental mobility $\tau(T)$ of P2VP near silica nanoparticle interfaces is two orders of magnitude slower than bulk with a slightly weaker temperature dependence.⁸⁰ Thus, achieving equilibration of chain conformations in a melt state in the Guiselin sense seems doubtful.

The older literature on polymer adsorption in solution noted the importance of substrate cleanliness on the resulting adsorbed layer amounts, where Granick et al. in particular examined how various substrate treatments and cleaning methods altered the resulting chain adsorption.²⁷² This is also true for the h_{ads} thicknesses obtained from solvent washing melt films, as is shown in Fig. 3.1b, where HF treatment consistently results in larger h_{ads} layers than substrates cleaned with piranha solution, for a given nominally equivalent solvent washing procedure. HF treated silicon results in an altered surface chemistry of Si–H, while piranha cleaning simply oxidizes the organics on the surface such that they can be readily washed off with water, and thus

leaves the SiO_x/Si surface chemistry of the silicon unchanged. The piranha solution is a mixture of concentrated H₂SO₄ and H₂O₂ that results in an exothermic reaction that can easily reach temperatures in excess of 120 °C, and as such it becomes highly hazardous and potentially explosive. Most publications actually note safety warnings associated with using piranha mixtures. We have found that HCl is a much safer acid mixture for substrate cleaning that also strongly oxidizes organics and leaves the silicon hydrolyzed. Figure 3.8 compares the adsorbed layer thicknesses h_{ads} measured after one, two, and three 30-min toluene washes for substrates cleaned with different methods. All films were vacuum annealed for 13 hours at either 150 °C or 120 °C, as indicated. The data demonstrate that our safer HCl cleaning method (30 min in 10 vol% HCl) is equivalent within error to the standard piranha cleaning procedure commonly used in the adsorption literature for samples annealed at both 150 °C and 120 °C, resulting in the same h_{ads} thickness after solvent washing. Data shown are the average of four samples with the error bars drawn in the figure representing the average sample-to-sample variability within a batch. We find this sample-to-sample error decreases progressively from ± 0.6 nm to ± 0.4 nm and ± 0.2 nm for one, two, and three toluene washes, respectively. We recognize that for the 150 °C annealed samples, the HCl cleaned substrates appear to result in slightly reduced h_{ads} thicknesses on average, albeit with overlapping sample-to-sample error bars. The more proper error for this comparison would probably be the batch-to-batch error of ± 1 nm, which would make the data for these two substrate cleaning procedures more equivalent. Given that the adsorbed layer thicknesses are the same and because HCl is safer and easier to use than piranha cleaning, Figure 3.7 was collected with HCl cleaned substrates.

Relevant to our discussion below that considers the impact of these $h_{\text{ads}}(t)$ studies on nanoconfinement investigations in thin films, in Figure 3.8 we also examined substrates that were toluene cleaned. Much of the literature on nanoconfined systems cleans silicon substrates by simply rinsing the silicon with toluene immediately prior

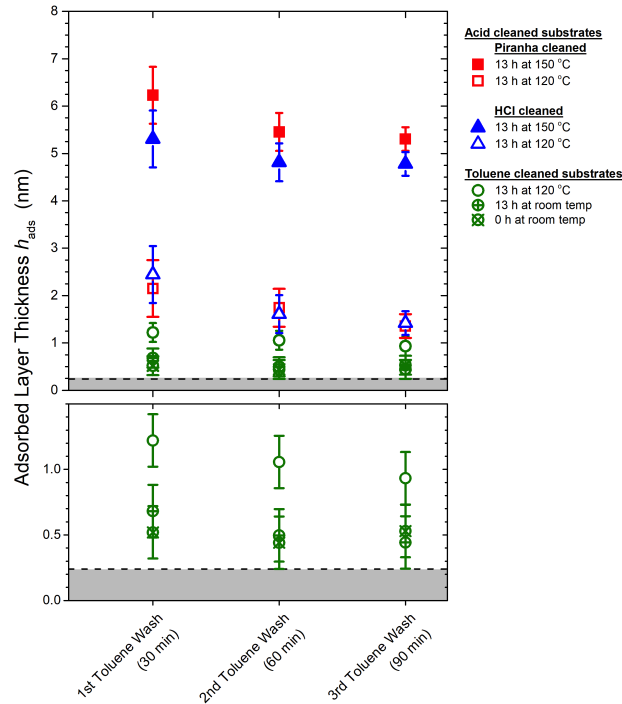


Figure 3.8: Comparison of the adsorbed layer thickness h_{ads} after one, two, or three 30 min washes in 100 mL of toluene, following 13 hours of annealing under vacuum at either 150 °C, 120 °C, or simply sitting at room temperature, on silicon substrates cleaned with either piranha solution (red squares), HCl acid (blue triangles), or simply toluene (green circles). Data shown represent the average and standard deviation of four samples each, and the gray bar with dashed line across the bottom of the graph represent the uncertainty in measuring zero adsorbed layer thickness, $h_{\text{ads}} \leq 0.24$ nm. The bottom portion is a zoomed in version of the toluene cleaned data.

to spin-coating the film. This minimalistic cleaning procedure is justified because silicon wafers come from the manufacturer pre-cleaned typically with some type of acid oxidizing solution and then packaged in a clean room environment. The most common annealing procedure followed in nanoconfinement studies is overnight under vacuum at $T_g^{\text{bulk}} + 20$ °C, which for PS with $T_g^{\text{bulk}} = 100$ °C means 120 °C. In our lab, over the years “overnight” has meant anywhere from 13-18 h. This explains our choice in Figure 3.8 for comparing annealing conditions at 120 °C for 13 hours, while the temperature of 150 °C is that most commonly used in the adsorption literature for PS. Compared to the more aggressive piranha and HCl cleaning procedures, toluene cleaned substrates lead to consistently smaller residual adsorbed layer thicknesses h_{ads}

under the same annealing and solvent washing conditions. The average sample-to-sample variability within a batch for the toluene cleaned data are noticeably smaller than what was observed for the piranha and HCl cleaned substrates, in most cases these were around ± 0.16 nm. As this would be smaller than the ± 0.2 nm error that we previously identified as the error for the ellipsometry measurement itself, we therefore opted to graph ± 0.2 nm for the error bars of the toluene cleaned data. It is clear that chain adsorption appears to be much less prevalent on toluene-cleaned compared to acid-cleaned substrates, which implies that in much of the nanoconfinement literature polymer adsorption is likely significantly less prevalent than suggested by chain adsorption studies done on acid-cleaned substrates and annealed under more aggressive conditions. We believe this strong impact of substrate cleaning method likely explains the slower growth and different shape of $h_{\text{ads}}(t)$ observed by Napolitano et al. in Figure 3.1a, which are for samples that were cleaned using organic solvents.²⁰⁰

Given the discussion associated with Figure 3.5 about the unexpected observations that time ‘sitting in a drawer’ had impact on the measured adsorbed layer thickness h_{ads} after solvent washing, we also include in Figure 3.8 data for films that were spin-coated onto toluene cleaned substrates and then left ‘sitting in a drawer’ overnight for 13 hours. Again this would not be an unusual circumstance given that experimentally it is common practice to leave samples ‘sitting in a drawer’ between measurements. As the h_{ads} thicknesses for toluene cleaned substrates are exceptionally small, we magnify this data in the lower region of Figure 3.8. We find that these samples never annealed above T_g , but left ‘sitting in a drawer’ at room temperature for 13 h, have roughly the same small adsorbed layer thickness $h_{\text{ads}} \approx 0.5$ nm, as samples simply spin-coated and washed off toluene cleaned substrates immediately. Tsui et al. previously measured the residual thickness h_{ads} for PS films spin-coated onto either piranha cleaned or HF treated silicon and immediately washed off, as a way to verify their solvent rinsing procedure, claiming $h_{\text{ads}} = 0$ was achieved for films that were never annealed.²¹¹ We

find the residual thickness h_{ads} after such a procedure is very small $h_{\text{ads}} < 0.5$ nm, but non-zero. This naturally leads to the question of what h_{ads} thickness should be properly considered $h_{\text{ads}} > 0$. As described above in Section 3.3.1 on the reliability of measuring h_{ads} with ellipsometry, we determined that values of $h_{\text{ads}} \leq 0.24$ nm should be reasonably considered as $h_{\text{ads}} \approx 0$ because it would be impossible to distinguish from natural variations in the native oxide layer thickness. In Figure 3.8, we depict this uncertainty in measuring zero h_{ads} adsorbed layer thickness as a gray bar. While the toluene cleaned data for samples that were never annealed above T_g come close to this h_{ads} minimum of 0.24 nm, they are still notably above it outside of experimental error. This observation is consistent with the literature on polymer adsorption in solution, where if you were to dip a clean silicon wafer into a dilute polymer solution, chains would naturally adsorb to the substrate leaving behind a small, but non-zero h_{ads} thickness.¹⁸⁶ This older literature established that even though polymer chains adsorbed on the substrate interface are quite mobile and can readily exchange with those in solution, there is an equilibrium adsorbed amount quickly reached in solution with a strong restoring force to maintain this surface saturation condition by balancing adsorption/desorption rates.¹⁸³

3.3.4 Impact of Adsorbed Layers on Film Average $T_g(h)$ and Physical Aging

Much of the recent literature on adsorbed layer formation in melt films has correlated measurements of the residual layer thickness $h_{\text{ads}}(t)$ after some given annealing and solvent washing conditions, with parallel measurements on samples showing changes in film properties and dynamics under equivalent annealing treatments.^{44,134,136,137,190–198} From this comparison, studies have argued that chain adsorption formed in the melt during this annealing process is responsible for numerous changes in nanoconfinement effects such as altering $T_g(h)$ reductions,^{137,190,193,205,206} increasing viscosity,^{134,191} and

altering other properties in thin films.^{44,195,201,204,208} Such a comparison on nominally equivalent, but different samples assumes that $h_{\text{ads}}(t)$ is a reliable and meaningful measure of some characteristic of the melt film prior to solvent washing. However, based on our observations, the adsorbed layer thickness h_{ads} seems to be largely determined by the solvent washing conditions used to expose it. Thus, to try and ascertain the impact of h_{ads} layers on melt film properties, we directly test the impact of different adsorbed layer thicknesses on the average glass transition temperature $T_g(h)$ and physical aging rate $\beta(h)$ of thin films by first explicitly forming a given adsorbed layer thickness h_{ads} following the protocols we elucidated above, and then embedding this known h_{ads} layer into a melt film.

In Figure 3.9, we compare the average $T_g(h)$ and $\beta(h)$ of $h \approx 31$ nm thick films that were formed by floating a PS layer of thickness h_{float} atop a previously formed adsorbed layer of a given thickness h_{ads} to create a total film thickness of $h_{\text{total}} = h_{\text{ads}} + h_{\text{float}} \approx 31$ nm. Specifically, in Figure 3.9 we compare (i) $h_{\text{total}} = 34.2$ nm with $h_{\text{ads}} = 6.9$ nm, (ii) $h_{\text{total}} = 33.1$ nm with $h_{\text{ads}} = 3.2$ nm, and (iii) a “regular” film of $h_{\text{total}} = 30.3$ nm ($h_{\text{ads}} = 0$) directly spin-coated onto a toluene-cleaned bare silicon substrate. The explicit preformed adsorbed layers were made by annealing bulk (>200 nm) PS films on HCl cleaned silicon under vacuum at 150 °C for either 23 h ($h_{\text{ads}} = 6.9$ nm) or 3 h ($h_{\text{ads}} = 3.2$ nm) and then rinsing once in toluene for 30 min, equivalent to the most common procedure used to make adsorbed layers from melt films. After capping with the additional PS layer, the $h_{\text{total}} = h_{\text{ads}} + h_{\text{float}}$ films were annealed for 2 hours at 170 °C under vacuum in an attempt to ensure good chain interpenetration between the top PS layer and underlying adsorbed layer. These annealing conditions used for merging the $h_{\text{ads}} + h_{\text{float}}$ layers were chosen to match our recent work where we capped end-tethered PS chains to investigate local T_g changes near the grafted substrate interface,²⁸ the conditions of which were based on literature studies for the interpenetration of end-grafted PS chains into a PS homopolymer

matrix, a system which has been well studied.²²⁰ For a matrix of high molecular weight homopolymer chains, interpenetration of end-tethered grafted chains occurs primarily via breathing mode relaxations of the grafted chains as they poke into the matrix.¹⁸⁸ Neutron reflectivity measurements by Clarke and Jones have characterized these timescales for various end-tethered and homopolymer chain lengths.^{189,273,274} For adsorbed chains comprised of tails, loops, and trains, we believe this analogy with end-grafted chains is reasonable for tails, but recognize that interpenetration of high molecular weight homopolymer chains with loops, especially tightly bound ones, would likely be a slower process and is still largely an open question.^{185,195} Neutron reflectivity measurements by Koga et al. have demonstrated that matrix PS chains can interpenetrate with “loosely adsorbed chains” (adsorbed layers comparable to those of the present study) with no significant evolution in the composition profile between 15 min and 24 h of annealing at 150 °C.⁴⁴ However, more recent adhesion measurements primarily with poly(ethylene oxide) (PEO) found adhesion strength between matrix chains and an adsorbed layer to be poorly correlated with interpenetration determined from neutron reflectivity profiles, although good adhesion strength was reported for PS matrix chains annealed with loosely adsorbed chains at 170 °C ($T \gg T_g$).¹⁹⁵

Case (iii) in Fig. 3.9 of a “regular” film corresponds to a sample that was only vacuum annealed overnight (13 h) at 120 °C, representing the most common sample preparation conditions used in the nanoconfinement literature. According to our data from Figure 3.8, when bulk films undergo this annealing condition and are then solvent washed with toluene, the resulting h_{ads} value is ≈ 1 nm. For a much thinner 31-nm thick film, we can estimate that such an annealed film would have a reduced h_{ads} value ≈ 0.5 nm after solvent washing based on the recent study by Napolitano et al.²⁰² demonstrating that $h_{\text{ads}}(t)$ values are significantly reduced when the initial film thickness is decreased. Small h_{ads} values ≈ 0.5 nm are comparable to h_{ads} values obtained when simply washing off any film in solvent, including films that were never

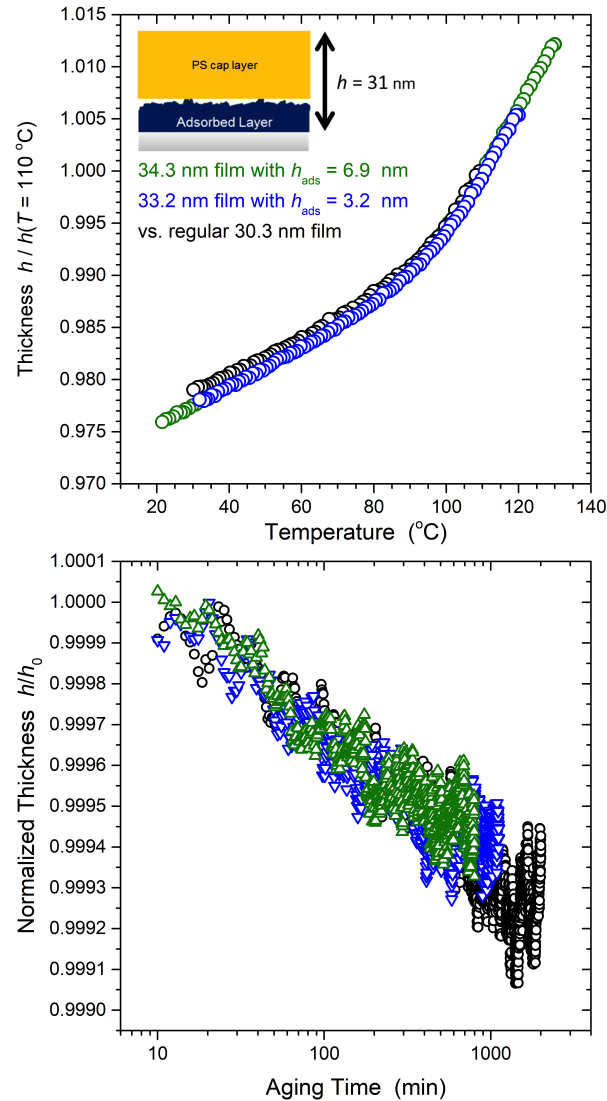


Figure 3.9: Comparison of PS films made with explicit adsorbed layers of thickness h_{ads} preformed on the surface followed by floating a layer of thickness h_{float} atop and annealing to create films of total thickness $h_{\text{total}} = h_{\text{ads}} + h_{\text{float}} \approx 31\text{ nm}$. Green data have $h_{\text{ads}} = 6.9\text{ nm}$, blue data $h_{\text{ads}} = 3.2\text{ nm}$, while black data are for a regular 30.3 nm thick film simply spin-coated onto the silicon wafer. (Top) Graphs the film thickness, normalized at $T = 110\text{ }^\circ\text{C}$, versus temperature used to determine the glass transition temperature $T_g = 93 \pm 1\text{ }^\circ\text{C}$ for all three samples. (Bottom) Graphs the film thickness, normalized at the start of the aging run $h_0(t_0 = 10\text{ min})$, as a function of aging time following a thermal quench from equilibrium above T_g to an aging temperature of $40\text{ }^\circ\text{C}$. Collapse of the data demonstrate no difference in the average glass transition and physical aging response for the three different kinds of samples.

annealed as shown in Fig. 3.8. The physics behind polymer adsorption in solution implies that simply putting a clean substrate into a solution with some polymer chains

will result in the chains coating the substrate and forming an adsorbed layer. Thus, it seems reasonable to consider this case (iii) condition of “regular” films to have $h_{\text{ads}} \approx 0$.

Figure 3.9 compares these three different samples with and without explicit h_{ads} layers, plotting the temperature-dependence of the film thickness $h(T)$, normalized to $h(T = 110 \text{ }^\circ\text{C})$, measured on cooling at $1 \text{ }^\circ\text{C}/\text{min}$, and the normalized thickness h/h_0 as a function of aging time following a rapid ($55 \text{ }^\circ\text{C}/\text{min}$) quench to an aging temperature of $40 \text{ }^\circ\text{C}$. The normalization condition h_0 represents the film thickness at an aging time of 10 min, following our previous works.^{29,38,253} All three samples show equivalent results, as can be visually seen in the figure by the superposition of the data. We note that multiple measurements on nominally identical samples typically show at least this much variation in the data.³⁸ The average glass transition temperature $T_g(h)$ of the films were determined in the usual manner from the intersection of linear fits to the liquid and glassy regimes, giving an average of $93 \pm 1 \text{ }^\circ\text{C}$ for all three samples. The physical aging rate characterizing the stability and densification of the glassy film as it evolves towards equilibrium is given by the slope of the data, and was measured to be on average $\beta = -d(h/h_0)/d(\log t) = 3.0 \pm 0.5 \times 10^{-4}$ for the three samples, equivalent to our previous works.^{29,38}

From these results, it appears that the presence or absence of an explicit adsorbed layer at the substrate interface does not affect the average glass transition temperature $T_g(h)$ and physical aging rate $\beta(h)$ of thin films. However, we recognize that *average* values may not fully represent *local* differences in dynamics near the interfaces. For example, the average $T_g(h)$ for PS films with PS chains end-grafted to the silica substrate have frequently shown little to no change in average $T_g(h)$ with the addition of the end-tethered chains.^{127,275,276} Yet, recent localized fluorescence measurements by Huang and Roth on samples designed to avoid competing free surface effects found that the local $T_g(z = 0)$ next to the silica substrate can increase by

as much as +50 K with low grafting densities of only $\sigma = 0.011$ chains/nm².²⁸ This apparent contradiction can be explained by the work of Lan and Torkelson²⁷⁷ that chemically labeled pyrene dye to different locations of PS brushes, demonstrating that the local T_g of the brush near the substrate interface was strongly increased by +36 K while the local T_g near the free surface was strongly reduced by -14 K. These strong differences in *local* T_g at different positions within the film occurred despite measurements of the *average* $T_g(h)$ of the brush being predominantly unaltered from bulk, suggesting that local changes at the two interfaces largely canceled each other out. Thus, measurements of the local T_g next to adsorbed layers would be warranted.

The closest such local T_g measurements that already exist in the literature is that of Priestley et al. where adsorbed layers of pyrene-labeled PS were capped with unlabeled PS films, measuring the T_g of the adsorbed layer itself.²⁰⁶ They reported that depending on the initial annealing conditions used to create adsorbed layers of pyrene-labeled PS after three 10-min toluene washes, the local T_g of the adsorbed layer was found to be reduced from bulk when initially capped with the unlabeled PS layer, after a short anneal of only 20 min at 120 °C. Subsequent annealing at 150 °C of the stacked films to amalgamate the two layers resulted in bulk T_g being recovered within a few hours. This time scale for slow interpenetration of the surface bound chains with an overlying polymer matrix is consistent with literature studies from the 1990s investigating the kinetics of end-grafted chains interpenetrating high molecular weight homopolymers.^{188,189,220,273,274} Adsorbed chains with some distribution of loops, tails, and trains could be expected to take even longer to achieve good interpenetration.^{185,195} Whereas tails can utilize relatively rapid breathing modes to penetrate into the overlying high molecular weight homopolymer,¹⁸⁸ loops would require the threading of the homopolymer chains, which could be a particularly slow process for small loops.¹⁸⁵ These results by Priestley et al.²⁰⁶ demonstrating that adsorbed chains recover bulk T_g with extended annealing conditions likely required to

achieve good interpenetration of surface bound chains with the overlying PS matrix, suggest that perhaps adsorbed layers within a melt do not exhibit T_g perturbations.

3.4 Conclusions: Summary, Implications and Open Questions

We began our investigation into adsorbed layers in 2016 when trying to understand some unexpected results demonstrating a molecular weight dependence to the physical aging behavior of thin PS films.³⁸ As the existing literature was proposing that chain adsorption in melt films may be altering dynamics in such thin films^{44,134,136,137,190–198} and that the adsorbed layer thickness measured increased with increasing molecular weight^{199,210,211} (as summarized in Fig. 3.1), we believed we should investigate and address the possibility that adsorbed layer formation may be responsible for the unexpected molecular weight dependent physical aging results we were observing in thin films. Our conclusions from this study³⁸ were that we could find no experimental evidence to support the hypothesis that chain adsorption was responsible for our observed molecular weight dependent aging behavior. No variation in the annealing or preparation conditions that were reported to increase chain adsorption altered the observed physical aging behavior, nor the pre-formation of explicit adsorbed layers within a thin film as demonstrated in Fig. 3.9 of the present review.

During the course of that investigation, we needed to identify an appropriate experimental protocol for forming adsorbed layers from melt films via solvent washing and convince ourselves that we understood how to reliably form residual adsorbed layers of a given thickness h_{ads} . This review is a summary of our understanding from that process. In short, our main conclusion is that once the films have been immersed in solvent, the resulting system of chains adsorbed to a surface in solution is fundamentally equivalent to that used to grow adsorbed layers in solution, thus the

same physics must apply.

3.4.1 Summary of Findings

Based on a survey of the disparate literature studies available at the time,^{192,199,206,210,211} we arrived at an experimental procedure most commonly used to form $h_{\text{ads}}(t)$ curves by solvent washing melt annealed films, where Figure 3.2 provides a summary of these steps. From our experimental efforts, we were forced to conclude that the residual adsorbed layer thickness $h_{\text{ads}}(t)$ formed from this process, where h_{ads} is measured after a given solvent washing condition as a function of annealing time t of the film at an elevated temperature in the melt state prior to washing, are far less reproducible than implied in the literature. The largest source of variability we found corresponds to samples made in different batches, where a batch represents a group of silicon wafers all piranha cleaned together. The logistics and safety of piranha cleaning means that there are a finite number (≤ 15 samples) that can be made together in a single batch. By binning data together from different batches, as demonstrated in Figure 3.4, we were able to reproduce $h_{\text{ads}}(t)$ curves comparable to those from the literature (as shown in Fig. 3.1). $h_{\text{ads}}(t)$ data where the entire curve is collected from a single batch of samples, as in Fig. 3.7, appear to be the most like those reported in the literature.

From our investigation of forming $h_{\text{ads}}(t)$ curves by solvent washing melt annealed films, we found that the residual adsorbed layer thickness h_{ads} is almost entirely dependent on the solvent washing conditions used. In our efforts to understand this process, we consulted the extensive, well-established older literature on chain adsorption in solution, reviewing in Section 3.1.2 the understanding developed about chain adsorption that is pertinent to the interpretation of forming residual adsorbed layers by solvent washing melt films. We found there to be a disconnect in conceptual interpretation between the assumptions being made in the recent literature regarding producing adsorbed layers by solvent washing of melt films and this older literature

on how adsorbed chains behave in solution that provides direct experimental evidence in contradiction to these assumptions. The recent literature believes that individual polymer segment–surface contacts are irreversibly adsorbed such that unadsorbed chains can be readily washed away from a film using a good solvent without disturbing the adsorbed chains and thereby “revealing” the structure of the adsorbed layer that is present within the film, a process which has come to be referred to as “Guiselin’s experiment”^{138,190,193,199–202} or “Guiselin’s approach”.^{195,203,204} This interpretation is based on a theoretical assumption by Guiselin²¹⁵ that is experimentally invalid.

Numerous studies from the older literature demonstrate that adsorbed chains in solution are quite mobile and readily exchange with those in solution,^{184,186,218,238,240,241,243} with more recent experimental evidence directly demonstrating adsorbed chains crawl and hop across the surface, even in the limit of strong adsorption.^{233,246–248} Misunderstanding about the reversible/irreversible nature of adsorbed chains is long standing, with a 1987 review by de Gennes¹⁸³ laying out the arguments and experimental evidence for the reversibility of adsorbed chains despite the total equilibrium adsorbed amount Γ of a given layer being strongly conserved, simply giving the illusion of irreversible adsorption. In his review, de Gennes explicitly argued that the countervailing viewpoint in favor of irreversibility, which claims that all polymer segment–surface contacts need to be detached at once for a chain to desorb, is “utterly wrong”.¹⁸³ The correct picture that emerges from all the experimental evidence is that individual polymer segment–surface contacts are not irreversibly adsorbed, but readily detach and exchange with solvent or other polymer segments on the same or different chain. With this continuous exchange of surface contacts, individual polymer chains can “unzip” from the surface and diffuse away.¹⁸³ Exchange experiments with a second “displacer” solvent also demonstrate reversibility with additional displacement of polymer chains observed when introducing a second solvent that has a more favorable interaction with the substrate,^{217,244,245} as defined by Silberberg’s adsorption energy parameter

χ_s (eq. 3.3).²³¹ Such mobility of adsorbed chains in solution and these differences in χ_s with solvent likely explain recent reports by Koga et al.²⁰⁴ and Beena Unni et al.²⁵² that residual h_{ads} adsorbed layers can end up dewetting in solution under some solvent conditions. Thus, the mobility of adsorbed polymer chains in solution means that the resulting residual adsorbed layer thickness h_{ads} remaining after solvent washing of films is primarily a representation of the solution conditions the films are washed in and likely bear little resemblance to any adsorbed state in the melt film. We find our experimental observations of the measured h_{ads} from solvent washing films to be consistent with this understanding from the older literature of polymer adsorption in solution.

We observe that part of the poor reproducibility of obtaining consistent $h_{\text{ads}}(t)$ values from following the experimental protocol outlined in Fig. 3.2 is that annealing at elevated temperatures above T_g is not required to form a perceived $h_{\text{ads}}(t)$ adsorbed layer. Simply having the films sit at room temperature for a few hours leads to densification of the films that make them harder to wash away, requiring longer exposure for the solvent to penetrate, swell, and dissolve the glassy film. Thus, for a given fixed solvent washing protocol, the remaining h_{ads} layer will be thicker giving the illusion of higher chain adsorption. This observation is consistent with the data shown by Koga et al.²¹⁰ that the long-time adsorbed layer thickness h_{∞} is independent of annealing temperature from 40-150 °C.

We also find that the substrate cleaning method strongly impacts the measured h_{ads} thickness, which is consistent with earlier work by Granick et al.²⁷² demonstrating that substrate cleaning treatment affects polymer adsorption in solution. As shown in Fig. 3.8, acid based cleaning methods like piranha and HCl solutions, typical of studies reporting adsorbed layer formation in melt films, consistently lead to larger h_{ads} values compared with simply rinsing the silicon wafer with an organic solvent like toluene. Tsui et al.²¹¹ and Koga et al.²¹⁰ have demonstrated that HF cleaned silicon

leads to even larger h_{ads} values than piranha cleaned silicon, as shown in Fig. 3.1b. For toluene cleaned silicon substrates, where the PS film was then annealed for 13 hours at only 120 °C, the sample preparation protocol most typical of studies in the nanoconfinement literature investigating property changes in thin films, the measured h_{ads} value is only ~ 1 nm, barely above the $h_{\text{ads}} \leq 0.24$ nm value we have concluded should be reasonably considered to be $h_{\text{ads}} \approx 0$ because it is impossible to distinguish from natural variations in the native oxide layer thickness.

To assess if the presence of an adsorbed layer h_{ads} could alter dynamics in thin films, we performed glass transition and physical aging measurements on samples with adsorbed chains. Given our observations that solvent washing does not provide a reliable measure of the possible presence of an adsorbed layer in films, we created films with an explicit preformed adsorbed layer of known thickness h_{ads} . These known h_{ads} layers were then placed in ≈ 31 nm thick films by capping the h_{ads} layer with layers h_{float} to create $h_{\text{total}} = h_{\text{ads}} + h_{\text{float}} \approx 31$ nm. As shown in Figure 3.9, the average $T_g(h_{\text{total}} \approx 31$ nm) of these films did not vary for films with different h_{ads} thicknesses, including those with zero h_{ads} layer. The average physical aging rate $\beta(h_{\text{total}} \approx 31$ nm) at 40 °C also did not differ with or without the presence of different h_{ads} values.

From this investigation into chain adsorption, we conclude that the use of some protocol like that outlined in Figure 3.2 to measure an h_{ads} layer thickness is sufficiently irreproducible, and more reflective of the solvent washing conditions used to extract the layer, that to infer some role of chain adsorption in melt films from correlations of such $h_{\text{ads}}(t)$ values with measurements of dynamics on parallel samples seems questionable at best. It would also appear that the absence or presence of placing an explicit adsorbed layer within a thin film does not alter the measured average $T_g(h)$ and $\beta(h)$ dynamics.

3.4.2 Open Questions

During this process, we also identified a number of open question which we believe are worthy of further research:

- Just because the *average* film $T_g(h)$ and $\beta(h)$ dynamics do not change, does not necessarily imply that adsorbed chains are not imparting some *local* change in these properties. For example, Lan and Torkelson²⁷⁷ recently demonstrated that PS brushes can have large gradients in local T_g with strongly elevated values near the substrate interface counteracted by reduced values near the free surface such that the average film $T_g(h)$ barely deviates from bulk despite this large gradient in local dynamics. Our group recently showed that low grafting density end-tethered chains can substantially increase the local $T_g(z)$ of the PS matrix near the substrate interface by as much as +50 K for only $\sigma = 0.011$ chains/nm².²⁸ As adsorbed chains contain an mixture of loops, tails, and trains, it is not not unrealistic to think that tails could be acting in a similar fashion to grafted end-tethered chains, and certainly the impact of loops bound to the surface is an open question. Thus, local measurements of the impact of adsorbed chains would be warranted and something our group is pursuing.
- An important open question related to the evaluation of whether adsorbed chains are locally impacting the dynamics of a polymer matrix is the temperature-dependent timescale needed for entanglement or interdiffusion of surface bound adsorbed chains with an overlying polymer matrix. Although tails could reasonably be interpreted in the context of end-tethered chains, for which much is known in this context,^{188,189,220,273,274} the entanglement of loops in particular may be entirely dependent on the homopolymer dynamics, which could be extremely long for high molecular weight chains. This was already identified as an open question in the context of adsorbed chains in polymer solution by Granick in 2002.¹⁸⁵ The experimental evaluation of the local impact of adsorbed chains in melts would likely

involve the assembly of some type of $h_{\text{ads}} + h_{\text{float}}$ sample with high molecular weight chains used to localize a fluorescent probe layer. Such long timescales needed for the interdiffusion of high molecular weight matrix chains with substrate bound chains to obtain sufficiently consolidated samples to remove the initially present free surface may explain the slow recovery of bulk T_g observed by Priestley et al.²⁰⁶ in their recent work. More recent work by Zuo et al. suggests that surface bound loops can modify dynamics in thin films, although the relative impact of small vs. large loops appears to be uncertain.^{193,278}

- The driving force for polymer adsorption in solution implies that simply inserting a clean substrate into a dilute polymer solution also results in a residual h_{ads} layer upon removal and drying of the substrate from solution.¹⁸⁶ These solution grown h_{ads} layers can be comparable in thickness to residual h_{ads} values obtained by solvent washing melt annealed films. Thus, a natural question would be to test whether there is any difference between these two types of adsorbed layers, especially given the significant polymer mobility of surface bound chains that occurs in solution.^{218,219,233,240,246–249} We have observed that films which were melt annealed at 150 °C for longer do result in thicker $h_{\text{ads}}(t)$ residual adsorbed layers after a given solvent washing condition. This suggests there is something different about these residual adsorbed layers that may reflect some slow evolution of substrate bound chains within the melt. However, as we have also observed that other factors which reduce film solubility, such as densification of the glassy film, also result in thicker $h_{\text{ads}}(t)$ residual adsorbed layers after a given solvent washing condition, it is possible that film annealing may simply reflect reduced film solubility requiring longer solvent washing times. This is also an open question we are pursuing in a subsequent publication.
- Theoretical efforts to understand polymer adsorption nearly all cite the same definition for the segmental “sticking” energy χ_s representing the favorable enthalpic

polymer segment–surface interaction that drives adsorption, eq. 3.3. This original definition formulated by Silberberg²³¹ is based on the *difference* ($u_s - u_s^0$) in interaction energies between a polymer segment–surface contact u_s exchanging with a solvent–surface contact u_s^0 . However, as explained in Section 3.1.2, for a melt film with no solvent present, the relevant exchange of surface contacts would be between two *equivalent* polymer segment–surface contacts. As this would not have any enthalpic energy gain, χ_s would be strictly zero by the definition of eq. 3.3. Perhaps if there were some favorable (e.g., hydrogen bonding) interaction between the polymer and substrate surface, there could be an enthalpic energy barrier that would need to be overcome for the exchange of polymer segment–surface contacts. This could conceivably be defined in terms of the difference in interaction energies between a polymer segment–surface contact and a polymer segment–segment contact in the bulk, but a different theoretical framework would be needed for this as this would not be equivalent to eq. 3.3. The other main factor driving adsorption in solution is the reduced miscibility of large chains in solution,¹⁸⁶ which is also not present in a melt film. Thus, it is not clear whether chain adsorption even occurs within melt films.

- Consistent with recent literature reports,^{192,199,200,206,210,211} we do observe that the residual $h_{\text{ads}}(t)$ thickness increases with increasing annealing time, where t represents the length of time the PS films were held in their melt state at 150 °C prior to being washed with some given solvent procedure. This is indicative of the films being harder to wash off. From an examination of our $h_{\text{ads}}(t)$ data in Figures 3.4, 3.5, 3.7, and 3.8, we do find some evidence suggesting that a slow restructuring of chain conformations near the substrate interface may be occurring within the melt films during this extended annealing at 150 °C. However, as any substrate bound chains will have considerable mobility and change conformation as soon as they are exposed to solvent, we believe inferring such information from any $h_{\text{ads}}(t)$ data

after solvent washing provides limited insight. There are some literature studies that have tried to measure in-situ the dynamics of surface bound chains within the melt as a function of different annealing conditions,^{134,191,206,265,279} but frequently these measurements still involve interpretation where $h_{\text{ads}}(t)$ data or literature reports thereof are used to attribute the changes to increased adsorption in the melt. There are also tracer diffusion studies reporting reduced mobility of chains near a substrate interface. Early work from the mid-1990s by Rafailovich et al. reported reduced diffusion from bulk of PS chains by up to 3 orders of magnitude near a SiOx/Si interface, scaling as $D_{\text{surf}} \sim N^{-1.5}$.²⁶³ In collaboration with Rubinstein, this was interpreted at the time as a “stickiness” of the interface where polymer segment–surface contacts increased the friction coefficient for reptation, where $N^{1/2}$ surface contacts per chain for Gaussian conformations gave the correct scaling. However, reduced diffusion by an order of magnitude persisted for an extended distance of ≈ 100 nm away from the interface indicating that direct surface contacts were not required.²⁶⁴ Split layer experiments suggested that entanglements with matrix chains that can span to the substrate interface were required to slow diffusion. At this point, all we can conclude is that this is still a major open question, with several results indicating that dynamics are slower near a substrate interface in the melt, although not all measurements are straightforward to interpret. It is unclear if the system is meaningfully evolving to some equilibrium state, which may or may not be different than the chain conformations of surface bound chains obtained in theta-solvent conditions, or if the dynamics are simply so slow that only non-equilibrium conformations are obtained.²⁸⁰

- Finally, given the commonalities between polymer–interface interactions in films and polymer nanocomposites (PNCs), a better understanding of chain adsorption in melts has broader implications than only in the film studies cited so far. Studies of PNCs frequently interpret the impact of nanofiller interfacial interactions on the

polymer matrix based on the presence of a “bound layer” at the surface of nanoparticles (NPs).^{77,281,282} In fact, a widespread procedure for determining the thickness δ of this bound layer is very similar to the Figure 3.2 procedure. A good solvent is used to dissolve away any unbound matrix chains, after which thermogravimetric analysis (TGA) is used to determine the remaining “bound” polymer to NP fraction, with δ calculated assuming a spherical shell of polymer with bulk density around the NP.⁷⁷ Other common themes between films and PNCs include, the requirement for good interpenetration between surface bound and matrix chains to cause observable changes in dynamics,^{80,282,283} as well as the reduced mobility of these surface bound chains. For PNC studies on P2VP/SiO₂-NPs where attractive hydrogen bonding interactions are present, reduced τ_α relaxation times of surface bound chains by two orders of magnitude have been reported.²⁸⁴ However, even in these strongly bonded systems, the surface bound chains are not irreversibly adsorbed, but can exchange with matrix chains.²⁶⁶ The strong temperature dependence observed for this exchange lifetime is consistent with reports from solution studies where surface coverage is shown to be reduced at higher temperatures when more thermal energy is available to overcome the predominantly temperature-independent binding energy of the surface bound chains.²³³ Given these similarities, there may be much that can be learned from making connections to the previously developed understanding about polymer adsorption in solution.

Chapter 4

Role of Solvent Washing

Conditions on the Creation of Adsorbed Layers from Melt Films and Its Impact on Local T_g Dynamics

4.1 Background

A number of studies have recently claimed that chain adsorption to substrate interfaces in the melt has strong impact on changing dynamics in thin films.^{44,134,136,137,190–198}

The amount of chain adsorption in melt films is evaluated by measuring the residual thickness $h_{\text{ads}}(t)$ remaining after a given solvent washing procedure on films that were annealed for some extended time t at an elevated temperature.^{192,199,200,206,210,211}

This procedure, which has become known as the “Guiselin experiment” or approach, assumes the solvent wash removes unadsorbed chains, leaving behind only the “irre-

versibly adsorbed” chains from the melt state.^{138,190,193,195,199–204} The most common protocol is to anneal polystyrene (PS) films at 150 °C (50 K above the glass transition temperature T_g) for tens of hours and then wash the films for 30 min in toluene (the spin-coating solvent).^{192,206,210,211} The measured values of $h_{\text{ads}}(t)$ are then correlated with property changes measured as a function of annealing time t made on parallel samples with nominally equivalent sample histories.^{44,134,136,137,190–198} Similar procedures are done with polymer nanocomposites to ascertain the “bound layer” by washing away matrix chains and assessing the amount of polymer remaining by thermogravimetric analysis (TGA).^{77,281}

We have recently reviewed this $h_{\text{ads}}(t)$ procedure for films and tested its reproducibility.²⁸⁵ From this evaluation we concluded that $h_{\text{ads}}(t)$ is not as reliable a measure as suggested by the recent literature because the residual thickness $h_{\text{ads}}(t)$ remaining is almost entirely determined by the solvent washing conditions used to expose the melt annealed films. We found our results to be consistent with the understanding developed on polymer adsorption in solution based on literature primarily spanning from the 1950-1990s.^{184,186,218,220,238,240,241,243} This well-established literature, as well as more recent studies, experimentally demonstrate that adsorbed chains in solution are highly mobile, diffusing across the surface via crawling and hopping mechanisms, even in the limit of strong adsorption (sticking energy $\chi_s \approx$ several kT).^{233,246–248} Already addressed in a 1987 review by de Gennes,¹⁸³ the notion of “irreversible adsorption” is a misnomer that arises from the strong driving force to maintain a given surface coverage in equilibrium. Even though this equilibrium adsorbed amount Γ_{eq} is strongly conserved, individual chains within the adsorbed layer are highly mobile, readily exchanging with other chains in solution.^{217,238,243–245} Individual polymer segment–surface contacts are continuously detaching and reattaching in thermal equilibrium, exchanging with solvent or other surface contacts on the same or different chain, resulting in an individual chain eventually “unzipping”

from the surface and drifting away, leading to the exchange of chains with those in solution. These experiments of adsorbed chains in solution invalidate the theoretical assumptions made by Guiselin²¹⁵ that have led to the above $h_{\text{ads}}(t)$ procedure favored by the recent literature.

In the present work, we follow up with measurements to address open questions that were identified from our recent review and evaluation of the $h_{\text{ads}}(t)$ procedure.²⁸⁵ What impact does continued solvent washing have on $h_{\text{ads}}(t)$ adsorbed layers formed by solvent washing melt films? Are there any differences between adsorbed layers grown directly in solution with those formed by solvent washing films? Does the presence of an h_{ads} layer have any impact on the local glass transition temperature T_g dynamics in a film, and if so, does it matter what kind of h_{ads} layer it is? We demonstrate that in the limit of long washing times, all $h_{\text{ads}}(t)$ layers tend towards the equilibrium desorbed amount $\Gamma_{\text{eq}}^{\text{des}} = h_{\text{ads}}/\rho$, where $h_{\text{ads}} = h_{\infty}^{\text{soln}}(c \rightarrow 0)$ observed for solution grown adsorbed layers upon decreasing solution concentration. This suggests that in equilibrium there is no difference between solution grown adsorbed layers and those formed by solvent washing melt films. However, we do observe that $h_{\text{ads}}(t)$ layers that were annealed for longer times in the melt ($t > 20$ h at 150 °C) are harder to wash off, requiring much longer in solution to reach equilibrium. This may reflect differences in chain conformations for surface bound chains or a significant pinning of unadsorbed chains that require extended restructuring of the adsorbed layer in solution before they can be released. Fluorescence measurements to evaluate the local T_g next to h_{ads} layers formed in different ways finds local T_g can be perturbed by up to ~ 30 K higher than bulk T_g for adsorbed layers formed from melt annealed films with little washing, provided good interpenetration is obtained with the adsorbed layer. In contrast, adsorbed layers formed in solution and adsorbed layers from melt films washed to equilibrium impart no perturbation to local T_g .

4.2 Experimental Methods

Polystyrene (PS) films were spin-coated from a 2.5 wt % solution of $M_w = 400$ kg/mol ($M_w/M_n = 1.06$) PS onto hydrogen chloride (HCl) cleaned Si at 800 rpm to produce bulk films (>200 nm), which were subsequently annealed under vacuum at 150 °C for up to 23 h and washed for 0 – 30+ hours in 100 mL of toluene to form a residual adsorbed layer following our established procedure based on literature protocols (see Chapter 3).²⁸⁵ Adsorbed layers were also grown directly from solution by placing HCl cleaned substrates into PS-toluene solutions of the same $M_w = 400$ kg/mol with concentrations varying from 5×10^{-3} mg/mL to 1 mg/mL. Samples annealed for long times and samples where the adsorbed layer were grown directly in solution were both washed in toluene solvent until a constant h_{ads} amount $h_{\infty}(c \rightarrow 0)$ was reached. During this procedure, samples were periodically removed from the solution and blown dry with nitrogen and measured with ellipsometry to determine the current adsorbed layer thickness h_{ads} before being placed back in the same solution, effectively measuring the kinetics of desorption of the adsorbed layer in solution. Adsorbed layers grown using the highest concentration solutions were also washed in pure toluene after reaching the equilibrium adsorbed amount $\Gamma_{\text{eq}}^{\text{ads}}(c)$ to measure the evolution of desorption in solution.

Adsorbed layers were also formed on HCl cleaned quartz substrates for use with fluorescence measurements, following the same procedure. To ensure the accurate measurement of the adsorbed layer thickness, equivalent adsorbed layers were simultaneously formed on SiOx–Si wafers and quartz substrates by placing both substrates in the same solution. Samples for local fluorescence measurements were constructed by floating a 12 nm thick pyrene-labeled-polystyrene (PS-Py) layer with 1.4 mol % pyrene content ($M_w = 672$ kg/mol, $M_w/M_n = 1.3$) directly onto the previously formed adsorbed layer, which was then capped by floating an additional 400 nm thick layer of neat PS ($M_w = 1,920$ kg/mol, $M_w/M_n = 1.26$, Pressure Chemical) above the

labeled layer. After floating the PS-Py layer samples were dried for 20+ min under a lamp to remove any residual water. Samples were then annealed following the procedure developed by Huang and Roth²⁸ for 2 h at 170 °C, which was designed to create good chain interpenetration for their singly end-grafted chains. We further annealed samples for 24 and 48 h at 170 °C to determine the annealing conditions needed for good interpenetration between the adsorbed layer and the local dye-labeled probe layer. After interpenetration of the dye layer with the adsorbed layer a bulk layer of PS was floated on top to cap the system and remove any perturbation from the free surface. The stack was then annealed for 20 min at 170 °C to consolidate the film and heal the PS-Py/bulk interface formed by the final floating step.

Once assembled samples were placed in a PTI fluorimeter with an Instec HCS402 heat stage and MK1000 temperature controller. The samples were heated to 130 °C (T_g+30 K) and the fluorescence emission spectrum was examined to determine the first emission peak for the sample. The sample was allowed to sit at this temperature for 10 min to ensure stability of the heater and fluorescence signal before measuring T_g on cooling from a higher temperature, usually 170 °C. T_g was measured by capturing the intensity at the first emission peak on cooling at 1 °C/min following our previous work.³⁰ After cooling the sample was reheated to the temperature of 130 °C and the fluorescence emission spectrum was collected and compared to the spectrum prior to measuring T_g . When measuring T_g from the higher temperature of 170 °C the heater was allowed to sit at 170 °C for no more than 5 min to ensure the heater and sample were thermally stable. Bulk T_g was measured on single layer PS films of 240 nm thickness with fluorescence and found to be 99 ± 3 °C.

time the samples spend in the polymer solution for three concentrations of 5×10^{-3} mg/mL, 0.1 mg/mL, and 1 mg/mL PS ($M_w=400$ kg/mol) in toluene. All concentrations show qualitatively the same behavior, where there is some initial growth of the adsorbed layer that eventually reaches a plateau $h_\infty(c)$, which represents the equilibrium adsorbed layer thickness for the solution. At the lowest concentration of 5×10^{-3} mg/mL adsorption takes place on such a slow time scale that we only plot the long time plateau found after 96 hours in solution, because in such extremely dilute solutions the kinetics for adsorption of the polymer chains is diffusion limited¹⁸⁶ as the chains must first find the substrate prior to adsorption. A concentration of 5×10^{-3} mg/mL was selected because it approximately corresponds to that for a 200 nm thick PS film (2 cm x 2 cm in extent) dissolved in 50 mL of toluene. A common sample washing condition used for the formation of adsorbed layers formed by solvent washing films.^{199,201,210,211,285}

The dashed adsorption curves in Figure 4.1 showing growth of $h_{\text{ads}}(t)$ are fits of the data to the form $h_{\text{ads}}(t) = h_\infty(c)(1 - e^{-t/\tau})$, where the fits show good agreement to the data. $h_\infty(c)$ is the long time equilibrium adsorbed layer thickness of the plateau and τ is a time constant that determines how long it takes for the adsorbed layer to form. Using this equation we have determined the long time equilibrium adsorbed layer thickness $h_\infty(c)$ to be 5.1 nm and 1.0 nm for adsorbed layers formed in the 1 mg/mL and 0.1 mg/mL concentration solutions respectively. We observe a concentration dependence for the long time equilibrium adsorbed layer thickness $h_\infty(c)$, in agreement with the classic adsorption isotherms presented in the literature where $\Gamma_{\text{eq}}^{\text{ads}}(c) = \rho h_\infty(c)$, where ρ is the density of the dried film because $h_\infty(c)$ comes from measurements of $h_{\text{ads}}(t)$, the dried film removed from solution. Additionally, the concentration also affects the time it takes to reach $h_\infty(c)$, which we determined from the time constant τ as 0.8 h and 3.1 h for adsorbed layers formed in the 1 mg/mL and 0.1 mg/mL concentrated solutions respectively.

We further examine the effects of concentration on the adsorbed amount by placing the samples made from our highest concentration ($c = 1$ mg/mL) in pure solvent after the equilibrium adsorbed amount $\Gamma_{\text{eq}}^{\text{ads}}(c)$ has formed. The red curve in Figure 4.1 shows the kinetics of the desorption process. This immersion of the samples in pure solvent quickly alters the adsorbed layer thickness, reaching a minimum limiting adsorbed layer thickness $h_{\infty}(c \rightarrow 0)$ on desorption. This new equilibrium adsorbed amount on desorption $\Gamma_{\text{eq}}^{\text{des}}(c \rightarrow 0)$ approaches that of the equilibrium adsorbed amount $\Gamma_{\text{eq}}^{\text{ads}}(c)$ for low concentrations formed by adsorbing to the substrate. The desorption of the adsorbed layer thickness $h_{\text{ads}}(t)$ between concentrations was fit to an exponential decay $h_{\text{ads}}(t) = h_{\infty}(c \rightarrow 0) + \Delta h(e^{-t/\tau})$ where $h_{\infty}(c \rightarrow 0)$ is the new limiting adsorbed layer thickness reached on desorption, Δh is the change in the adsorbed layer thickness, and τ is a time constant for the rate of desorption. We find from our fit that $\tau = 0.02$ h and $h_{\infty}(c \rightarrow 0) = 1.6$ nm for 1 mg/mL grown layers desorbed to this new equilibrium adsorbed amount.

Adsorbed layers grown in more dilute solutions at long times are also highlighted in Figure 4.1. Data for an adsorbed layer formed in the limit of extremely dilute concentrations ($c = 5 \times 10^{-3}$ mg/mL) is given by the orange filled triangle. These data show the same $h_{\infty}(c)$ as adsorbed layers grown from solutions with concentrations of 0.1 mg/mL (blue triangle). This adsorbed layer thickness is the adsorbed layer thickness for polymers in the limit extremely dilute concentrations. Notably the minimum limiting adsorbed layer thickness formed on desorption $h_{\infty}(c \rightarrow 0)$ (red triangle) is equivalent within experimental error. These limiting values for the adsorbed layer thickness formed in solution in the limit of extremely low concentration $h_{\infty}^{\text{soln}}(c \rightarrow 0)$ are highlighted by the dashed red box surrounding these data. We have averaged all the data in the highlighted red box of Figure 4.1 and determined the thickness to be $h_{\infty}^{\text{soln}}(c \rightarrow 0) = 1.2 \pm 0.4$ nm.

These measurements shown in Fig. 4.1 are similar to the classic polymer adsorp-

tion from solution experiments presented in the literature dating back to the 1950s.²¹⁶ Historically these experiments were done such that the adsorbed amount was measured at some long-time equilibrium adsorbed value, where this equilibrium adsorbed amount $\Gamma_{\text{eq}}^{\text{ads}}(c)$ was plotted versus concentration c producing what is called an adsorption isotherm, which can be determined from our data as the long time plateau values for the adsorbed layer thickness $h_{\infty}(c)$ times density ρ , $\Gamma_{\text{eq}}^{\text{ads}}(c) = \rho h_{\infty}(c)$, where $\rho = 1.05 \text{ g/cm}^3$ is the bulk density for PS. The bulk density is used because the adsorbed layer thicknesses are measured as dry films without solvent present.²⁸⁵ Although we focus primarily on the dilute regime, where few studies have examined adsorption, we do note that at a concentration 1 mg/mL our data give an equilibrium adsorbed amount consistent with literature reports.^{216,286}

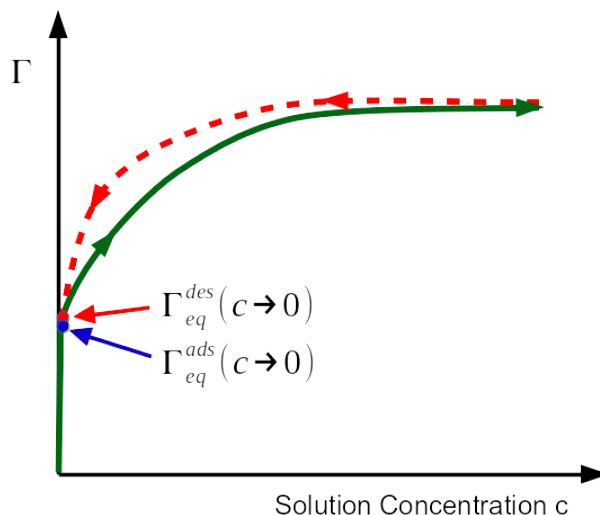


Figure 4.2: Schematic of the adsorption and desorption process by increasing then decreasing the solution concentration based on literature experimental data.¹⁸⁶ On adsorption, very little solution concentration is needed to saturate the surface with an adsorbed layer. On desorption, hysteresis is typically observed with a non-zero limiting adsorbed amount remaining at zero concentration.

Desorption by reducing the bulk concentration of the solution to zero is far less studied. Typically hysteresis is observed and the final adsorbed layer thickness does not reduce to zero.^{186,287} Figure 4.2 illustrates a schematic of the adsorption-desorption process based on experimental data in the literature.¹⁸⁶ If one plots the

adsorbed amount Γ as a function of bulk solution concentration, on adsorption (green curve) Γ initially increases very quickly as chains in solution preferentially coat the substrate surface and very little polymer is needed to obtain surface saturation. This is why the limiting adsorbed layer thickness $h_{\infty}(c)$ formed for the blue and orange data at extremely low concentration are identical. Further increases in solution concentration will drive more chains to the surface such that surface crowding effects will cause rearrangements and increases in the adsorbed layer thickness. However, the $\Gamma_{\text{eq}}^{\text{ads}}(c)$ curve quickly saturates as the surface can only accommodate so many chains. On desorption when the solution concentration is reduced, polymer chains will desorb from the surface, which then add to the solution concentration and a new equilibrium is formed $\Gamma_{\text{eq}}^{\text{des}}(c)$. Even when the bulk concentration is reduced to zero, the desorption is not complete because very few chains need desorb before the solution concentration is a small non-zero quantity again, and in equilibrium the system prefers maintaining a high surface concentration of chains.¹⁸⁶ Kinetically the desorption process is a logarithmically limiting process where the rate of desorption depends on the surface concentration of chains, which will become extremely slow as the surface concentration decreases.^{186,288} Even though equilibrium is maintained on desorption, complete desorption of the adsorbed layer into solvent is extremely slow and can thus never be completed.¹⁸⁶ Koga et al. has shown that a non-zero adsorbed layer thickness remains even after solvent washing PS adsorbed layers in toluene for up to 150 days.²¹⁰

An alternative method of forming adsorbed layers is by solvent washing polymer films.^{199,201,210,211,285} Films of initial thickness $h > 200$ nm were prepared by using different annealing times of 3 h, 6 h, and 23 h at 150 °C under vacuum before being placed in toluene to measure the dissolution of the polymer film. Figure 4.3 shows the evolution of the adsorbed layer thickness $h_{\text{ads}}(t)$ as a function of time the films spend in solution, where films were placed in toluene and measured progressively throughout

the washing process. If we compare the shortest washing times in the figure (~ 1 h) we see that there is an increase in adsorbed layer thickness with longer annealing time at 150 °C, as shown in the inset of Figure 4.3, for samples annealed 3, 6, and 23 h, as reported elsewhere in the literature.^{199,201,210,211,285} With progressive washing we observe that films annealed for the shortest time of 3 h evolve to a limiting adsorbed layer thickness $h_{\infty}^{\text{film}}(c \rightarrow 0)$ of ~ 1 nm in less than 5 hours, where it exhibits a plateau. Data annealed for 6 and 23 h also reach this same limiting adsorbed layer thickness $h_{\infty}^{\text{film}}(c \rightarrow 0)$, but require longer washing to evolve to this limiting value, with the 23 h data requiring over 100 hours in solvent. The retardation of this process for films annealed for long times well above T_g may be due to some evolution of the structure of the polymer chains during annealing. We associate this plateau with the film reaching its long time steady state adsorbed layer thickness $h_{\infty}^{\text{film}}(c) = 1.3 \pm 0.6$ nm.

For comparison, in Figure 4.3 we also plot the dashed fit curves to the solution data from Figure 4.1. We find the limiting adsorbed layer thicknesses obtained from solvent washing films $h_{\infty}^{\text{film}}(c) = 1.3 \pm 0.6$ nm to be experimentally equivalent to the limiting adsorbed layer thickness obtained in solution $h_{\infty}^{\text{soln}}(c \rightarrow 0) = 1.2 \pm 0.4$ nm, both evolving to the same limiting value highlighted by the red dashed box in Figure 4.3. We interpret this evolution of the adsorbed layer thickness as the polymer chains in the film leaving the substrate in a process similar to desorption of an adsorbed layer grown in solution. Upon dissolution of the film, an adsorbed layer in solution is formed where the concentration is that of an extremely dilute solution with $c \rightarrow 0$. This perhaps should not be surprising as we chose our lowest concentration to approximate the concentration of a bulk polymer film, with an area of 2 cm \times 2 cm, completely dissolved in 50-100 mL of solution. The continual evolution of the adsorbed layers formed by washing melt annealed films, even for films that were annealed for long times (23 h at 150 °C), to the $h_{\infty}^{\text{soln}}(c \rightarrow 0)$ value for dilute solutions indicates that these adsorbed layers are reaching the same limiting value and strongly

suggests that these adsorbed layers may be equivalent. After many hours in solvent, the system should be equivalent to an equilibrium adsorbed layer in solution. We note previous literature works claiming to use solvent washing as a way of revealing the adsorbed layer supposedly present within the melt annealed film typically stop washing at much shorter times, citing an apparent plateau after only 30-90 min²⁰⁴ of washing, contrary to what we observe here.

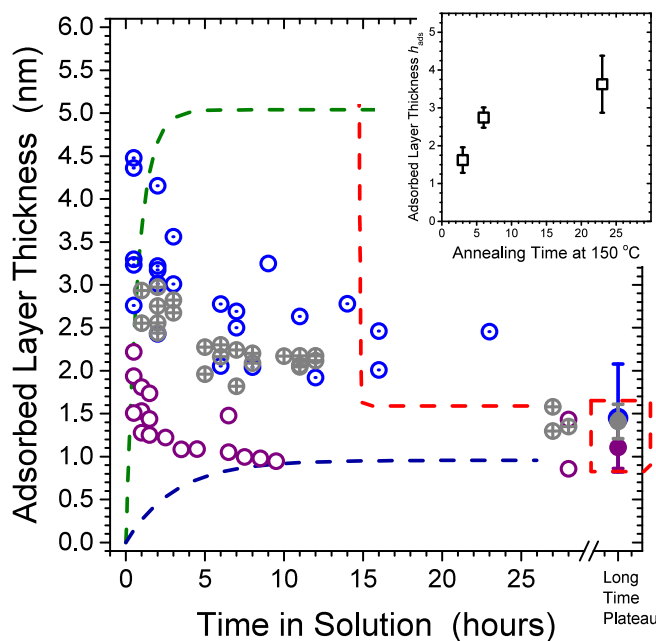


Figure 4.3: Plot of the adsorbed layer thickness versus the time spent in pure solvent (toluene) after annealing films at 150 °C for 3 h (purple open circles), 6 h (gray crossed circles), and 23 h (blue dotted circles). Adsorbed layers washed for extended periods of time show a continual decrease in the adsorbed layer thickness until they reach a minimum limiting adsorbed layer thickness $h_{\infty}^{\text{film}}(c \rightarrow 0)$, where these long time plateau values are shown as filled circles. The adsorbed layer thickness for the long time plateau are the averages of data after reaching the long time steady state adsorbed layer thickness where no further decrease in the adsorbed layer thickness was detected. For reference, the dashed curves are the fits to the data in Figure 4.1 showing the trends for the adsorbed layers in solution. The inset shows the adsorbed amount after 30 minutes of washing as a function of annealing time for the film at 150 °C .

While determining the exact structure of the adsorbed layers is not possible in this work, for the adsorbed layers grown in solution prior literature provides some in-

formation suggesting that we likely have two different regimes for adsorption.¹⁸⁶ For adsorption at our highest concentrations of 1 mg/mL the relatively fast adsorption combined with the relatively weak favorability for adsorption (small sticking energy χ_s ²³¹) suggests that the adsorbed layer formed will likely be dominated by loop structures with relatively short trains to due polymer chains competing for space on the surface. However, in the extremely dilute case for the concentration 5×10^{-3} mg/mL, where chains are able to more easily spread out on the surface, the adsorbed layer formed could be more train dominated with fewer loops. We consider below whether such differences in the distribution of trains, loops, and tails in the structure of these adsorbed layers may create differences in the local T_g dynamics of the system. We also can consider potential differences in structure for films spin-coated from solution to those that were annealed for long times, where freshly spin-coated films could have different conformations prior to annealing than after annealing for long times well above T_g . This in turn could affect the time necessary for these structures to equilibrate in solution to the structure of an equilibrium adsorbed layer in the limit of extremely dilute solutions. Work by Dhinojwala et al.¹³⁴ that used sum frequency generation to look at the local surface orientation of monomers for adsorbed layers grown from solution in comparison to spin-coated films, found no difference between them. Thus, at least prior to annealing, local monomer contacts at the substrate interface are initially the same. Our findings in Fig. 4.2 indicate that even though it takes longer to wash films annealed for long times above T_g to the long time limiting adsorbed layer thickness $h_\infty^{\text{film}}(c \rightarrow 0)$, the fact that these films have the same limiting adsorbed layer thickness as adsorbed layers formed in solution $h_\infty^{\text{soln}}(c \rightarrow 0)$ suggests that there are likely similarities in the final structure of these adsorbed layers.

Chain adsorption in solution is controlled by a competition between a favorable sticking energy χ_s for monomers in contact with the surface and the entropy cost to deform the chain. In the extremely dilute regime, chains are able to spread out on the

substrate and find their independent equilibrium conformations without interacting with other chains. However, at higher concentrations when more than one chain is adsorbing to a given area of the substrate, surface competition between chains can alter their conformations. Limited surface contacts will result in a distribution of chain conformations with some chains more strongly or weakly adsorbed.²³⁶ Granick et al. has shown that such film restructuring can take many hours in solution.²¹⁸

When a polymer film is placed in pure solvent, solvent enters the film and chains diffuse away. This process continues until a solvent swollen adsorbed layer remains near the substrate surface. Initially the surface concentration of this adsorbed layer is extremely high such that chains likely have limited mobility. It is also likely that unadsorbed chains with no direct substrate contacts may be pinned under loops of adsorbed chains. Even though this adsorbed layer may be far from an equilibrium adsorbed layer formed in solution, the same physics must apply to the system. Over time in solution, the adsorbed layer will slowly restructure with monomer-substrate contacts desorbing and readsorbing on the surface allowing some chains to diffuse away. As more chains diffuse away, the remaining chains will slowly form an adsorbed layer that is similar to one formed in dilute solutions with the process being similar to desorption.

Figure 4.4 presents a schematic summary of the evolution of the adsorbed layers formed both in solution and by solvent washing of films annealed above T_g . We show the adsorbed layer thickness $h_{\text{ads}}(t)$ for different times in solution, comparing the differences in how the adsorbed layer evolves for both melt films and adsorbed layers grown in solution. We highlight the equivalence of the adsorbed layer thickness for films annealed in the melt and washed for long times $h_{\infty}^{\text{film}}(c \rightarrow 0)$ to the desorption of adsorbed layers formed in solution $h_{\infty}^{\text{soln}}(c \rightarrow 0)$, as well as adsorbed layers grown at extremely dilute concentrations.

The similarity in the limiting thickness of the adsorbed layer for films equilibrated

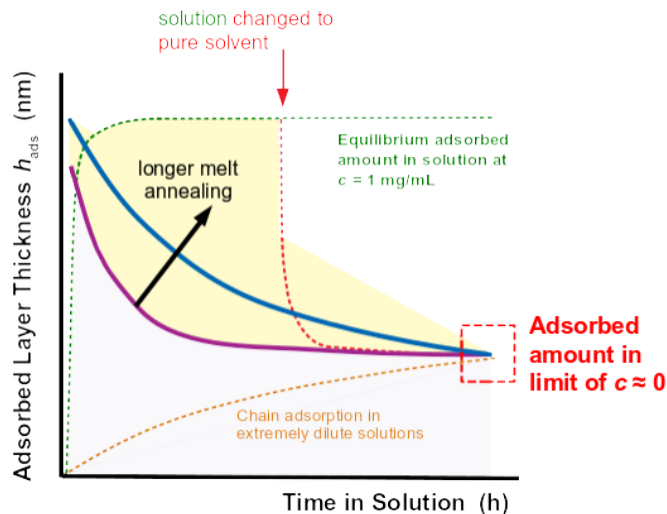


Figure 4.4: Depiction of the regimes for creating adsorbed layers, where we show representative curves to guide the eye of adsorbed layer thickness versus time in solution for various cases of annealed films washed in solvent and adsorbed layers grown directly in solution. The solid curves illustrate the evolution of the adsorbed layer for films annealed above T_g as a function of time the films spend in pure solvent (toluene) after annealing. Slower kinetics of desorption is observed for films annealed longer as indicated by the black arrow highlighting the effect of annealing on desorption kinetics for these films. Dashed curves represent films grown in solution and thus the adsorption and desorption kinetics in solution. The red box indicates the minimum limiting adsorbed layer thickness $h_\infty(c \rightarrow 0)$ in the limit of very low concentration.

in solution to the limiting adsorbed layer thickness found in solution suggests that the underlying structure of these films is the same. We now consider whether this similarity in structure is a possible indication of the local T_g dynamics being the same irregardless of the way in which the adsorbed layers were formed. We cannot say with any certainty why films annealed for the longest times require longer to reach its limiting thickness, but we speculate this is due to differences in the structure of adsorbed layers formed from washing off films that were well annealed. Thus it would be reasonable to believe that well annealed films with minimal washing may show differences in the local T_g dynamics to those grown in our lowest concentration solution, which still yet may show different dynamics to films grown in our highest concentration solutions.

4.3.2 Local $T_g(z = 0)$ next to an adsorbed layer

We consider now what impact the presence of these different adsorbed layers have on the local $T_g(z = 0)$ of a PS matrix next to such an adsorbed layer. We address this by comparing T_g locally adjacent to the adsorbed layers with that for a local dye-labeled layer adjacent to a Si–SiOx substrate with no adsorbed layer present, which we show exhibits a bulk $T_g = 100 \pm 2$ °C. We also consider whether there is a difference in perturbation to the local T_g dynamics imparted by adsorbed layers either formed by solvent washing melt annealed films or grown in solution, because if the structure of these adsorbed layers are different they could possibly result in different impacts to local $T_g(z = 0)$. Thus a change in local T_g could perhaps inform us about differences in the structure of these adsorbed layers. Comparing T_g for adsorbed layers formed by solvent washing of melt annealed films at short and long washing times to adsorbed layers grown directly in solution with similar adsorbed layer thicknesses $h_{\text{ads}}^{\text{soln}}(c)$ may indicate differences in local structure of the adsorbed layer as previously discussed. We are especially interested in comparing adsorbed layers formed to reach $h_{\infty}^{\text{film}}(c \rightarrow 0)$ and $h_{\infty}^{\text{soln}}(c \rightarrow 0)$, which appear to merge to the same long time limiting value.

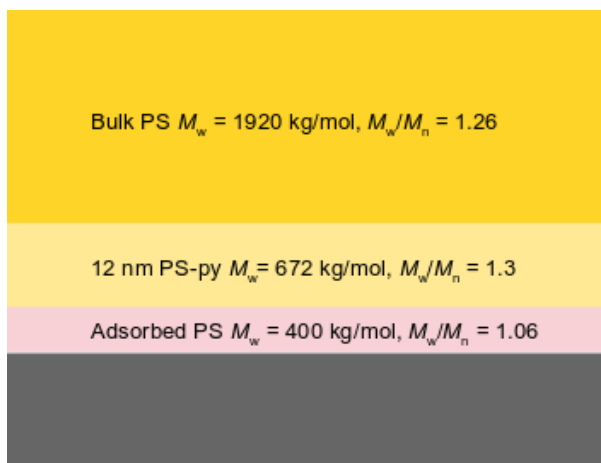


Figure 4.5: Schematic of the film geometry used to measure the local fluorescence adjacent to the adsorbed layer.

To measure the local T_g dynamics adjacent to the adsorbed layer we will first

form our adsorbed layers as described above, either directly grown in solution or by annealing films above T_g and washing them in solvent for extended periods of time. After this we will stack a 12 nm thick pyrene labeled PS layer (PS-Py) immediately atop the adsorbed layer and anneal the system for a minimum of 2 h at 170°C to allow for tails and possibly loops of the adsorbed layer to interpenetrate the dye-labeled layer. After the dye-labeled layer is interpenetrated with the adsorbed layer, a bulk layer is placed on top to cap the film creating samples where the localized dye-labeled layer is probing the T_g dynamics next to the adsorbed layer without any impact of free surface effects. Prior to the T_g measurements, samples are further annealed for 20 min at 170 °C to ensure the individual layers formed a consolidated sample with no air gaps. A schematic of the sample geometry is shown in Figure 4.5 for clarity. The only things that will be changed between measurements is how we form our adsorbed layers allowing us to compare the impact of different kinds of adsorbed layers on the local T_g , and the amount of annealing for chain interpenetration, to inform us about the potential differences that loops and tails may have on the local T_g dynamics.

One preparation condition we must consider first is what annealing is appropriate to produce good chain interpenetration of the dye-labeled chains with the adsorbed layer for both loops and tails of adsorbed chains. Previous work on end-grafted chains has demonstrated that in the melt end grafted chains will extend into the the matrix polymer by having the grafted chain ends ‘poke’ into the polymer matrix via chain end “breathing modes”.¹⁸⁸ O’Connor and McLeaish proposed a dynamical model consisting of multiple timescales to predict how end grafted chains could intermix into a cross-linked polymer elastomer matrix based on the grafted polymer chain ends being able to quickly penetrate into the polymer matrix and then relax on a much slower times scale to an equilibrium conformation via slower “breathing modes” similar to the motion of star polymers.¹⁸⁸ Clarke, then used neutron reflectivity to experimentally determine the time scales for which such end-grafted chains interpenetrate with

a polymer matrix.²⁷⁴ These works led Huang and Roth to choose a time scale of 2 h at 170 °C to create good interpenetration of their singly end-grafted polymer chains with the polymer matrix.²⁸ However, adsorbed layers consist of two main structural elements that would require interpenetration: tails, which presumably behave similar to the end-grafted polymer chains, and loops, which could require much more annealing to get good chain interpenetration due to their additional topological constraints. The inability of loops to interpenetrate on the same time scale as tails arises due to the requirement for the matrix to thread through the loop via reptation of the PS-Py chains. This process is controlled by the dye-labeled layer molecular weight (672 kg/mol) as well as the size of the loops, with relatively large loops being easier for the labeled chains to thread than tiny loops that are more tightly bound to the substrate and do not extend as far into the polymer layers. We therefore explore the effect that interpenetration annealing time has on the local T_g to inform us about the possible role chain interpenetration plays. The assumption here is that longer annealing facilitates more interpenetration with loops due to reptation of the PS-Py labeled layer, where tails likely are already well interpenetrated.

Figure 4.6 plots the normalized fluorescence intensity at a wavelength of 379 nm for the sample geometry described above as a function of temperature on cooling for two different kinds of adsorbed layers interpenetrated for either 2 hours or 24 hours at 170 °C. The adsorbed layers were formed either directly in solution with 1 mg/mL concentration or by washing films annealed for 23 h in the melt for 30 min. We then varied the time that the dye-labeled layer was annealed to interpenetrate into this adsorbed layer at 170 °C. For samples where the adsorbed layer was formed directly in solution we observed that 2 h of interpenetration resulted in a reduction in T_g by 7 °C ($T_g = 93 \pm 2^\circ\text{C}$) adjacent to the adsorbed layer compared to the T_g of a dye labeled layer adjacent to a bare Si-SiOx substrate ($T_g = 100 \pm 2^\circ\text{C}$), which we will use as our measure of bulk T_g . However, when these films were instead annealed

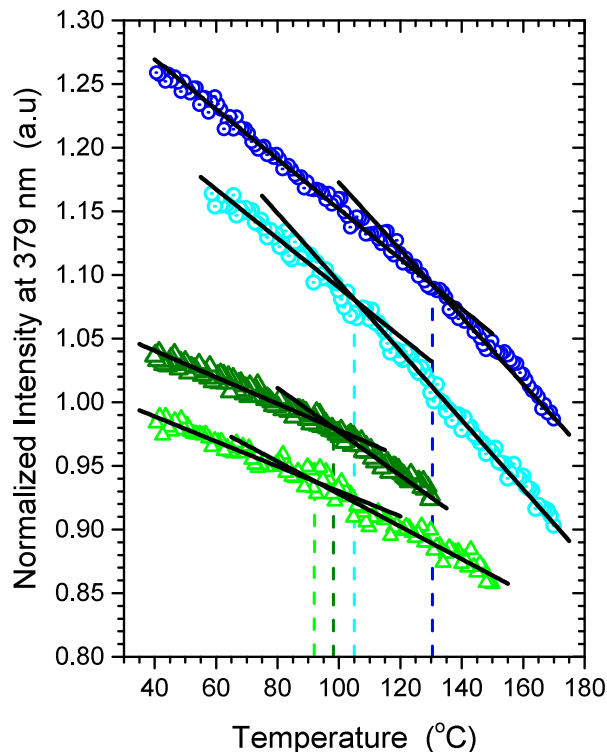


Figure 4.6: Plot of the normalized fluorescence intensity at $\lambda = 379$ nm vs temperature for a local probe layer adjacent to adsorbed layers formed in either a 1 mg/mL solution (light green and dark green triangles) or by washing for 30 minutes films annealed in the melt for 23 h at 150 °C (cyan and blue circles with a dot). The light green and cyan data were made by annealing the dye labeled layer atop the adsorbed layer for only 2 hours at 170 °C to get chain interpenetration following the procedure utilized by Huang and Roth.²⁸ The dark green and blue data are adsorbed layers that were interpenetrated for much longer 24 hours at 170 °C, causing an increase in T_g compared to the less well interpenetrated samples. Data are offset on the y axis for easy reading.

for 24 h at 170 °C to facilitate further chain interpenetration we observed that films with adsorbed layers grown directly in solution recover bulk T_g . In contrast, samples formed by washing of melt annealed films interpenetrated for only 2 h at 170 °C showed a modest increase in T_g of 5 K ($T_g = 105 \pm 2^\circ\text{C}$). Yet those melt washed films, when interpenetrated for 24 h at 170 °C exhibited a large increase in T_g of almost 30 K ($T_g = 128 \pm 2^\circ\text{C}$).

We verified that additional annealing to form good chain interpenetration does not alter T_g further after 24 h of annealing. Figure 4.7 plots the measured T_g of the

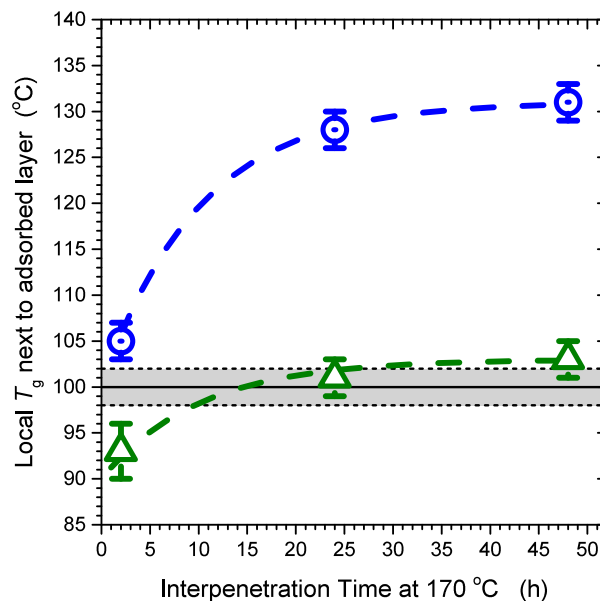


Figure 4.7: Plot of local T_g for a dye-labeled layer adjacent to the adsorbed layer as a function of the time the dye-labeled layer was allowed to interpenetrate the adsorbed layer at 170 °C. The blue circles with a dot are for adsorbed layers formed by 30 minutes of solvent washing films that were annealed for 23 h at 150 °C and the green open triangles are for adsorbed layers grown directly in a 1 mg/mL solution. The black solid line represents the local T_g for a Py-PS labeled layer on bare SiOx with $T_g = 100 \pm 2^\circ\text{C}$ with the dashed lines giving the standard deviation reported in this study. The dashed blue and green curves are to guide the eye.

local dye-labeled layer adjacent to adsorbed layers formed by either solvent washing for 30 min films annealed in the melt for 23 h or grown directly in solution, at 1 mg/mL concentration. The plot shows that as you anneal longer to facilitate better interpenetration of the dye-labeled layer into the adsorbed layer that T_g increases, apparently reaching a plateau after 24 h. This plateau in interpenetration time indicates that the chains are sufficiently interpenetrated, likely with loops, and further interpenetration with the adsorbed layer may not be possible or may not affect T_g .

This increase in T_g locally adjacent to the adsorbed layer is likely due to the interpenetration of tails and possibly loops, acting like end grafted chains.^{28,278} The necessity for more annealing to create good chain interpenetration suggests that the loops are somehow important to the local dynamics, where loops presumably are harder to interpenetrate by the dye-labeled layer due to their topological constraints

of being pinned on the surface on both ends. It is not clear what mechanism exists for the loops to alter the local T_g dynamics, nor is it clear if the loops are capable of allowing polymer chains to thread between individual loops or if they merely collapse and extend into the polymer matrix as a looped strand similar to singly end grafted chains.

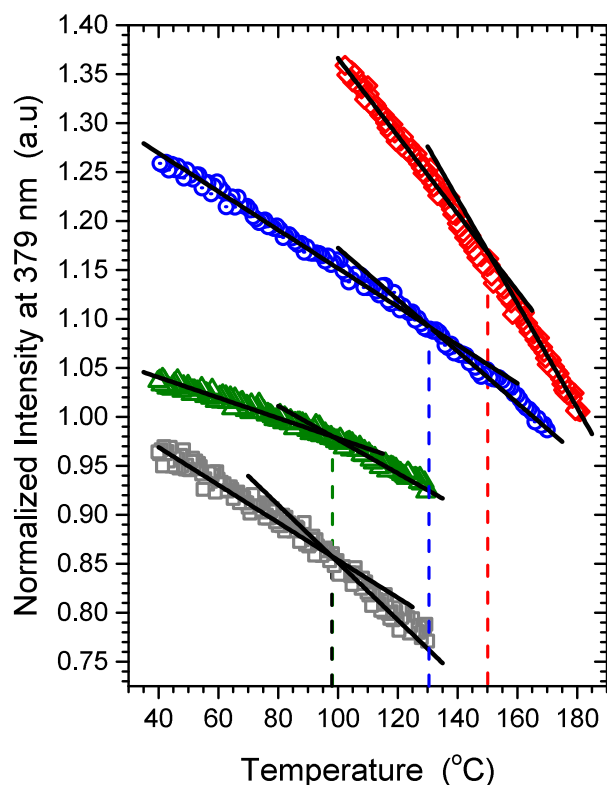


Figure 4.8: Plot of the normalized fluorescence intensity at $\lambda = 379$ nm vs temperature for a local probe layer adjacent to adsorbed layers made directly from a 1 mg/mL solution (green triangles) or from films annealed at 150°C for 23 h and washed for 30 minutes (blue circles with a dot), where both samples were interpenetrated for 24 h at 170 °C. The red diamonds are a local fluorescence measurement adjacent to a chemically end grafted polymer brush from Huang and Roth,²⁸ where a large increase in $T_g = 150$ °C was observed at a relatively low grafting density $\sigma = 0.011$ chains/nm². Data for a local probe layer adjacent to a HCl cleaned SiOx substrate is shown as gray squares for reference, where the T_g measured is 100 °C, the same as bulk. Data are offset on the y axis for easy reading.

These results suggest that adsorbed layers formed directly in solution may have a different local structure than those formed by solvent washing of melt annealed films.

The lower T_g for adsorbed layers formed in solution may be indicative of a highly loop dominated layer that even with good chain interpenetration is fundamentally different than singly end grafted chains, such that extensive annealing of the interface may be required to properly heal. We have shown that after 24 h of annealing at 170 °C the interface appears to be healed and T_g adjacent to the adsorbed layers formed directly in solution exhibit bulk-like T_g . Figure 4.7 also shows that longer annealing has no effect on the adsorbed layers grown in solution, where 48 h of annealing shows the same local T_g as 24 h for adsorbed layers grown directly in solution. This indicates that the adsorbed layers grown directly in solution may be highly loop dominated, possibly by large loops, where interpenetration merely allows for recovery of bulk T_g . In contrast, adsorbed layers formed by washing off melt annealed films show a significant T_g increase when the adsorbed layer and Py-PS dye layer are allowed to achieve good interpenetration. The timescale for this interpenetration suggests that the adsorbed layers formed are also dominated by loops, however the large increase in T_g above bulk suggests that if these adsorbed layers are similarly loop dominated like the adsorbed layers grown in the 1 mg/mL solution, that the loops in these adsorbed layers from well annealed films somehow behave differently than those present in adsorbed layers grown in solution. This could be due to a difference in the size of loops or distribution of loop sizes between these adsorbed layers formed by solvent washing of melt annealed films or grown directly in solution. However, the exact role of loops and loop size on the local T_g dynamics remains an open question.

We examine now the local T_g adjacent to adsorbed layers formed both by solvent washing of melt annealed films and compare these to adsorbed layers grown directly in solution, and to singly end grafted polymer chains from Huang and Roth²⁸ and a bare SiO_x-Si substrate. Figure 4.8 plots the normalized fluorescence intensity at a wavelength of 379 nm for four different sample geometries as a function of temperature on cooling. Both the bare substrate and the film with an adsorbed layer formed

directly in a solution of 1 mg/mL exhibit a T_g that is equivalent to bulk of 101 ± 2 and 100 ± 2 °C, respectively. For adsorbed layers formed by washing of melt annealed films we find that there is a substantial increase in T_g ($T_g = 128 \pm 2$ °C) of ~ 30 °C compared to bulk T_g , similar to the ($T_g = 150 \pm 2$ °C) 50 °C increase seen by Huang and Roth²⁸ adjacent to singly end grafted polymer chains. The structure of the end grafted polymer chains in the work of Huang and Roth are well characterized in the literature as being dependent on the grafting density. Here we are comparing T_g for our adsorbed layers to their largest T_g increase at their grafting density of $\sigma = 0.011$ chains/nm². This grafting density is relatively low compared to what would be considered a “true brush” where the chains are forced to extend up from the substrate. Instead the structure of the chains at the grafting density that showed the largest T_g increase in the work by Huang and Roth are mushroom like within the mushroom-to-brush transition region still having Gaussian random walk conformations. These end grafted chains also show a 50 K T_g increase after only 2 h of annealing at 170 °C for chain interpenetration, significantly less than the 24 h at the same temperature required in this work for a more moderate increase in T_g of only ~ 30 K. This is likely because end grafted chains have no loop structures and as such are able to quickly penetrate into the dye-labeled layer limited only by the grafted chain’s molecular weight.

We now can return to adsorbed layers washed in solution to their long time limiting adsorbed layer thickness $h_\infty(c \rightarrow 0)$. Figure 4.9 plots the fluorescence emission intensity versus temperature measured on cooling at 1K/min, comparing the local T_g imparted by adsorbed layers formed by washing films to the long time limiting adsorbed layer thickness $h_\infty^{\text{film}}(c \rightarrow 0)$ after being annealed for 23 h at 150 °C. For these data the dye-labeled layer was allowed to interpenetrate the adsorbed layers for either 2 h or 24 h at 170 °C. We find that T_g for these data are not strikingly different unlike for the films washed for only 30 minutes described above. Interpenetration for 2 h shows a $T_g = 109 \pm 2$ °C, and 24 h of interpenetration shows a $T_g = 107 \pm 2$ °C. We

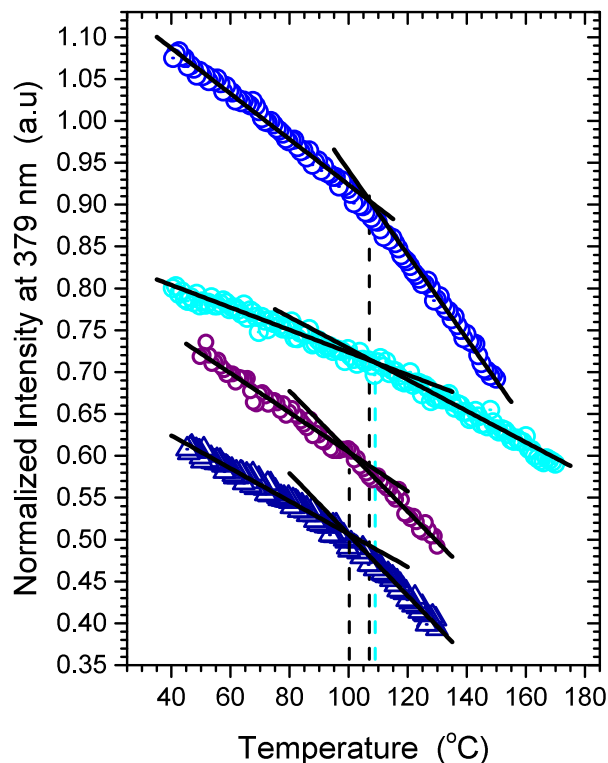


Figure 4.9: Plot of the normalized fluorescence intensity at $\lambda = 379$ nm vs temperature for a local probe layer adjacent to adsorbed layers formed by washing off melt annealed films for 100+ h to the limiting adsorbed layer thickness $h_{\text{ads}}^{\text{film}}(c \rightarrow 0)$ mg/mL (circles with a dot). Data were collected for both 2 h (light blue dotted symbols) and 24 h (blue dotted circles) of interpenetration at 170 °C. We also show data for an adsorbed layer formed by washing a film to its limiting adsorbed layer thickness $h_{\text{ads}}^{\text{film}}(c \rightarrow 0)$ that was annealed in the melt for 3 h at 150 °C with 2 h of interpenetration for the Py-PS layer (purple open circles). Data are also shown for adsorbed layers formed in a 0.1 mg/mL solution (dotted dark blue triangles) that had been interpenetrated at 170 °C for 2 h. The drop lines show the measured T_g for each data set showing no significant shift to a higher T_g with more interpenetration for films annealed well above T_g and washed to the limiting adsorbed layer thickness $h_{\text{ads}}(c \rightarrow 0)$. Data are offset on the y axis for easy reading.

also show data for the local T_g next to an adsorbed layer grown from a 0.1 mg/mL solution, where the adsorbed layer was interpenetrated at 170 °C for 2 h, giving a $T_g = 100 \pm 2^\circ\text{C}$. Because T_g does not depend strongly on chain interpenetration for films in the limit of $h_{\infty}^{\text{film}}(c \rightarrow 0)$, we are able to compare these data to our data for the local T_g adjacent to the equilibrium adsorbed layers grown in the limit of low concentration $h_{\infty}^{\text{soln}}(c \rightarrow 0)$ even with only 2 h of annealing at 170 °C to interpenetrate

the dye-labeled layer. In both cases we see that T_g is equivalent to bulk, or slightly higher than bulk by $\lesssim 7$ °C.

This indicates that an adsorbed layer grown in the dilute concentration of 0.1 mg/mL $h_\infty^{\text{soln}}(c \rightarrow 0)$ does not affect T_g , similar to adsorbed layers grown in solution at the higher concentration of 1 mg/mL. Furthermore, adsorbed layers formed by washing off melt annealed films in solution for sufficiently long times also appear to only moderately at best affect T_g , despite adsorbed layers from melt films with only 30 min of washing increasing T_g by ~ 30 K. It is worth noting, that by choosing a long 23 h of annealing we have limited our ability to reach this long time limiting regime by requiring extensive washing. For adsorbed layers annealed for merely 3 h and washed to the long time limiting adsorbed layer thickness $h_\infty^{\text{film}}(c \rightarrow 0)$ we observed no increase in T_g with 2 h of annealing at 170 °C the dye-labeled layer to facilitate chain interpenetration. Therefore, it seems likely the slight increase in T_g that appears to persist for the adsorbed layers formed by washing off melt annealed films for 23 h may be due to insufficient washing to reach the long time limiting adsorbed layer thickness $h_\infty^{\text{film}}(c \rightarrow 0)$. Overall it appears that adsorbed layers washed to the $h_\infty(c \rightarrow 0)$ limit do not affect T_g .

To understand why T_g is the same for all samples in the long time limit $h_\infty(c \rightarrow 0)$, we must consider again the potential structure of the adsorbed layer in this system. Adsorbed layers formed in the limit of extremely dilute solutions $h_\infty^{\text{soln}}(c \rightarrow 0)$ are known to be able to spread out on the surface and form long trains, with relatively few loops. By forming long flat trains with few loops the fraction of the adsorbed layer that can interpenetrate with the dye-labeled layer is reduced. As such, we would expect that annealing to interpenetrate for longer would not affect T_g significantly because there simply are not that many loops for the dye-labeled layer to interpenetrate with. This is what we believe is also occurring for adsorbed layer formed by washing films to the long time limiting adsorbed layer thickness $h_\infty^{\text{film}}(c \rightarrow 0)$. At most there is

only a modest increase in local T_g with relatively small amount of annealing for the dye-labeled layer to interpenetrate and effectively no increase in T_g with additional annealing to promote chain interpenetrate due to a lack of adsorbed layer structures to interpenetrate with. This would mean that the dominant structure to affect T_g may be the individual tails of the adsorbed layer. In that case T_g would increase relative to the effective grafting density of these tails.

These results indicate that not only is the adsorbed amount the same for films washed extensively to their limiting value as it is for adsorbed layers grown directly in dilute solutions, but that their structures in this regime may be the same as well. This is supported by the local T_g measurements in the presence of these adsorbed layers as well as the lack of a strong dependence of T_g on the annealing time required for chain interpenetration of the dye-labeled layers into the adsorbed layer. This hints that while tails certainly affect local T_g , the difference between adsorbed layers structure formed by washing off melt annealed films to their limiting adsorbed layer thickness $h_\infty(c \rightarrow 0)$ and those washed for shorter times is key to altering the T_g dynamics adjacent to an adsorbed layer. We have speculated that this difference is that one structure may be loop dominated, however further work is required to solidify and more carefully distinguish the impact that loops have from tails. This work likely will involve better controlling of the structure at the surface by replacing the adsorbed layers with some form of doubly end grafted chains as a substitute for loop structures.

4.4 Conclusions

We measured the evolution of adsorbed layer thickness formed from directly growing an adsorbed layer in solution and from washing melt films after annealing for various amounts of time. The evolution of the thickness of the adsorbed layer measured suggests all adsorbed layers washed in pure solvent evolve to the same final thickness

for sufficiently long washing times. This is because in solution, adsorbed layers are mobile and evolve to an equilibrium desorbed amount $\Gamma_{\text{eq}}^{\text{des}}(c)$. The limiting adsorbed layer thickness $h_{\infty}(c \rightarrow 0)$ that remains is equivalent to the adsorbed layer thickness grown in extremely dilute solutions.

We also examined the effects that these adsorbed layers have on the local T_g of the polymer adjacent to the adsorbed layer using a local fluorescence technique. We find that similar to singly end grafted chains, adsorbed polymers formed by solvent washing 23 h annealed films for only 30 min there is an increase of up to 30 °C to the local T_g , if the adsorbed layer is allowed to form good chain interpenetration with the labeled dye layer. We also determined that for solution grown adsorbed layers at 1 mg/mL there was no strong effect on the local T_g of the polymer film for sufficiently well interpenetrated films. Furthermore, for adsorbed layers washed to the long time limiting adsorbed layer thickness $h_{\infty}^{\text{film}}(c \rightarrow 0)$ no large changes in T_g were observed, and less annealing time at 170 °C was required for the dye-labeled layer to interpenetrate, possibly due to the nature of the adsorbed layers in extremely dilute solutions concentrations. The question of how loops may affect T_g in these adsorbed layers compared to tails remains an open question that deserves further examination.

Adsorbed layers are an often discussed topic in the confinement community,^{199,201,210,211,285} with the adsorbed layer often being presented as having a large impact on the film dynamics in confined films. Here we showed that specific pre-formed adsorbed layers can alter the local T_g under certain conditions. However, many open questions remain about the exact mechanism for how these dynamics are altered. Furthermore we show that you cannot merely decouple the effects of solvent washing from the effects that the adsorbed layer has on T_g because as soon as a film is placed in a solvent, whatever polymer chains are at the substrate will inherently follow the physics of polymer adsorption in solution and evolve to the limiting adsorbed layer thickness at low concentrations. What happens to the structure of the adsorbed layer from the

beginning of washing until it reaches its final limiting adsorbed amount is an open question that is beyond the current scope of this project.

Chapter 5

Outlook and open questions

In this dissertation we presented a series of experimental results that demonstrated the effects that chain connectivity and entropy have on glassy dynamics in confined polymer systems. In this chapter we will conclude my putting these results into context and summarizing the primary results of my work.

Chapter 2 presented a direct study of the effect that molecular weight has on the physical aging behavior of thin polymer glasses. A representative ultra-high molecular weight PS ($M_w = 6,790$ kg/mol) showed $\sim 45\%$ on average faster physical aging than a representative merely high molecular weight PS ($M_w = 400$ kg/mol) for films with a thickness less than 80 nm. However, bulk films showed no change to their physical aging rate with molecular weight and furthermore no difference in the glass transition temperature was found in bulk or thin films. The interpretation for this was concluded to be due to chain connectivity altering the gradient in dynamics emanating from the free surface, where physical aging was believed to be more sensitive to the chain connectivity effects in confinement than T_g . The chapter ended with a rigorous discussion of possible explanations for this surprising increase in β for thin films of ultra-high molecular weights (MWs $> 6,500$ kg/mol) relative to nominally identical films of merely high molecular weights (MWs $< 3,500$ kg/mol), which included sam-

ple preparation procedure, comparisons of film thickness to R_g , and changes in film density in thin ultra-high molecular weight films. The observed increase in β was attributed to a diminished breadth in the gradient in dynamics emanating from the free surface in thin ultra-high molecular weight films. Due to the literature suggestions in the field at the time, chain adsorption was also considered as one possible explanation for the faster physical aging in thin polymer films of ultra-high MWs $> 6,500$ kg/mol. However, our efforts to test this concluded that the possible presence of adsorbed layers did not show any affect on the average physical aging rate β or T_g in thin, 31-nm thick PS films. Due to potential differences in the average and local properties in thin films, this work led to a more thorough exploration of polymer adsorption presented in later chapters.

Chapter 3 presented a study on the reproducibility and reliability of the procedure presented in the literature for forming adsorbed layers by solvent washing of films that were previously annealed extensively in the melt. We found that the assumptions behind the procedure known as “Guiselin’s experiment” were not experimentally viable based on the historic literature of adsorption in solution. We explored the formation of adsorbed layers by examining the effect that each step in the procedure has on the reproducibility of the experimentally measured residual layer thickness $h_{\text{ads}}(t)$, finding that the experimental results were less reproducible than previously reported. We also showed that the annealing of bulk films well above T_g to form an $h_{\text{ads}}(t)$ adsorbed layer appeared to be an unnecessary step as comparable adsorbed layers could be formed merely by allowing samples to sit at room temperature for extended periods of time prior to solvent washing. We concluded that much of the variability in the measure of adsorbed layers stemmed from samples being allowed to sit in a drawer between different steps in the procedure, where we showed that leaving samples in a drawer created a denser less porous film that would be more difficult to wash off than freshly spin-coated films. However, when we controlled for this parameter we still

observed less reproducible $h_{\text{ads}}(t)$ adsorption curves than commonly presented in the literature. We go on to describe how these adsorbed layers are innately influenced by the the exact solvent washing procedure they undergo prior to measuring the adsorbed layer thickness. This finding was supported and discussed in the context of the rich literature on polymer adsorption from solution. We concluded that once solvent is present in the system the adsorbed layer must follow the same physics of adsorbed chains in solution. The evolution of adsorbed layer thickness with additional washing was consistent with how adsorbed layers behave in solution.

Building on the work in Chapter 3, Chapter 4 presented a series of experiments that tested whether the adsorbed layers formed by solvent washing of melt annealed films would create equivalent adsorbed layers to those grown in solutions. We began by exploring the formation of adsorbed layers in solutions of different concentrations, focusing primarily on extremely dilute solutions in the concentration regime similar to dissolving a bulk film in 50-100 mL of pure solvent. We examined the effects that extended solvent washing has on the adsorbed layers formed from washing of melt annealed films and showed that for films washed for tens of hours the adsorbed layer thickness formed is the same as the equilibrium adsorbed layer thickness formed in such low concentration solutions. We then focused on the local T_g dynamics adjacent to different adsorbed layers both grown directly in solution at varying concentrations, but also formed by washing of melt annealed films for short (30 min) and long (10s of hours) times. We found that the adsorbed layers formed by solvent washing of melt annealed films for 23 h at 150 °C for short times (30 min) show a 30 K increase to local T_g of PS, but only when the dye-labeled layer is well interpenetrated with the adsorbed layer for 24 h at 170 °C. We interpret this as being the dye-labeled chains achieving good chain interpenetration with the adsorbed layer structure, possibly due to the dye labeled layer being able to thread through loop structures of the adsorbed layer. The local T_g adjacent to adsorbed layers washed for tens of hours in solvent

showed no changes to local T_g , as did adsorbed layers grown in solution, so long as good chain interpenetration was achieved.

I end this thesis with a series of open questions that my research has lead to:

- What is the molecular mechanism for chain connectivity and entropic effects to modify glassy dynamics near an interface?
- How do trains, loops, and tails individually impact the local dynamics of polymer films? This question could be more directly probed if the structure could be forced to be fixed in the system, perhaps by doubly grafting chain ends to form fixed loops in the system to explore their contribution.
- Why do adsorbed layers formed by solvent washing films annealed in the melt for extensive amounts of time require longer in solvent to reach equilibrium than films annealed for less or no time in the melt state? Could there be subtle differences in entanglements and local structure that prevent solvent from penetrating as easily allowing individual chains to wash away?

Bibliography

- [1] C. B. Roth and R. R. Baglay, “Fundamentals of polymer glasses”, in *Polymer glasses*, edited by C. B. Roth (CRC Press Taylor and Francis, Boca Raton, 2016) Chap. 1, pp. 3–22.
- [2] C. A. Angell, “Formation of glasses from liquids and biopolymers”, *Science* **267**, 1924–1935 (1995).
- [3] W. Kob, *Soft and Fragile Matter: Nonequilibrium Dynamics, Metastability and Flow*, edited by M. E. Cates and M. R. Evans (Scottish Universities Summer School in Physics, Bristol, 2000), pp. 259–284.
- [4] S. Kim, S. A. Hewlett, C. B. Roth, and J. M. Torkelson, “Confinement effects on glass transition temperature, transition breadth, and expansivity: Comparison of ellipsometry and fluorescence measurements on polystyrene films”, *Eur. Phys. J. E* **30**, 83 (2009).
- [5] L. C. E. Struik, *Physical Aging in Amorphous Polymers and Other Materials* (Elsevier Scientific Publishing Company, Amsterdam, 1978).
- [6] Z. Fakhraai and J. A. Forrest, “Probing Slow Dynamics in Supported Thin Polymer Films”, *Phys. Rev. Lett.* **95**, 025701 (2005).
- [7] R. Greiner and F. R. Schwarzl, “Thermal contraction and volume relaxation of amorphous polymers”, *Rheologica Acta* **23**, 378–395 (1984).

- [8] R. Casalini, K. L. Ngai, C. G. Robertson, and C. M. Roland, “alpha- and beta-Relaxations in Neat and Antiplasticized Polybutadiene”, *J. Polym. Sci. Part B Polym. Phys.* **38**, 1841–1847 (2000).
- [9] G. Adam and J. H. Gibbs, “On the Temperature Dependence of Cooperative Relaxation Properties in Glass-Forming Liquids”, *J. Chem. Phys.* **43**, 139–146 (1965).
- [10] T. G. Fox and P. J. Flory, “The glass temperature and related properties of polystyrene. influence of molecular weight”, *Journal of Polymer Science* **14**, 315–319 (1954).
- [11] P. G. Santangelo and C. M. Roland, “Molecular weight dependence of fragility in polystyrene”, *Macromolecules* **31**, 4581–4585 (1998).
- [12] G. B. McKenna, *Glass formation and glassy behavior*, edited by C. Booth and C. Price, vol2 (Pergamon, Oxford, 1989), pp. 311–362.
- [13] Q. Li and S. L. Simon, “Enthalpy recovery of polymeric glasses: Is the theoretical limiting liquid line reached?”, *Polymer (Guildf)*. **47**, 4781–4788 (2006).
- [14] E. A. Baker, P. Rittigstein, J. M. Torkelson, and C. B. Roth, “Streamlined ellipsometry procedure for characterizing physical aging rates of thin polymer films”, *Journal of Polymer Science Part B; polymer Physics* **47**, 2509–2519 (2009).
- [15] S. L. Simon, D. J. Plazek, J. W. Sobieski, and E. T. McGregor, “Physical aging of a polyetherimide: Volume recovery and its comparison to creep and enthalpy measurements”, *J. Polym. Sci. Part B Polym. Phys.* **35**, 929–936 (1997).
- [16] S. Simon, J. Sobieski, and D. Plazek, “Volume and enthalpy recovery of polystyrene”, *Polymer (Guildf)*. **42**, 2555–2567 (2001).
- [17] J. Keddie, R. Jones, and R. Cory, “Size-Dependent Depression of the Glass Transition Temperature in Polymer Films .”, *Europhys. Lett.* **27**, 59–64 (1994).

- [18] C. J. Ellison and J. M. Torkelson, “The distribution of glass-transition temperatures in nanoscopically confined glass formers”, *Nat. Mater.* **2**, 695–700 (2003).
- [19] C. J. Ellison, M. K. Mundra, and J. M. Torkelson, “Impacts of Polystyrene Molecular Weight and Modification to the Repeat Unit Structure on the Glass Transition Nanoconfinement Effect and the Cooperativity Length Scale”, *Macromolecules* **38**, 1767–1778 (2005).
- [20] Y. Lee, K. C. Bretz, F. W. Wise, and W. Sachse, “Picosecond acoustic measurements of longitudinal wave velocity of submicron polymer films”, *Appl. Phys. Lett.* **69**, 1692–1694 (1996).
- [21] T. B. Karim and G. B. McKenna, “Evidence of surface softening in polymers and their nanocomposites as determined by spontaneous particle embedment”, *Polymer (Guildf)*. **52**, 6134–6145 (2011).
- [22] C. M. Stafford, C. Harrison, K. L. Beers, A. Karim, E. J. Amis, M. R. VanLandingham, H. C. Kim, W. Volksen, R. D. Miller, and E. E. Simonyi, “A buckling-based metrology for measuring the elastic moduli of polymeric thin films”, *Nat. Mater.* **3**, 545–550 (2004).
- [23] J. Y. Chung, A. J. Nolte, and C. M. Stafford, “Surface wrinkling: a versatile platform for measuring thin-film properties.”, *Adv. Mater.* **23**, 349–68 (2011).
- [24] J. A. Forrest, K. Dalnoki-Veress, and J. R. Dutcher, “Brillouin light scattering studies of the mechanical properties of thin freely standing polystyrene films”, *Phys. Rev. E* **58**, 6109–6114 (1998).
- [25] C. J. Ellison and J. M. Torkelson, “Sensing the glass transition in thin and ultrathin polymer films via fluorescence probes and labels”, *J. Polym. Sci. Part B Polym. Phys.* **40**, 2745–2758 (2002).

- [26] R. R. Baglay and C. B. Roth, “Communication: experimentally determined profile of local glass transition temperature across a glassy-rubbery polymer interface with a tg difference of 80 k”, *The Journal of Chemical Physics* **143**, 111101 (2015).
- [27] R. R. Baglay and C. B. Roth, “Experimental Study of the Influence of Periodic Boundary Conditions: Effects of Finite Size and Faster Cooling Rates on Dissimilar Polymer–Polymer Interfaces”, *ACS Macro Lett.* **6**, 887–891 (2017).
- [28] X. Huang and C. B. Roth, “Optimizing the Grafting Density of Tethered Chains to Alter the Local Glass Transition Temperature of Polystyrene near Silica Substrates: The Advantage of Mushrooms over Brushes”, *ACS Macro Letters* **7**, 269–274 (2018).
- [29] J. E. Pye, K. A. Rohald, E. A. Baker, and C. B. Roth, “Physical aging in ultrathin polystyrene films: Evidence of a gradient in dynamics at the free surface and its connection to the glass transition temperature reductions”, *Macromolecules* **43**, 8296–8303 (2010).
- [30] P. M. Rauscher, J. E. Pye, R. R. Baglay, and C. B. Roth, “Effect of Adjacent Rubbery Layers on the Physical Aging of Glassy Polymers”, *Macromolecules* **46**, 9806–9817 (2013).
- [31] Z. Yang, Y. Fujii, F. K. Lee, C.-h. Lam, and O. K. C. Tsui, “Glass Transition Dynamics and Surface Layer Mobility in Unentangled Polystyrene Films”, *Science* **328**, 1676–1679 (2010).
- [32] F. Chen, D. Peng, C.-H. Lam, and O. K. C. Tsui, “Viscosity and Surface-Promoted Slippage of Thin Polymer Films Supported by a Solid Substrate”, *Macromolecules* **48**, 5034–5039 (2015).

- [33] K. Geng and O. K. C. Tsui, “Effects of Polymer Tacticity and Molecular Weight on the Glass Transition Temperature of Poly(methyl methacrylate) Films on Silica”, *Macromolecules* **49**, 2671–2678 (2016).
- [34] T. Lan and J. M. Torkelson, “Methacrylate-based polymer films useful in lithographic applications exhibit different glass transition temperature-confinement effects at high and low molecular weight”, *Polymer (Guildf)*. **55**, 1249–1258 (2014).
- [35] D. Qi, C. R. Daley, Y. Chai, and J. A. Forrest, “Molecular weight dependence of near surface dynamical mechanical properties of polymers”, *Soft Matter* **9**, 8958 (2013).
- [36] E. C. Glor and Z. Fakhraai, “Facilitation of interfacial dynamics in entangled polymer films”, *The Journal of Chemical Physics* **141**, 194505 (2014).
- [37] E. C. Glor, R. J. Composto, and Z. Fakhraai, “Glass Transition Dynamics and Fragility of Ultrathin Miscible Polymer Blend Films”, *Macromolecules* **48**, 6682–6689 (2015).
- [38] M. F. Thees and C. B. Roth, “Unexpected Molecular Weight Dependence to the Physical Aging of Thin Polystyrene Films Present at Ultra-High Molecular Weights”, *Journal of Polymer Science Part B-Polymer Physics* **57**, 1224–1238 (2019).
- [39] S. Napolitano and M. Wübbenhorst, “The lifetime of the deviations from bulk behaviour in polymers confined at the nanoscale”, *Nature Communications* **2**, 260 (2011).
- [40] N. G. Perez-de-Eulate, M. Sferrazza, D. Cangialosi, and S. Napolitano, “Irreversible Adsorption Erases the Free Surface Effect on the T_g of Supported Films of Poly(4-tert-butylstyrene)”, *ACS Macro Lett.* **6**, 354–358 (2017).

- [41] C. Housmans, M. Sferrazza, and S. Napolitano, “Kinetics of Irreversible Chain Adsorption”, *Macromolecules* **47**, 3390–3393 (2014).
- [42] M. J. Burroughs, S. Napolitano, D. Cangialosi, and R. D. Priestley, “Direct Measurement of Glass Transition Temperature in Exposed and Buried Adsorbed Polymer Nanolayers”, *Macromolecules* **49**, 4647–4655 (2016).
- [43] T. Koga, N. Jiang, P. Gin, M. K. Endoh, S. Narayanan, L. B. Lurio, and S. K. Sinha, “Impact of an irreversibly adsorbed layer on local viscosity of nanoconfined polymer melts”, *Physical Review Letters* **107**, 1–5 (2011).
- [44] N. Jiang, J. Wang, X. Di, J. Cheung, W. Zeng, M. K. Endoh, T. Koga, and S. K. Satija, “Nanoscale adsorbed structures as a robust approach for tailoring polymer film stability”, *Soft Matter* **12**, 1801–1809 (2016).
- [45] J. A. Forrest and K. Dalnoki-Veress, “The glass transition in thin polymer films”, *Adv. Colloid Interface Sci.* **94**, 167–195 (2001).
- [46] M. D. Ediger and J. A. Forrest, “Dynamics near Free Surfaces and the Glass Transition in Thin Polymer Films: A View to the Future”, *Macromolecules* **47**, 471–478 (2014).
- [47] C. B. Roth and J. R. Dutcher, “Glass transition and chain mobility in thin polymer films”, *Journal of Electroanalytical Chemistry* **584**, International Symposium on Material Processing for Nanostructured Devices 2003, 13–22 (2005).
- [48] J. Baschnagel and F. Varnik, “Computer simulations of supercooled polymer melts in the bulk and in confined geometry”, *Journal of Physics: Condensed Matter* **17**, R851–R953 (2005).
- [49] M. Alcoutlabi and G. B. McKenna, “Effects of confinement on material behaviour at the nanometre size scale”, *Journal of Physics: Condensed Matter* **17**, R461–R524 (2005).

- [50] O. K. C. Tsui, “Anomalous dynamics of polymer films”, in *Polymer thin films*, edited by O. K. C. Tsui and T. P. Russel (World Scientific, Singapore, 2008) Chap. 11, pp. 267–294.
- [51] S. Napolitano, E. Glynos, and N. B. Tito, “Glass transition of polymers in bulk, confined geometries, and near interfaces”, *Reports Prog. Phys.* **80**, 036602 (2017).
- [52] C. B. Roth, J. E. Pye, and R. R. Baglay, “Correlating glass transition and physical aging in thin polymer films”, in *Polymer glasses*, edited by C. B. Roth (CRC Press Taylor and Francis, Boca Raton, 2016) Chap. 5, pp. 181–204.
- [53] J. E. Pye and C. B. Roth, “Physical aging of polymer films quenched and measured free-standing via ellipsometry: controlling stress imparted by thermal expansion mismatch between film and”, *Macromolecules* **46**, 9455–63 (2013).
- [54] D. Cangialosi, A. Alegría, and J. Colmenero, “Effect of nanostructure on the thermal glass transition and physical aging in polymer materials”, *Progress in Polymer Science* **54-55**, 128–147 (2016).
- [55] P. Z. Hanakata, J. F. Douglas, and F. W. Starr, “Interfacial mobility scale determines the scale of collective motion and relaxation rate in polymer films.”, *Nat. Commun.* **5**, 4163 (2014).
- [56] P. Z. Hanakata, B. A. Pazmiño Betancourt, J. F. Douglas, and F. W. Starr, “A unifying framework to quantify the effects of substrate interactions, stiffness, and roughness on the dynamics of thin supported polymer films”, *J. Chem. Phys.* **142**, 234907 (2015).
- [57] J. E. Pye, K. A. Rohald, E. A. Baker, and C. B. Roth, “Physical Aging in Ultrathin Polystyrene Films: Evidence of a Gradient in Dynamics at the Free Surface and Its Connection to the Glass Transition Temperature Reductions”, *Macromolecules* **43**, 8296–8303 (2010).

- [58] R. J. Lang and D. S. Simmons, “Interfacial dynamic length scales in the glass transition of a model freestanding polymer film and their connection to cooperative motion”, *Macromolecules* **46**, 9818–9825 (2013).
- [59] A. Shavit and R. A. Riggleman, “Physical aging, the local dynamics of glass-forming polymers under nanoscale confinement”, *Journal of Physical Chemistry B* **118**, 9096–9103 (2014).
- [60] J. D. Stevenson and P. G. Wolynes, “On the surface of glasses”, *The Journal of Chemical Physics* **129**, 234514 (2008).
- [61] N. B. Tito, J. E. Lipson, and S. T. Milner, “Lattice model of mobility at interfaces: Free surfaces, substrates, and bilayers”, *Soft Matter* **9**, 9403–9413 (2013).
- [62] S. Mirigian and K. S. Schweizer, “Communication: slow relaxation, spatial mobility gradients, and vitrification in confined films”, *The Journal of Chemical Physics* **141**, 161103 (2014).
- [63] S. Mirigian and K. S. Schweizer, “Theory of activated glassy relaxation, mobility gradients, surface diffusion, and vitrification in free standing thin films”, *The Journal of Chemical Physics* **143**, 244705 (2015).
- [64] S. Mirigian and K. S. Schweizer, “Influence of chemistry, interfacial width, and non-isothermal conditions on spatially heterogeneous activated relaxation and elasticity in glass-forming free standing films”, *The Journal of Chemical Physics* **146**, 203301 (2017).
- [65] C. B. Roth, K. L. McNerny, W. F. Jager, and J. M. Torkelson, “Eliminating the Enhanced Mobility at the Free Surface of Polystyrene: Fluorescence Studies of the Glass Transition Temperature in Thin Bilayer Films of Immiscible Polymers”, *Macromolecules* **40**, 2568–2574 (2007).

- [66] C. J. Ellison and J. M. Torkelson, “The distribution of glass-transition temperatures in nanoscopically confined glass formers.”, *Nature Materials* **2**, 695–700 (2003).
- [67] R. D. Priestley, C. J. Ellison, L. J. Broadbelt, and J. M. Torkelson, “Structural relaxation of polymer glasses at surfaces, interfaces, and in between”, *Science* **309**, 456–459 (2005).
- [68] R. D. Priestley, M. K. Mundra, N. J. Barnett, L. J. Broadbelt, and J. M. Torkelson, “Effects of nanoscale confinement and interfaces on the glass transition temperatures of a series of poly(n-methacrylate) films”, *Australian Journal of Chemistry* **60**, 765 (2007).
- [69] D. S. Fryer, R. D. Peters, E. J. Kim, J. E. Tomaszewski, J. J. De Pablo, P. F. Nealey, C. C. White, and W. L. Wu, “Dependence of the glass transition temperature of polymer films on interfacial energy and thickness”, *Macromolecules* **34**, 5627–5634 (2001).
- [70] R. P. White, C. C. Price, and J. E. G. Lipson, “Effect of interfaces on the glass transition of supported and freestanding polymer thin films”, *Macromolecules* **48**, 4132–4141 (2015).
- [71] Z. Fakhraai and J. A. Forrest, “Measuring the surface dynamics of glassy polymers.”, *Science* **319**, 600–4 (2008).
- [72] S. F. Swallen, K. : Kearns, M. K. Mapes, Y. S. Kim, R. J. McMahon, M. D. Ediger, T. Wu, L. Yu, and S. Satija, “Organic Glasses with Exceptional Thermodynamic and Kinetic Stability”, *Science* **315**, 353–356 (2007).
- [73] L. Zhu, C. W. Brian, S. F. Swallen, P. T. Straus, M. D. Ediger, and L. Yu, “Surface self-diffusion of an organic glass”, *Physical Review Letters* **106**, 256103 (2011).

- [74] C. M. Bates, T. Seshimo, M. J. Maher, W. J. Durand, J. D. Cushen, L. M. Dean, G. Blachut, C. J. Ellison, and C. G. Willson, “Polarity-Switching Top Coats Enable Orientation of Sub-10-nm Block Copolymer Domains”, *Science* **338**, 775–779 (2012).
- [75] B. W. Rowe, B. D. Freeman, and D. R. Paul, “Physical aging of ultrathin glassy polymer films tracked by gas permeability”, *Polymer (Guildf)*. **50**, 5565–5575 (2009).
- [76] P. Rittigstein, R. D. Priestley, L. J. Broadbelt, and J. M. Torkelson, “Model polymer nanocomposites provide an understanding of confinement effects in real nanocomposites”, *Nature Materials* **6**, 278–282 (2007).
- [77] N. Jouault, J. F. Moll, D. Meng, K. Windsor, S. Ramcharan, C. Kearney, and S. K. Kumar, “Bound Polymer Layer in Nanocomposites”, *ACS Macro Letters* **2**, 371–374 (2013).
- [78] S. Cheng, A. P. Holt, H. Wang, F. Fan, V. Bocharova, H. Martin, T. Etampawala, B. T. White, T. Saito, N.-G. Kang, M. D. Dadmun, J. W. Mays, and A. P. Sokolov, “Unexpected Molecular Weight Effect in Polymer Nanocomposites”, *Physical Review Letters* **116**, 038302 (2016).
- [79] S. Cheng, V. Bocharova, A. Belianinov, S. Xiong, A. Kisliuk, S. Somnath, A. P. Holt, O. S. Ovchinnikova, S. Jesse, H. Martin, T. Etampawala, M. Dadmun, and A. P. Sokolov, “Unraveling the Mechanism of Nanoscale Mechanical Reinforcement in Glassy Polymer Nanocomposites”, *Nano Letters* **16**, 3630–3637 (2016).
- [80] A. P. Holt, V. Bocharova, S. Cheng, A. M. Kisliuk, B. T. White, T. Saito, D. Uhrig, J. P. Mahalik, R. Kumar, A. E. Imel, T. Etampawala, H. Martin, N. Sikes, B. G. Sumpter, M. D. Dadmun, and A. P. Sokolov, “Controlling

- Interfacial Dynamics: Covalent Bonding versus Physical Adsorption in Polymer Nanocomposites”, *ACS Nano* **10**, 6843–6852 (2016).
- [81] S. Merabia, P. Sotta, and D. R. Long, “Unique plastic and recovery behavior of nanofilled elastomers and thermoplastic elastomers (payne and mullins effects)”, *Journal of Polymer Science Part B: Polymer Physics* **48**, 1495–1508 (2010).
- [82] C. Declet-Perez, E. M. Redline, L. F. Francis, and F. S. Bates, “Role of localized network damage in block copolymer toughened epoxies”, *ACS Macro Letters* **1**, 338–342 (2012).
- [83] R. Y. F. Liu, Y. Jin, A. Hiltner, and E. Baer, “Probing nanoscale polymer interactions by forced-assembly”, *Macromolecular Rapid Communications* **24**, 943–948 (2003).
- [84] R. J. Lang, W. L. Merling, and D. S. Simmons, “Combined Dependence of Nanoconfined T_g on Interfacial Energy and Softness of Confinement”, *ACS Macro Letters* **3**, 758–762 (2014).
- [85] R. R. Baglay and C. B. Roth, “Experimental Study of the Influence of Periodic Boundary Conditions: Effects of Finite Size and Faster Cooling Rates on Dissimilar Polymer–Polymer Interfaces”, *ACS Macro Letters* **6**, 887–891 (2017).
- [86] V. Sethuraman, V. Pryamitsyn, and V. Ganesan, “Influence of molecular weight and degree of segregation on local segmental dynamics of ordered block copolymers”, *Journal of Polymer Science Part B: Polymer Physics* **54**, 859–864 (2016).
- [87] F. S. Bates, M. A. Hillmyer, T. P. Lodge, C. M. Bates, K. T. Delaney, and G. H. Fredrickson, “Multiblock Polymers: Panacea or Pandora’s Box?”, *Science* (80-.). **336**, 434–440 (2012).

- [88] N. P. Balsara and K. M. Beers, “Proton conduction in materials comprising conducting domains with widths less than 6nm”, *European Polymer Journal* **47**, Designer polymers: Controlled synthesis, structure-property relationships and applications (Dedicated to Professor Nikos Hadjichristidis in recognition of his contribution to polymer science), 647–650 (2011).
- [89] Z. Yang, Y. Fujii, F. K. Lee, C.-H. Lam, and O. K. C. Tsui, “Glass transition dynamics and surface layer mobility in unentangled polystyrene films”, *Science* **328**, 1676–1679 (2010).
- [90] K. Paeng, S. F. Swallen, and M. D. Ediger, “Direct measurement of molecular motion in freestanding polystyrene thin films”, *Journal of the American Chemical Society* **133**, 8444–8447 (2011).
- [91] O. K. Tsui, T. P. Russell, and C. J. Hawker, “Effect of interfacial interactions on the glass transition of polymer thin films”, *Macromolecules* **34**, 5535–5539 (2001).
- [92] D. Christie, C. Zhang, J. Fu, B. Koel, and R. D. Priestley, “Glass transition temperature of colloidal polystyrene dispersed in various liquids”, *Journal of Polymer Science Part B: Polymer Physics* **54**, 1776–1783 (2016).
- [93] J. L. Keddie, R. A. L. Jones, and R. A. Cory, “Interface and surface effects on the glass-transition temperature in thin polymer films”, *Faraday Discussions* **98**, 219 (1994).
- [94] R. S. Tate, D. S. Fryer, S. Pasqualini, M. F. Montague, J. J. de Pablo, and P. F. Nealey, “Extraordinary elevation of the glass transition temperature of thin polymer films grafted to silicon oxide substrates”, *The Journal of Chemical Physics* **115**, 9982–9990 (2001).
- [95] E. C. Glor, G. V. Angrand, and Z. Fakhraai, “Exploring the broadening and the existence of two glass transitions due to competing interfacial effects in

- thin, supported polymer films”, *The Journal of Chemical Physics* **146**, 203330 (2017).
- [96] O. K. C. Tsui and H. F. Zhang, “Effects of chain ends and chain entanglement on the glass transition temperature of polymer thin films”, *Macromolecules* **34**, 9139–9142 (2001).
- [97] J. E. Pye and C. B. Roth, “Two Simultaneous Mechanisms Causing Glass Transition Temperature Reductions in High Molecular Weight Freestanding Polymer Films as Measured by Transmission Ellipsometry”, *Physical Review Letters* **107**, 235701 (2011).
- [98] D. Qi, C. R. Daley, Y. Chai, and J. A. Forrest, “Molecular weight dependence of near surface dynamical mechanical properties of polymers”, *Soft Matter* **9**, 8958 (2013).
- [99] T. Lan and J. M. Torkelson, “Methacrylate-based polymer films useful in lithographic applications exhibit different glass transition temperature-confinement effects at high and low molecular weight”, *Polymer (Guildf)*. **55**, 1249–1258 (2014).
- [100] S. Askar, T. Wei, A. W. Tan, and J. M. Torkelson, “Molecular weight dependence of the intrinsic size effect on T_g in AAO template-supported polymer nanorods: A DSC study”, *The Journal of Chemical Physics* **146**, 203323 (2017).
- [101] K. Geng, F. Chen, and O. K. Tsui, “Molecular-weight dependent t_g depression of silica-supported poly(-methyl styrene) films”, *Journal of Non-Crystalline Solids* **407**, 7th IDMRCS: Relaxation in Complex Systems, 296–301 (2015).
- [102] K. Geng and O. K. C. Tsui, “Effects of Polymer Tacticity and Molecular Weight on the Glass Transition Temperature of Poly(methyl methacrylate) Films on Silica”, *Macromolecules* **49**, 2671–2678 (2016).

- [103] J. M. Torres, C. M. Stafford, and B. D. Vogt, “Manipulation of the Elastic Modulus of Polymers at the Nanoscale : Influence of UV-Ozone Cross-Linking and Plasticizer”, *ACS Nano* **4**, 5357–5365 (2010).
- [104] J. M. Torres, C. Wang, E. B. Coughlin, J. P. Bishop, R. A. Register, R. A. Riggleman, C. M. Stafford, and B. D. Vogt, “Influence of Chain Stiffness on Thermal and Mechanical Properties of Polymer Thin Films”, *Macromolecules* **44**, 9040–9045 (2011).
- [105] A. Shavit and R. A. Riggleman, “Influence of Backbone Rigidity on Nanoscale Confinement Effects in Model Glass-Forming Polymers”, *Macromolecules* **46**, 5044–5052 (2013).
- [106] Z. Yang, A. Clough, C.-H. Lam, and O. K. C. Tsui, “Glass Transition Dynamics and Surface Mobility of Entangled Polystyrene Films at Equilibrium”, *Macromolecules* **44**, 8294–8300 (2011).
- [107] R. N. Li, F. Chen, C.-H. Lam, and O. K. C. Tsui, “Viscosity of PMMA on Silica: Epitome of Systems with Strong Polymer–Substrate Interactions”, *Macromolecules* **46**, 7889–7893 (2013).
- [108] F. Chen, D. Peng, Y. Ogata, K. Tanaka, Z. Yang, Y. Fujii, N. L. Yamada, C.-H. Lam, and O. K. C. Tsui, “Confinement Effect on the Effective Viscosity of Plasticized Polymer Films”, *Macromolecules* **48**, 7719–7726 (2015).
- [109] W. Bisbee, J. Qin, and S. T. Milner, “Finding the Tube with Isoconfigurational Averaging”, *Macromolecules* **44**, 8972–8980 (2011).
- [110] E. Glynos, B. Frieberg, H. Oh, M. Liu, D. W. Gidley, and P. F. Green, “Role of Molecular Architecture on the Vitrification of Polymer Thin Films”, *Physical Review Letters* **106**, 1–4 (2011).
- [111] B. Frieberg, E. Glynos, G. Sakellariou, and P. F. Green, “Physical Aging of Star-Shaped Macromolecules”, *ACS Macro Letters* **1**, 636–640 (2012).

- [112] B. Frieberg, E. Glynos, and P. F. Green, “Structural relaxations of thin polymer films”, *Physical Review Letters* **108**, 1–5 (2012).
- [113] B. R. Frieberg, E. Glynos, M. Stathouraki, G. Sakellariou, and P. F. Green, “Glassy Dynamics of Polymers with Star-Shaped Topologies: Roles of Molecular Functionality, Arm Length, and Film Thickness”, *Macromolecules* **50**, 3719–3725 (2017).
- [114] E. Glynos, K. J. Johnson, B. Frieberg, A. Chremos, S. Narayanan, G. Sakellariou, and P. F. Green, “Free Surface Relaxations of Star-Shaped Polymer Films”, *Physical Review Letters* **119**, 1–5 (2017).
- [115] S.-f. Wang, Z. Jiang, S. Narayanan, and M. D. Foster, “Dynamics of Surface Fluctuations on Macrocyclic Melts”, *Macromolecules* **45**, 6210–6219 (2012).
- [116] B. Liu, S. Narayanan, D. T. Wu, and M. D. Foster, “Polymer film surface fluctuation dynamics in the limit of very dense branching”, *Macromolecules* **46**, 3190–3197 (2013).
- [117] S.-f. Wang, S. Yang, J. Lee, B. Akgun, D. T. Wu, and M. D. Foster, “Anomalous Surface Relaxations of Branched-Polymer Melts”, *Physical Review Letters* **111**, 1–5 (2013).
- [118] Q. He, S. Narayanan, D. T. Wu, and M. D. Foster, “Confinement Effects with Molten Thin Cyclic Polystyrene Films”, *ACS Macro Letters* **5**, 999–1003 (2016).
- [119] F. Zhang, Q. He, Y. Zhou, S. Narayanan, C. Wang, B. D. Vogt, and M. D. Foster, “Anomalous Confinement Slows Surface Fluctuations of Star Polymer Melt Films”, *ACS Macro Letters* **7**, 834–839 (2018).
- [120] J. M. Torres, C. M. Stafford, D. Uhrig, and B. D. Vogt, “Impact of chain architecture (branching) on the thermal and mechanical behavior of polystyrene

- thin films”, *Journal of Polymer Science Part B: Polymer Physics* **50**, 370–377 (2012).
- [121] T. B. Karim and G. B. McKenna, “Comparison of surface mechanical properties among linear and star polystyrenes: Surface softening and stiffening at different temperatures”, *Polymer (Guildf)*. **54**, 5928–5935 (2013).
- [122] L. Zhang, R. Elupula, S. M. Grayson, and J. M. Torkelson, “Major Impact of Cyclic Chain Topology on the T_g -Confinement Effect of Supported Thin Films of Polystyrene”, *Macromolecules* **49**, 257–268 (2016).
- [123] X. Huang and C. B. Roth, “Optimizing the Grafting Density of Tethered Chains to Alter the Local Glass Transition Temperature of Polystyrene near Silica Substrates: The Advantage of Mushrooms over Brushes”, *ACS Macro Letters* **7**, 269–274 (2018).
- [124] M. Hénot, A. Chennevière, E. Drockenmuller, K. Shull, L. Léger, and F. Restagno, “Influence of grafting on the glass transition temperature of PS thin films”, *The European Physical Journal E* **40**, 11 (2017).
- [125] T. Lan and J. M. Torkelson, “Substantial spatial heterogeneity and tunability of glass transition temperature observed with dense polymer brushes prepared by ARGET ATRP”, *Polymer (Guildf)*. **64**, 183–192 (2015).
- [126] T. Lan and J. M. Torkelson, “Fragility-Confinement Effects: Apparent Universality as a Function of Scaled Thickness in Films of Freely Deposited, Linear Polymer and Its Absence in Densely Grafted Brushes”, *Macromolecules* **49**, 1331–1343 (2016).
- [127] J. L. Keddie and R. A. L. Jones, “Glass Transition Behavior in Ultra-thin Polystyrene Films”, *Israel Journal of Chemistry* **35**, 21–26 (1995).
- [128] A. Clough, D. Peng, Z. Yang, and O. K. C. Tsui, “Glass transition temperature of polymer films that slip”, *Macromolecules* **44**, 1649–1653 (2011).

- [129] H. Lee, H. Ahn, S. Naidu, B. S. Seong, D. Y. Ryu, D. M. Trombly, and V. Ganesan, “Glass Transition Behavior of PS Films on Grafted PS Substrates”, *Macromolecules* **43**, 9892–9898 (2010).
- [130] H. Lee, V. Sethuraman, Y. Kim, W. Lee, D. Y. Ryu, and V. Ganesan, “Non-monotonic Glass Transition Temperature of Polymer Films Supported on Polymer Brushes”, *Macromolecules* **51**, 4451–4461 (2018).
- [131] Y. Shin, H. Lee, W. Lee, and D. Y. Ryu, “Glass Transition and Thermal Expansion Behavior of Polystyrene Films Supported on Polystyrene-Grafted Substrates”, *Macromolecules* **49**, 5291–5296 (2016).
- [132] S. Sun, H. Xu, J. Han, Y. Zhu, B. Zuo, X. Wang, and W. Zhang, “The architecture of the adsorbed layer at the substrate interface determines the glass transition of supported ultrathin polystyrene films”, *Soft Matter* **12**, 8348–8358 (2016).
- [133] G. Uğur, B. Akgun, Z. Jiang, S. Narayanan, S. Satija, and M. D. Foster, “Effect of tethering on the surface dynamics of a thin polymer melt layer”, *Soft Matter* **12**, 5372–5377 (2016).
- [134] Y. Zhou, Q. He, F. Zhang, F. Yang, S. Narayanan, G. Yuan, A. Dhinojwala, and M. D. Foster, “Modifying Surface Fluctuations of Polymer Melt Films with Substrate Modification”, *ACS Macro Letters* **6**, 915–919 (2017).
- [135] S. D. Vianna, F. Y. Lin, M. A. Plum, H. Duran, and W. Steffen, “Dynamics of ultra-thin polystyrene with and without a (artificial) dead layer studied by resonance enhanced dynamic light scattering”, *The Journal of Chemical Physics* **146** (2017).
- [136] S. Napolitano, S. Capponi, and B. Vanroy, “Glassy dynamics of soft matter under 1D confinement: How irreversible adsorption affects molecular packing,

- mobility gradients and orientational polarization in thin films”, *Eur. Phys. J. E* **36**, 61 (2013).
- [137] N. G. Perez-de-Eulate, M. Sferrazza, D. Cangialosi, and S. Napolitano, “Irreversible Adsorption Erases the Free Surface Effect on the Tg of Supported Films of Poly(4-tert-butylstyrene)”, *ACS Macro Letters* **6**, 354–358 (2017).
- [138] D. N. Simavilla, W. Huang, P. Vandestruck, J.-P. Ryckaert, M. Sferrazza, and S. Napolitano, “Mechanisms of Polymer Adsorption onto Solid Substrates”, *ACS Macro Lett.* **6**, 975–979 (2017).
- [139] A. Panagopoulou and S. Napolitano, “Irreversible Adsorption Governs the Equilibration of Thin Polymer Films”, *Physical Review Letters*. **119**, 097801 (2017).
- [140] P. Gin, N. Jiang, C. Liang, T. Taniguchi, B. Akgun, S. K. Satija, M. K. Endoh, and T. Koga, “Revealed Architectures of Adsorbed Polymer Chains at Solid-Polymer Melt Interfaces”, *Physical Review Letters* **109**, 265501 (2012).
- [141] N. Jiang, J. Shang, X. Di, M. K. Endoh, and T. Koga, “Formation Mechanism of High-Density, Flattened Polymer Nanolayers Adsorbed on Planar Solids”, *Macromolecules* **47**, 2682–2689 (2014).
- [142] M. Sen, N. Jiang, J. Cheung, M. K. Endoh, T. Koga, D. Kawaguchi, and K. Tanaka, “Flattening Process of Polymer Chains Irreversibly Adsorbed on a Solid”, *ACS Macro Letters* **5**, 504–508 (2016).
- [143] N. Jiang, J. Cheung, Y. Guo, M. K. Endoh, T. Koga, G. Yuan, and S. K. Satija, “Stability of Adsorbed Polystyrene Nanolayers on Silicon Substrates”, *Macromol. Chem. Phys.* **219**, 1–10 (2018).
- [144] Y. Fujii, Z. Yang, J. Leach, H. Atarashi, K. Tanaka, and O. K. C. Tsui, “Affinity of Polystyrene Films to Hydrogen-Passivated Silicon and Its Relevance to the T g of the Films”, *Macromolecules* **42**, 7418–7422 (2009).

- [145] W. Zhang and L. Yu, “Surface Diffusion of Polymer Glasses”, *Macromolecules* **49**, 731–735 (2016).
- [146] C. B. Roth and R. R. Baglay, *Polymer Glasses*, edited by C. B. Roth (CRC Press, Taylor and Francis Group, Boca Raton, 2016), pp. 3–22.
- [147] F. W. Starr, J. F. Douglas, and S. Sastry, “The relationship of dynamical heterogeneity to the Adam-Gibbs and random first-order transition theories of glass formation”, *The Journal of Chemical Physics* **138** (2013).
- [148] B. A. Pazmiño Betancourt, J. F. Douglas, and F. W. Starr, “String model for the dynamics of glass-forming liquids”, *The Journal of Chemical Physics* **140**, 204509 (2014).
- [149] C. M. Evans, H. Deng, W. F. Jager, and J. M. Torkelson, “Fragility is a key parameter in determining the magnitude of T_g-confinement effects in polymer films”, *Macromolecules* **46**, 6091–6103 (2013).
- [150] J. A. Forrest and J. Mattsson, “Reductions of the glass transition temperature in thin polymer films: probing the length scale of cooperative dynamics”, *Physical Review E* **61**, R53–R56 (2000).
- [151] J. Mattsson, J. a. Forrest, and L. Börjesson, “Quantifying glass transition behavior in ultrathin free-standing polymer films”, *Physical Review E* **62**, 5187–5200 (2000).
- [152] C. G. Campbell and B. D. Vogt, “Examination of the influence of cooperative segmental dynamics on the glass transition and coefficient of thermal expansion in thin films probed using poly(n-alkyl methacrylate)s”, *Polymer (Guildf)*. **48**, 7169–7175 (2007).
- [153] S. Butler and P. Harrowell, “Glassy relaxation at surfaces: The correlation length of cooperative motion in the facilitated kinetic Ising model”, *The Journal of Chemical Physics* **95**, 4466–4470 (1991).

- [154] J. M. Hutchinson, “Physical aging of polymers”, *Progress in Polymer Science* **20**, 703–760 (1995).
- [155] G. B. McKenna and S. L. Simon, “50th anniversary perspective : challenges in the dynamics and kinetics of glass-forming polymers”, *Macromolecules* **50**, 5333–6361 (2017).
- [156] A. S. Marshall and S. E. B. Petrie, “Rate-determining factors for enthalpy relaxation of glassy polymers. Molecular weight”, *Journal of Applied Physics* **46**, 4223–4230 (1975).
- [157] Y. Ding, A. Kisliuk, and A. P. Sokolov, “When Does a Molecule Become a Polymer?”, *Macromolecules* **37**, 161–166 (2004).
- [158] S. Mirigian and K. S. Schweizer, “Dynamical Theory of Segmental Relaxation and Emergent Elasticity in Supercooled Polymer Melts”, *Macromolecules* **48**, 1901–1913 (2015).
- [159] P. C. Hiemenz and T. P. Lodge, *Polymer Chemistry*, 2nd (CRC Press, Taylor and Francis Group, Boca Raton, FL, 2007).
- [160] X. Huang and C. B. Roth, “Changes in the temperature-dependent specific volume of supported polystyrene films with film thickness”, *Journal of Chemical Physics* **144**, 234903 (2016).
- [161] L. J. Fetters, N. Hadjichristidis, J. S. Lindner, and J. W. Mays, *Molecular Weight Dependence of Hydrodynamic and Thermodynamic Properties for Well-Defined Linear Polymers in Solution*, 1994.
- [162] G. F. Meyers, B. M. DeKoven, and J. T. Seitz, “Is the molecular surface of polystyrene really glassy?”, *Langmuir* **8**, 2330–2335 (1992).
- [163] J. Malek, “Rate-determining factors for structural relaxation in non-crystalline materials I. Stabilization period of isothermal volume relaxation”, *Thermochimica Acta* **313**, 181–190 (1998).

- [164] Y. P. Koh, S. Gao, and S. L. Simon, “Structural recovery of a single polystyrene thin film using flash dsc at low aging temperatures”, *Polymer* **96**, 182–187 (2016).
- [165] Y. P. Koh and S. L. Simon, “The glass transition and enthalpy recovery of a single polystyrene ultrathin film using Flash DSC”, *Journal of Chemical Physics* **146** (2017).
- [166] Y. P. Koh and S. L. Simon, “Enthalpy recovery of ultrathin polystyrene film using flash dsc”, *Polymer* **143**, 40–45 (2018).
- [167] L. A. G. Gray, S. W. Yoon, W. a. Pahner, J. E. Davidheiser, and C. B. Roth, “Importance of Quench Conditions on the Subsequent Physical Aging Rate of Glassy Polymer Films”, *Macromolecules* **45**, 1701–1709 (2012).
- [168] A. J. Kovacs, “Transition vitreuse dans les polymeres amorphes. Etude phénornénologique”, *Fortschritte der hochpolymeren-forschung* **3**, 394–507 (1963).
- [169] S. Kawana and R. A. L. Jones, “Character of the glass transition in thin supported polymer films”, *Physical Review E* **63**, 1–6 (2001).
- [170] J. A. Forrest, K. Dalnoki-Veress, and J. R. Dutcher, “Interface and chain confinement effects on the glass transition temperature of thin polymer films”, *Physical Review E* **56**, 5705–5716 (1997).
- [171] S. Kim, S. A. Hewlett, C. B. Roth, and J. M. Torkelson, “Confinement effects on glass transition temperature, transition breadth, and expansivity: Comparison of ellipsometry and fluorescence measurements on polystyrene films”, *European Physical Journal E* **30**, 83–92 (2009).
- [172] M. K. Mundra, C. J. Ellison, P. Rittigstein, and J. M. Torkelson, “Fluorescence studies of confinement in polymer films and nanocomposites: Glass transition temperature, plasticizer effects, and sensitivity to stress relaxation and local polarity”, *Eur. Phys. J. Spec. Top.* **141**, 143–151 (2007).

- [173] S. Askar, C. M. Evans, and J. M. Torkelson, “Residual stress relaxation and stiffness in spin-coated polymer films: Characterization by ellipsometry and fluorescence”, *Polymer (Guildf)*. **76**, 113–122 (2015).
- [174] M. Born and E. Wolf, *Principles of Optics* (Cambridge University Press, New York, 2006).
- [175] N. W. Ashcroft and N. D. Mermin, *Solid State Physics* (Saunders College Publishing, 1976).
- [176] R. P. White and J. E. G. Lipson, “Polymer Free Volume and Its Connection to the Glass Transition”, *Macromolecules* **49**, 3987–4007 (2016).
- [177] C. W. Frank, V. Rao, M. M. Despotopoulou, R. F. W. Pease, W. D. Hinsberg, R. D. Miller, and J. F. Rabolt, “Structure in Thin and Ultrathin Spin-Cast Polymer Films”, *Science (80-.)*. **273**, 912–915 (1996).
- [178] J. Ferry, *Viscoelastic properties of polymers* (Wiley, 1980).
- [179] D. J. Plazek and V. M. O’Rourke, “Viscoelastic behavior of low molecular weight polystyrene”, *J. Polym. Sci. Part A-2 Polym. Phys.* **9**, 209–243 (1971).
- [180] C. Roth and J. Dutcher, *Soft Materials*, edited by J. R. Dutcher and A. G. Marangoni, January 2005 (CRC Press, Oct. 2004), pp. 1–38.
- [181] J. Y. Chung, T. Q. Chastek, M. J. Fasolka, H. W. Ro, and C. M. Stafford, “Quantifying Residual Stress in Nanoscale Thin Polymer Films via Surface Wrinkling”, *ACS Nano* **3**, 844–852 (2009).
- [182] K. R. Thomas and U. Steiner, “Direct stress measurements in thin polymer films”, *Soft Matter* **7**, 7839 (2011).
- [183] P. G. de Gennes, “Polymers at an interface; a simplified view”, *Advances In Colloid And Interface Science* **27**, 189–209 (1987).

- [184] M. A. Cohen Stuart and G. J. Fleer, “Adsorbed Polymer Layers in Nonequilibrium Situations”, *Annual Review of Materials Science* **26**, 463–500 (1996).
- [185] S. Granick, “Perspective: Kinetic and mechanical properties of adsorbed polymer layers”, *European Physical Journal E* **9**, 421–424 (2002).
- [186] G. J. Fleer, M. A. Cohen Stuart, J. M. H. M. Scheutjens, T. Cosgrove, and B. Vincent, *Polymers at Interfaces* (Chapman & Hall, London, UK, 1993).
- [187] D. Nieto Simavilla, W. Huang, C. Housmans, M. Sferrazza, and S. Napolitano, “Taming the Strength of Interfacial Interactions via Nanoconfinement”, *ACS Central Science* **4**, 755–759 (2018).
- [188] K. P. O’Connor and T. C. B. McLeish, “Molecular velcro”: dynamics of a constrained chain into an elastomer network”, *Macromolecules* **26**, 7322–7325 (1993).
- [189] C. J. Clarke, R. A. L. Jones, and A. S. Clough, “The effect of matrix molecular weight on the kinetics of formation of end-adsorbed polystyrene layers from the melt”, *Polymer (Guildf)*. **37**, 3813–3817 (1996).
- [190] S. Napolitano and M. Wubbenhorst, “The lifetime of the deviations from bulk behaviour in polymers confined at the nanoscale”, *Nature Communications* **2**, 260 (2011).
- [191] T. Koga, N. Jiang, P. Gin, M. K. Endoh, S. Narayanan, L. B. Lurio, and S. K. Sinha, “Impact of an Irreversibly Adsorbed Layer on Local Viscosity of Nanoconfined Polymer Melts”, *Physical Review Letters* **107**, 225901 (2011).
- [192] N. Jiang, J. Shang, X. Di, M. K. Endoh, and T. Koga, “Formation Mechanism of High-Density, Flattened Polymer Nanolayers Adsorbed on Planar Solids”, *Macromolecules* **47**, 2682–2689 (2014).

- [193] S. Sun, H. Xu, J. Han, Y. Zhu, B. Zuo, X. Wang, and W. Zhang, “The architecture of the adsorbed layer at the substrate interface determines the glass transition of supported ultrathin polystyrene films”, *Soft Matter* **12**, 8348–8358 (2016).
- [194] A. Panagopoulou and S. Napolitano, “Irreversible Adsorption Governs the Equilibration of Thin Polymer Films”, *Physical Review Letters* **119**, 097801 (2017).
- [195] N. Jiang, M. Sen, W. Zeng, Z. Chen, J. M. Cheung, Y. Morimitsu, M. K. Endoh, T. Koga, M. Fukuto, G. Yuan, S. K. Satija, J.-M. Y. Carrillo, and B. G. Sumpter, “Structure-induced switching of interpolymer adhesion at a solid–polymer melt interface”, *Soft Matter* **14**, 1108–1119 (2018).
- [196] N. Jiang, M. Sen, M. K. Endoh, T. Koga, E. Langhammer, P. Björn, and M. Tsige, “Thermal Properties and Segmental Dynamics of Polymer Melt Chains Adsorbed on Solid Surfaces”, *Langmuir* **34**, 4199–4209 (2018).
- [197] A. Debot, P. Tripathi, and S. Napolitano, “Solution filtering affects the glassy dynamics of spincoated thin films of poly(4-chlorostyrene)”, *European Physical Journal E* **42**, 102 (2019).
- [198] X. Li and X. Lu, “Interfacial Irreversibly and Loosely Adsorbed Layers Abide by Different Evolution Dynamics”, *ACS Macro Letters* **8**, 1426–1431 (2019).
- [199] C. Housmans, M. Sferrazza, and S. Napolitano, “Kinetics of Irreversible Chain Adsorption”, *Macromolecules* **47**, 3390–3393 (2014).
- [200] D. N. Simavilla, A. Panagopoulou, and S. Napolitano, “Characterization of Adsorbed Polymer Layers: Preparation, Determination of the Adsorbed Amount and Investigation of the Kinetics of Irreversible Adsorption”, *Macromolecular Chemistry And Physics* **219**, 1700303 (2018).

- [201] M.-L. Braatz, L. I. Meléndez, M. Sferrazza, and S. Napolitano, “Unexpected impact of irreversible adsorption on thermal expansion: Adsorbed layers are not that dead”, *Journal of Chemical Physics* **146**, 203304 (2017).
- [202] D. N. Simavilla, W. Huang, C. Housmans, M. Sferrazza, and S. Napolitano, “Taming the Strength of Interfacial Interactions via Nanoconfinement”, *ACS Central Science* **4**, 755–759 (2018).
- [203] M. Sen, N. Jiang, J. Cheung, M. K. Endoh, T. Koga, D. Kawaguchi, and K. Tanaka, “Flattening Process of Polymer Chains Irreversibly Adsorbed on a Solid”, *ACS Macro Letters* **5**, 504–508 (2016).
- [204] N. Jiang, J. Cheung, Y. Guo, M. K. Endoh, T. Koga, G. Yuan, and S. K. Satija, “Stability of Adsorbed Polystyrene Nanolayers on Silicon Substrates”, *Macromolecular Chemistry And Physics* **219**, 1700326 (2018).
- [205] S. Napolitano and D. Cangialosi, “Interfacial Free Volume and Vitrification: Reduction in Tg in Proximity of an Adsorbing Interface Explained by the Free Volume Holes Diffusion Model”, *Macromolecules* **46**, 8051–8053 (2013).
- [206] M. J. Burroughs, S. Napolitano, D. Cangialosi, and R. D. Priestley, “Direct Measurement of Glass Transition Temperature in Exposed and Buried Adsorbed Polymer Nanolayers”, *Macromolecules* **49**, 4647–4655 (2016).
- [207] A. B. Unni, G. Vignaud, J. P. Chapel, J. Giermanska, J. K. Bal, N. Delorme, T. Beuvier, S. Thomas, Y. Grohens, and A. Gibaud, “Probing the Density Variation of Confined Polymer Thin Films via Simple Model-Independent Nanoparticle Adsorption”, *Macromolecules* **50**, 1027–1036 (2017).
- [208] H. Jeong, S. Napolitano, C. B. Arnold, and R. D. Priestley, “Irreversible Adsorption Controls Crystallization in Vapor-Deposited Polymer Thin Films”, *Journal of Physical Chemistry Letters* **8**, 229–234 (2017).

- [209] H. K. Nguyen, M. Labardi, M. Lucchesi, P. Rolla, and D. Prevosto, “Plasticization in Ultrathin Polymer Films: The Role of Supporting Substrate and Annealing”, *Macromolecules* **46**, 555–561 (2013).
- [210] P. Gin, N. Jiang, C. Liang, T. Taniguchi, B. Akgun, S. K. Satija, M. K. Endoh, and T. Koga, “Revealed Architectures of Adsorbed Polymer Chains at Solid-Polymer Melt Interfaces”, *Physical Review Letters* **109**, 265501 (2012).
- [211] Y. Fujii, Z. Yang, J. Leach, H. Atarashi, K. Tanaka, and O. K. C. Tsui, “Affinity of Polystyrene Films to Hydrogen-Passivated Silicon and Its Relevance to the T-g of the Films”, *Macromolecules* **42**, 7418–7422 (2009).
- [212] H. Fujiwara, *Spectroscopic Ellipsometry: Principles and Applications* (John Wiley & Sons, Ltd., West Sussex, England, 2007).
- [213] S. Napolitano and M. Sferrazza, “How irreversible adsorption affects interfacial properties of polymers”, *Advances In Colloid And Interface Science* **247**, 172–177 (2017).
- [214] C. J. Durning, B. O’Shaughnessy, U. Sawhney, D. Nguyen, J. Majewski, and G. S. Smith, “Adsorption of Poly(methyl methacrylate) Melts on Quartz”, *Macromolecules* **32**, 6772–6781 (1999).
- [215] O. Guiselin, “Irreversible Adsorption of a Concentrated Polymer Solution”, *Europhysics Letters* **17**, 225–230 (1992).
- [216] E. Jenckel and B. Rumbach, “Über die Adsorption von hochmolekularen Stoffen aus der Lösung”, *Zeitschrift für Elektrochemie und angewandte physikalische Chemie* **55**, 612–618 (1951).
- [217] M. A. C. Stuart, G. J. Fleer, and J. M. H. M. Scheutjens, “Displacement of polymers. I. Theory. Segmental adsorption energy from polymer desorption in binary solvents”, *Journal of Colloid And Interface Science* **97**, 515–525 (1984).

- [218] S. Granick, in *Physics of Polymer Surfaces and Interfaces*, edited by I. C. Sanchez (I. C. Sanchez, Ed.; Butterworth-Heinemann, Boston, 1992) Chap. 10: Dynamics of Adsorption and Desorption at Polymer/Solid Interfaces, pp. 227–244.
- [219] J. F. Douglas, H. M. Schneider, P. Frantz, R. Lipman, and S. Granick, “The origin and characterization of conformational heterogeneity in adsorbed polymer layers”, *Journal of Physics-Condensed Matter* **9**, 7699–7718 (1997).
- [220] R. A. L. Jones and R. W. Richards, *Polymers at Surfaces and Interfaces* (Cambridge University Press, Cambridge, UK, 1999).
- [221] W. Norde, “Adsorption of proteins from solution at the solid-liquid interface”, *Advances In Colloid And Interface Science* **25**, 267–340 (1986).
- [222] R. R. Netz and D. Andelman, “Neutral and charged polymers at interfaces”, *Physics Reports* **380**, 1–95 (2003).
- [223] H.-J. Butt, K. Graft, and M. Kappl, *Physics and Chemistry of Interfaces* (Wiley-VCH Verlag GmbH, Weinheim, Germany, 2013).
- [224] A. W. Adamson and A. P. Gast, *Physical Chemistry of Surfaces, 6th Edition* (Wiley, New York, 1997).
- [225] H. Swenson and N. P. Stadie, “Langmuir’s Theory of Adsorption: A Centennial Review”, *Langmuir* **35**, 5409–5426 (2019).
- [226] J. M. H. M. Scheutjens and G. J. Fleer, “Statistical theory of the adsorption of interacting chain molecules. 1. Partition function, segment density distribution, and adsorption isotherms”, *J Phys Chem* **83**, 1619–1635 (1979).
- [227] J. M. H. M. Scheutjens and G. J. Fleer, “Statistical theory of the adsorption of interacting chain molecules. 2. Train, loop, and tail size distribution”, *J Phys Chem* **84**, 178–190 (1980).

- [228] P. G. de Gennes, “Scaling theory of polymer adsorption”, *Journal de Physique* **37**, 1445–1452 (1976).
- [229] M. Aubouy, O. Guiselin, and E. Raphael, “Scaling Description of Polymer Interfaces: Flat Layers”, *Macromolecules* **29**, 7261–7268 (1996).
- [230] T. Wang, J. Yan, H. Yuan, J. Xu, H. Y. Lam, X. Yu, C. Lv, B. Du, and O. K. C. Tsui, “Tg Confinement Effect of Random Copolymers of 4-tert-Butylstyrene and 4-Acetoxy styrene with Different Compositions”, *ACS Macro Letters* **8**, 1280–1284 (2019).
- [231] A. Silberberg, “The Adsorption of Flexible Macromolecules. Part I. The Isolated Macromolecule at a Plane Interface”, *J Phys Chem* **66**, 1872–1883 (1962).
- [232] A. Silberberg, “Adsorption of flexible macromolecules. iv. effect of solvent–solute interactions, solute concentration, and molecular weight”, *The Journal of Chemical Physics* **48**, 2835–2851 (1968).
- [233] C. Yu and S. Granick, “Revisiting Polymer Surface Diffusion in the Extreme Case of Strong Adsorption”, *Langmuir* **30**, 14538–14544 (2014).
- [234] H. M. Schneider and S. Granick, “Kinetic traps in polymer adsorption: exchange of polystyrene between the adsorbed state and a good solvent”, *Macromolecules* **25**, 5054–5059 (1992).
- [235] M. Rubinstein and R. H. Colby, *Polymer Physics* (Oxford University Press, Oxford; New York, 2003).
- [236] H. M. Schneider, P. Frantz, and S. Granick, “The Bimodal Energy Landscape When Polymers Adsorb”, *Langmuir* **12**, 994–996 (1996).
- [237] M. M. Santore, “Dynamics in adsorbed homopolymer layers: Understanding complexity from simple starting points”, *Current Opinion In Colloid & Interface Science* **10**, 176–183 (2005).

- [238] E. Pefferkorn, A. Haouam, and R. Varoqui, “Kinetics of exchange between adsorbed and free polymers at a solid/liquid interface”, *Macromolecules* **22**, 2677–2682 (1989).
- [239] P. Frantz and S. Granick, “Kinetics of polymer adsorption and desorption”, *Physical Review Letters* **66**, 899–902 (1991).
- [240] H. E. Johnson and S. Granick, “Exchange kinetics between the adsorbed state and free solution: poly(methyl methacrylate) in carbon tetrachloride”, *Macromolecules* **23**, 3367–3374 (1990).
- [241] J. F. Douglas, H. E. Johnson, and S. Granick, “A Simple Kinetic Model of Polymer Adsorption and Desorption”, *Science* **262**, 2010–2012 (1993).
- [242] H. E. Johnson, J. F. Douglas, and S. Granick, “Topological influences on polymer adsorption and desorption dynamics”, *Physical Review Letters* **70**, 3267–3270 (1993).
- [243] E. Pefferkorn, A. Carroy, and R. Varoqui, “Dynamic behavior of flexible polymers at a solid/liquid interface”, *Journal of Polymer Science: Polymer Physics Edition* **23**, 1997–2008 (1985).
- [244] G. P. van der Beek, M. A. Cohen Stuart, G. J. Fleer, and J. E. Hofman, “A chromatographic method for the determination of segmental adsorption energies of polymers. Polystyrene on silica”, *Langmuir* **5**, 1180–1186 (1989).
- [245] G. P. van der Beek, M. A. Cohen Stuart, G. J. Fleer, and J. E. Hofman, “Segmental adsorption energies for polymers on silica and alumina”, *Macromolecules* **24**, 6600–6611 (1991).
- [246] J. Zhao and S. Granick, “How Polymer Surface Diffusion Depends on Surface Coverage”, *Macromolecules* **40**, 1243–1247 (2007).

- [247] C. Yu, J. Guan, K. Chen, S. C. Bae, and S. Granick, “Single-Molecule Observation of Long Jumps in Polymer Adsorption”, *ACS Nano* **7**, 9735–9742 (2013).
- [248] K. H. Nagamanasa, H. Wang, and S. Granick, “Liquid-Cell Electron Microscopy of Adsorbed Polymers”, *Advanced Materials* **29**, 1703555 (2017).
- [249] M. J. Skaug, J. Mabry, and D. K. Schwartz, “Intermittent Molecular Hopping at the Solid-Liquid Interface”, *Physical Review Letters* **110**, 256101 (2013).
- [250] H. G. Tompkins, *A User’s Guide to Ellipsometry* (Academic Press, Inc., San Diego, CA, 1993).
- [251] S. Napolitano, C. Rotella, and M. Wubbenhorst, “Can Thickness and Interfacial Interactions Univocally Determine the Behavior of Polymers Confined at the Nanoscale?”, *ACS Macro Letters* **1**, 1189–1193 (2012).
- [252] A. Beena Unni, G. Vignaud, J. K. Bal, N. Delorme, T. Beuvier, S. Thomas, Y. Grohens, and A. Gibaud, “Solvent Assisted Rinsing: Stability/Instability of Ultrathin Polymer Residual Layer”, *Macromolecules* **49**, 1807–1815 (2016).
- [253] E. A. Baker, P. Rittigstein, J. M. Torkelson, and C. B. Roth, “Streamlined ellipsometry procedure for characterizing physical aging rates of thin polymer films”, *Journal of Polymer Science Part B-Polymer Physics* **47**, 2509–2519 (2009).
- [254] C. M. Herzinger, B. Johs, W. A. McGahan, J. A. Woollam, and W. Paulson, “Ellipsometric determination of optical constants for silicon and thermally grown silicon dioxide via a multi-sample, multi-wavelength, multi-angle investigation”, *Journal of Applied Physics* **83**, 3323–3336 (1998).
- [255] N. L. Thomas and A. H. Windle, “A Theory of Case II Diffusion”, *Polymer* **23**, 529–542 (1982).

- [256] J. S. Papanu, D. W. Hess, A. T. Bell, and D. S. Soane, “In Situ Ellipsometry to Monitor Swelling and Dissolution of Thin Polymer Films”, *Journal of the Electrochemical Society* **136**, 1195–1200 (1989).
- [257] J. S. Papanu, D. W. Hess, D. S. Soane, and A. T. Bell, “Dissolution of Thin Poly(methyl methacrylate) Films in Ketones, Binary Ketone/Alcohol Mixtures, and Hydroxy Ketones”, *Journal of the Electrochemical Society* **136**, 3077–3083 (1989).
- [258] H. Coll and C. Searles, “Solvent permeation rates and ageing phenomena in polymer coatings”, *Polymer* **29**, 1266–1272 (1988).
- [259] D. Meng, K. Zhang, and S. K. Kumar, “Size-dependent penetrant diffusion in polymer glasses”, *Soft Matter* **14**, 4226–4230 (2018).
- [260] H. Richardson, I. Lopez-Garcia, M. Sferrazza, and J. L. Keddie, “Thickness dependence of structural relaxation in spin-cast, glassy polymer thin films”, *Physical Review E* **70**, 051805 (2004).
- [261] H. Richardson, M. Sferrazza, and J. L. Keddie, “Influence of the glass transition on solvent loss from spin-cast glassy polymer thin films”, *European Physical Journal E* **12**, S87–S91 (2003).
- [262] J. M. Hutchinson, “Physical Aging of Polymers”, *Progress In Polymer Science* **20**, 703–760 (1995).
- [263] X. Zheng, B. B. Sauer, J. G. Vanalsten, S. A. Schwarz, M. H. Rafailovich, J. Sokolov, and M. Rubinstein, “Reptation Dynamics of a Polymer Melt near an Attractive Solid Interface”, *Physical Review Letters* **74**, 407–410 (1995).
- [264] X. Zheng, M. H. Rafailovich, J. Sokolov, Y. Strzhemechny, S. A. Schwarz, B. B. Sauer, and M. Rubinstein, “Long-range effects on polymer diffusion induced by a bounding interface”, *Physical Review Letters* **79**, 241–244 (1997).

- [265] J. Choi, N. Clarke, K. I. Winey, and R. J. Composto, “Polymer Diffusion from Attractive and Athermal Substrates”, *Macromolecules* **50**, 3038–3042 (2017).
- [266] A. M. Jimenez, D. Zhao, K. Misquitta, J. Jestin, and S. K. Kumar, “Exchange Lifetimes of the Bound Polymer Layer on Silica Nanoparticles”, *ACS Macro Letters* **8**, 166–171 (2019).
- [267] F. Chen, K. Takatsuji, D. Zhao, X. Yu, S. K. Kumar, and O. K. C. Tsui, “Unexpected thermal annealing effects on the viscosity of polymer nanocomposites”, *Soft Matter* **13**, 5341–5354 (2017).
- [268] S. Alexander, “Adsorption of chain molecules with a polar head a scaling description”, *Journal de Physique* **38**, 983–987 (1977).
- [269] P. G. de Gennes, “Conformations of Polymers Attached to an Interface”, *Macromolecules* **13**, 1069–1075 (1980).
- [270] A. Casoli, M. Brendlé, J. Schultz, P. Auroy, and G. Reiter, “Friction Induced by Grafted Polymeric Chains”, *Langmuir* **17**, 388–398 (2001).
- [271] B. O’Shaughnessy and D. Vavylonis, “Non-equilibrium in adsorbed polymer layers”, *Journal of Physics-Condensed Matter* **17**, R63–R99 (2005).
- [272] P. Frantz and S. Granick, “Surface preparation of silicon for polymer adsorption studies”, *Langmuir* **8**, 1176–1182 (1992).
- [273] C. J. Clarke, “The kinetics of polymer brush penetration in to a high molecular weight matrix”, *Polymer* **37**, 4747–4752 (1996).
- [274] C. J. Clarke, R. A. L. Jones, J. L. Edwards, K. R. Shull, and J. Penfold, “The Structure of Grafted Polystyrene Layers in a Range of Matrix Polymers”, *Macromolecules* **28**, 2042–2049 (1995).

- [275] M. Hénot, A. Chenneviere, E. Drockenmuller, K. Shull, L. Léger, and F. Restagno, “Influence of grafting on the glass transition temperature of PS thin films”, *European Physical Journal E* **40**, 11 (2017).
- [276] A. Clough, D. Peng, Z. Yang, and O. K. C. Tsui, “Glass Transition Temperature of Polymer Films That Slip”, *Macromolecules* **44**, 1649–1653 (2011).
- [277] T. Lan and J. M. Torkelson, “Substantial spatial heterogeneity and tunability of glass transition temperature observed with dense polymer brushes prepared by ARGET ATRP”, *Polymer* **64**, 183–192 (2015).
- [278] B. Zuo, H. Zhou, M. J. B. Davis, X. Wang, and R. D. Priestley, “Effect of Local Chain Conformation in Adsorbed Nanolayers on Confined Polymer Molecular Mobility”, *Physical Review Letters* **122**, 217801 (2019).
- [279] H. K. Nguyen, S. Sugimoto, A. Konomi, M. Inutsuka, D. Kawaguchi, and K. Tanaka, “Dynamics Gradient of Polymer Chains near a Solid Interface”, *ACS Macro Letters* **8**, 1006–1011 (2019).
- [280] S. Chandran, J. Baschnagel, D. Cangialosi, K. Fukao, E. Glynos, L. M. C. Janssen, M. Müller, M. Muthukumar, U. Steiner, J. Xu, S. Napolitano, and G. Reiter, “Processing Pathways Decide Polymer Properties at the Molecular Level”, *Macromolecules* **52**, 7146–7156 (2019).
- [281] S. K. Kumar, V. Ganesan, and R. A. Riggleman, “Perspective: Outstanding theoretical questions in polymer-nanoparticle hybrids”, *Journal of Chemical Physics* **147**, 020901 (2017).
- [282] F. W. Starr, J. F. Douglas, D. Meng, and S. K. Kumar, “Bound Layers “Cloak” Nanoparticles in Strongly Interacting Polymer Nanocomposites”, *ACS Nano* **10**, 10960–10965 (2016).

- [283] W. Zhang, J. F. Douglas, and F. W. Starr, “Effects of a “bound” substrate layer on the dynamics of supported polymer films”, *Journal of Chemical Physics* **147**, 044901 (2017).
- [284] A. P. Holt, P. J. Griffin, V. Bocharova, A. L. Agapov, A. E. Imel, M. D. Dadmun, J. R. Sangoro, and A. P. Sokolov, “Dynamics at the Polymer/Nanoparticle Interface in Poly(2-vinylpyridine)/Silica Nanocomposites”, *Macromolecules* **47**, 1837–1843 (2014).
- [285] M. F. Thees, J. A. McGuire, and C. B. Roth, “Review and Reproducibility of Forming Adsorbed Layers From Solvent Washing of Melt Annealed Films”, *Soft Matter*, submitted January x (2020).
- [286] M. Kawaguchi, K. Maeda, T. Kato, and A. Takahashi, “Preferential Adsorption of Monodisperse Polystyrene on Silica Surface”, *Macromolecules* **17**, 1666–1671 (1984).
- [287] G. Kraus and J. Dugone, “Adsorption of Elastomers on Carbon Black”, *Ind. Eng. Chem.* **47**, 1809–1816 (1955).
- [288] J. C. Dijt, M. A. Cohen Stuart, and G. J. Fleer, “Kinetics of polymer adsorption and desorption in capillary flow”, *Macromolecules* **25**, 5416–5423 (1992).